THE UNIVERSITY *of* EDINBURGH

FAST NEUTRON POLARIZATION STUDIES

by

AHMED MOHAMED ALSORAYA, B.Sc.

Thesis submitted for the degree of

DOCTOR OF PHILOSOPHY

University of Edinburgh

August 1976

ABSTRACT.

A considerable disagreement exists between the various experimental results on the polarization of neutrons from the $^{2}H(d,n)^{3}He$ reaction. Some of these results indicate a peak in the polarization near 100 keV incident deuteron energy, and others do not. All but one of the experimental results differ significantly from the theoretical prediction of polarization by Boersma.

Because of the confused situation regarding the polarization of D-D neutrons and because of the theoretical interest in the results of this reaction and its practical value for users of low energy accelerators, the neutron polarization has been measured in the range from 35 to 275 keV average deuteron energy at a reaction angle of 45° Lab. The polarization is inferred from measurement of the left-right asymmetry induced in elastic scattering from helium at $\sim 120^{\circ}$ Lab. The polarimeter employed in the experiment consists of a helium gas scintillator detector and two neutron detectors. The three detectors are mounted on a rotatable cradle.

An automatic control system has been designed and constructed from TTL Logical integrated circuits, to enable the polarimeter to be rotated to the desired position for false asymmetry elimination. This system and a direct interface with a computer have helped to achieve a completely automatic data collection

system which has increased the running time to 24 hours per day.

The method of measurement utilises a pulse shape discrimination technique for gamma ray rejection and a coincidence technique for background reduction. Both real plus random and random coincidences between each side detector and the gas scintillator are recorded and used to gate four pulse height spectra of associated ^{4}He recoils in the gas scintillator.

The analysing power of the helium scattering is calculated from the phase shifts of Hoop and Barschall, and averaged over the geometry of the helium scintillator and the side detector cells.

The results of the measurements show that the value of the polarization ranges from -0.080 ± 0.011 at 35 keV average deuteron energy, to -0.150 ± 0.007 at 275 keV average deuteron energy. A comparison with the theoretical calculation based on an expression given by Boersma for the prediction of neutron polarization, has been made and shows very good agreement. The present results agree very well with recently published values of neutron polarization by Sikkema and Steendam and Lugo. The agreement is excellent since the three experimental techniques are very different, and all results agree with the theoretical calculation from the expression given by Boersma.

DECLARATION.

I hereby certify that this thesis has been composed by myself and that the experimental work reported herein has been performed completely by myself.

CONTENTS.

CHAPTER 4.

CHAPTER 5.

CHAPTER 1.

INTRODUCTION.

CHAPTER 1.

INTRODUCTION.

1.1 Introduction.

The $^{2}H(d,n)^{3}He$ reaction as a source of monoenergetic neutrons has been the subject of both experimental and theoretical investigations with the aim of obtaining more information about the nuclear forces involved in the reaction. Among the first studies on the available reaction cross section data was that of Konopinski and Teller [1]. By using the method of partial waves in their analysis, they were able to conclude that a large amount of spin-orbit coupling is involved in the reaction. By adopting this conclusion, Wolfenstein[2] in 1948 was able to predict that the outgoing neutrons should be polarized even if the incident deuterons as well as the target nuclei are unpolarized. Schwinger [3] had already pointed out in 1946 a method for detecting neutron polarization by elastically scattering them from light nuclei.

The first experiments which showed that the neutrons produced in a reaction are polarized, and that polarization can be detected by elastic scattering from light nuclei were reported in 1953. Huber and Baumgartner [4] and Ricamo [5,6], using carbon as polarization analyser, managed to observe the polarization of the neutrons produced from the D-D reaction.

Since then a large number of experiments have been performed to measure the polarization of neutrons from different reactions. A review article by Haeberli [7] in Fast Neutron Physics cites most of the important references up to 1962, while the tabulated review of Galloway [8] is an important source of more recent developments up to 1971.

The situation regarding the polarization of neutrons produced from the D-D reaction in the energy range above 500 keV is very confusing. Purser et al [9] have collected the polarization data reported for deuteron energies above 2 MeV and for reaction angles near 45° in the centre of mass system. In this region two polarization curves can be drawn through two groups of points representing the available neutron polarization values. These two curves indicate polarization values which differ by more than 20% over most of the energy range from 2 to 11 MeV and, in fact, differ in sign from about 4.5 to 8 MeV. No satisfactory explanation has been given for the large discrepancies. Recently, Galloway et al [10] have published a new set of data covering the energy range from 1.1 to 5.4 MeV using the same polarimeter as the present experiment. Their polarization values were discussed both in relation to previously reported discrepant values and to the Beiduck, Pruett and Konopinski [11] description of D-D reaction. As this energy region is beyond the limit of the present experiment, no further mention will be made of it here.

The situation regarding the polarization of neutrons in the energy range below 500 keV is not much clearer. In order to compare the data of the different experiments, a survey of the existing neutron polarization data published since 1957 for reaction angles near 45^{o} in the laboratory system, and in the relevant energy range is provided in section 1.4 which includes a brief description of the experimental techniques used in the measurements.

1.2 Measurement of Neutron Polarization.

A typical arrangement for a neutron polarization experiment is shown in figure 1. An unpolarized charged particle beam strikes an unpolarized target T. Let $\vec{P}_n(\theta_1)$ be the polarization of the neutrons emitted from the reaction at angle θ_1 , then we have the relation :

$$\vec{P}_n(\theta_1) = \vec{n}_1 P_n(\theta_1) \qquad 1.2.1$$

where $\vec{n}_1$ is a unit vector normal to the reaction plane.

$$\vec{n}_1 = \vec{k}_1 \times \vec{k}_2 \qquad 1.2.2$$

Here $\vec{k}_1$ is a unit vector in the direction of the incident charged particles and $\vec{k}_2$ is a unit vector in the direction of the emitted neutrons. The magnitude of $P_n(\theta_1)$ is defined as :

$$P_n(\theta_1) = \frac{N+ - N-}{N+ + N-} \qquad 1.2.3$$

Figure 1. Typical geometry for fast neutron polarization experiments showing the unit vectors $\vec{k}_1$, $\vec{k}_2$, $\vec{k}_2'$ in the direction of the incident charged particle, emitted neutron, and scattered neutron, respectively. $\vec{n}_1$ and $\vec{n}_2$ are unit axial vectors.

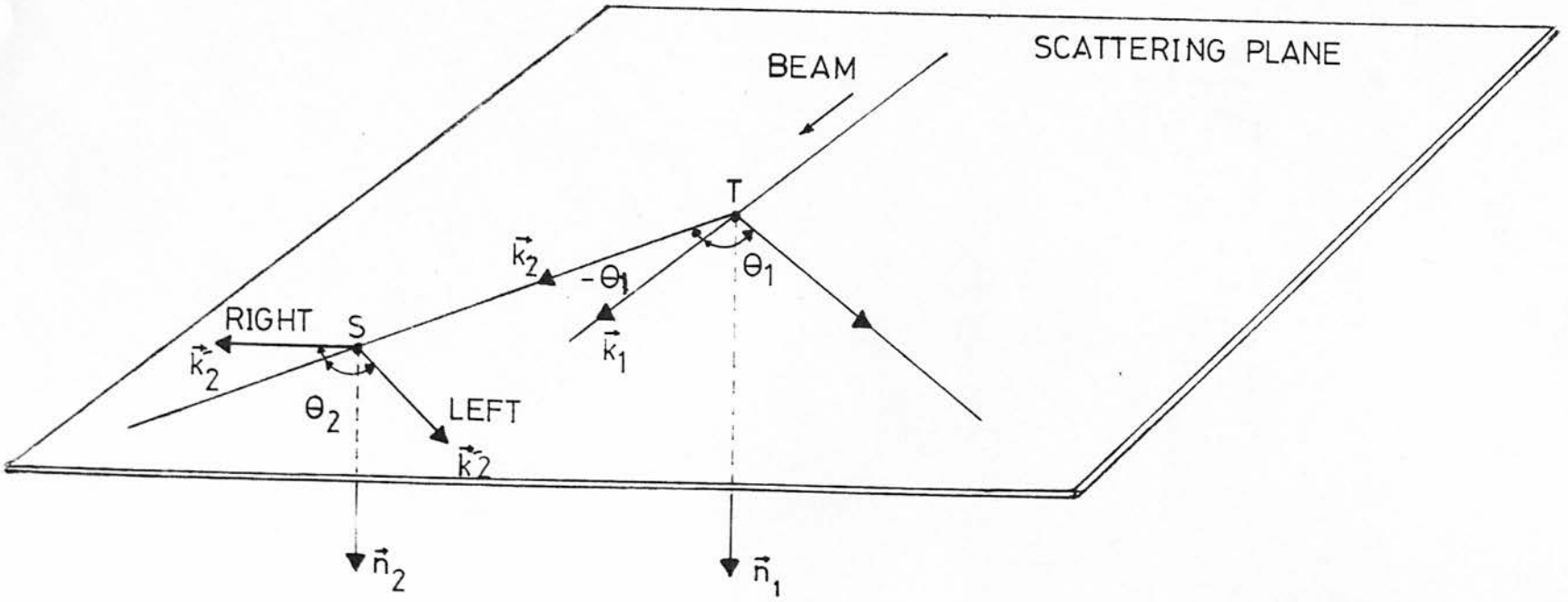
SCATTERING PLANE
BEAM
T
$\vec{k}_2$
$-\theta_1$
θ_1
$\vec{k}_1$
RIGHT
S
$\vec{k}_2$
θ_2
LEFT
$\vec{k}_2$
$\vec{n}_2$
$\vec{n}_1$

where N+ and N- are the numbers of neutrons with spin parallel and antiparallel to $\vec{n}_1$ respectively.

As conventional neutron detectors are not sensitive to the neutron spin orientation, a special method has to be employed to measure polarization. The most commonly used process to measure the neutron polarization is to scatter the neutrons elastically from a second target composed of spin zero nuclei.

Let $\vec{P}_s(\theta_2)$ be the polarization of an initially unpolarized neutron beam after scattering through an angle θ_2 from a target S of spin zero nuclei. Then we can write $\vec{P}_s(\theta_2)$ as :

$$\vec{P}_s(\theta_2) = \vec{n}_2 P_s(\theta_2) \qquad 1.2.4$$

where $\vec{n}_2$ is a unit vector normal to the scattering plane :

$$\vec{n}_2 = \vec{k}_2 \times \vec{k}_2' \qquad 1.2.5$$

Here $\vec{k}_2$ and $\vec{k}_2'$ are the unit vectors in the direction of the incident and scattered neutrons respectively.

Lepor [42] was the first to analyse the polarization of neutrons due to elastic scattering. It was shown that if the neutron beam from the first target is polarized, the differential cross section in the second reaction depends not only on the scattering angle θ_2 but also on the azimuthal angle ϕ . The angle ϕ is defined by the relation :

$$\cos \phi = \vec{n}_1 \cdot \vec{n}_2 \qquad 1.2.6$$

The differential cross section for the scattering of a polarized neutron beam is given by the formula :

$$\sigma(\theta_2, \phi) = \sigma_u(\theta_2)[1 + P_n(\theta_1) P_s(\theta_2) \cos \phi] \qquad 1.2.7$$

where $\sigma_u(\theta_2)$ is the differential cross section for the scattering of an unpolarized neutron beam at θ_2.

In figure 1, the position of the neutron detectors is not shown. Two neutron detectors are placed so as to measure at a fixed scattering angle θ_2, the flux I for azimuthal angles $\phi = 0$ and $\phi = \pi$. These two side detectors are arbitrarily distinguished by labelling them right $\phi = 0$ and left $\phi = \pi$. The intensities measured by these detectors can be simply related to the polarization product by the expression for the left - right asymmetry ε :

$$\varepsilon = \frac{\sigma(\theta_2, 0) - \sigma(\theta_2, \pi)}{\sigma(\theta_2, 0) + \sigma(\theta_2, \pi)} = \frac{I_R - I_L}{I_R + I_L} \qquad 1.2.8$$

From equations 1.2.7 and 1.2.8 we can derive the relation :

$$\varepsilon = P_n(\theta_1) P_s(\theta_2) = \frac{I_R - I_L}{I_R + I_L} \qquad 1.2.9$$

As can be seen from equation 1.2.9, a direct measurement of P_n or P_s is not possible. However, if $P_s(\theta_2)$ can be calculated by the method of Lepore experimental measurements of ε can be used to determine the required polarization $P_n(\theta_1)$. If the source polarization $P_n(\theta_1)$ is known, the reaction may be used

to measure the polarization in the scattering from other nuclei.

The experimental problems which arise in neutron polarization measurements are very similar to those involved in neutron angular distribution measurements. While polarization measurements are simpler in that the only relative intensities are required, the precision required of the asymmetry measurement is high. Also, since the determination of the polarization depends upon measurement of the asymmetry, it is important that any false or instrumental asymmetries should be eliminated.

1.3 False and Instrumental Asymmetries.

One major cause of false asymmetry is introduced when the detector position is changed from right to left. It is a relatively easy task to keep the scatterer to detector distance constant but to reproduce the angular setting is frequently rather difficult. If the cross section changes rapidly with angle, the angular setting is quite critical. One method which can be used to eliminate any false asymmetry due to the angular setting effect is to reverse the incident polarization vector $\vec{P}_n = \vec{n}_1 P_n$ (equation 1.2.1) instead of moving the detector from the right to the left. This is done by rotating the complete assembly of detectors, scatterer and shielding from θ_1 to $-\theta_1$ (figure 1), the rotation taking place about an axis which is

normal to the scattering plane and passes through the neutron - producing target. Errors in the position of the detectors average out provided the assembly is rotated exactly about the centre of the target. Another method which gives a similar effect can be achieved by reversing the vector $\vec{P}_s = \vec{n}_2 P_s$ (equation 1.2.4). This is done by accurately rotating the assembly of scatterer and detectors about the axis defined by the centres of the target and the scatterer.

If two detectors are used simultaneously, the data accumulation time can be reduced by a factor of two and by rotation any difference in their detection efficiencies will be cancelled.

Equation (1.2.9) gives the neutron polarization in terms of the scattering asymmetry and the scatterer analysing power on the assumption of equal detection efficiency for the right and the left side detector. In practice the right and the left detection efficiencies may be slightly different because detection volumes, detection thresholds and electronic timing may all be unequal. The effects of this instrumental asymmetry may be cancelled by a suitable experimental method as explained below.

Equation (1.2.7) may be rewritten, modified to include the more general case and using a more standard notation to give the number of scattered neutrons to the right as :

$$I_R \propto I d_R \sigma(\theta) [\, 1 + P_n P_s(\theta) \,] \qquad 1.3.1$$

and the number of scattered neutrons to the left as :

$$I_L \propto I d_L \sigma(\theta) [\, 1 - P_n P_s(\theta) \,] \qquad 1.3.2$$

where d_R and d_L are detection efficiencies of the right and left side detectors, respectively. I is the number of neutrons incident on the scatterer.

Using equations (1.2.9) , (1.3.1) and (1.3.2) we can write :

$$P_n P_s(\theta) = \frac{I_R - I_L(d_R/d_L)}{I_R + I_L(d_R/d_L)} \qquad 1.3.3$$

The method used in this work to eliminate d_R/d_L was to interchange the right and left side detectors and make new polarization measurements. Let quantities referring to the first run be subscripted 1, and to the second interchanged run be subscripted 2. Equation (1.3.3) becomes :

$$P_n P_s(\theta) = \frac{I_{R1} - I_{L1}(d_{R1}/d_{L1})}{I_{R1} + I_{L1}(d_{R1}/d_{L1})} \qquad 1.3.4$$

for the first run, and

$$P_n P_s(\theta) = \frac{I_{R2} - I_{L2}(d_{R2}/d_{L2})}{I_{R2} + I_{L2}(d_{R2}/d_{L2})} \qquad 1.3.5$$

for the second run.

But :

$$d_{R2} / d_{L2} = d_{L1} / d_{R1}$$

since the only difference between the runs is an interchange of right and left side detectors and this interchange is assumed not to affect the detection efficiencies.

By using equations (1.3.3), (1.3.4) and (1.3.5) we can get :

$$P_n P_s(\theta) = \frac{A - 1}{A + 1} \qquad (1.3.6)$$

where :

$$A = \sqrt{\frac{I_{R1}\, I_{R2}}{I_{L1}\, I_{L2}}}$$

In practice, the polarization measurements were made with frequent interchange between the first and second positions to eliminate any effects from long term changes in the detection efficiency ratio.

Another method of eliminating instrumental asymmetry is to rotate the neutron polarization through 180° effectively changing the sign of P_n. This was proposed and first used by Hillman, Stafford and Whitehead [63]. The direction of polarization $P_n(\theta)$ was rotated by means of a magnetic field in the region between the target and the polarization analyser. The field was along the direction of motion of the neutrons, and was produced by an air core solenoid through which the neutrons passed. The solenoid current was chosen such that the

neutron spin precessed through 90°, so that depending on the sense of current flow, the polarization vector became parallel or opposite to the vector $\vec{n}_1 \times \vec{k}_2$ (figure 1). As a result, the scattering plane was placed perpendicular to the reaction plane. The asymmetry was measured by reversing the solenoid current, the counters remaining fixed. This eliminates all instrumental asymmetry, provided the accelerator beam and the detectors are properly shielded from the magnetic field.

In the present experiment two interchangeable neutron detectors were used instead of the magnetic field method. Equation 1.3.6 was used in the analysis of the present data, to eliminate the effect of any difference in the detection efficiency of the two neutron detectors.

1.4 Polarization of $D(d,n)^3He$ Neutrons in the Energy Range Below 500 keV.

Because of the discrepancies in the reported polarization values, a brief description of all the previous work for deuteron energies below 500 keV is presented in this section. Before this is done, however, it should be pointed out that, in order to determine the polarization of a neutron beam, scattering from a suitable target must be employed. All of the measurements described below utilised scattering from either helium or carbon as polarization analyser. In every case the analysing power was calculated from either n - ^4He or n - ^{12}C scattering phase

shifts, respectively. For the neutron energies involved in the $D(d,n)^3He$ studies, there exist two angular regions where the analysing power is large, i.e., forward scattering angles near $\theta_2 = 65^\circ$ and backscattering angles near $\theta_2 = 135^\circ$ in the centre of mass system. Each investigation was carried out using scattering angles near either one or the other of these angles. Fig.(2) shows the angular distribution in the centre of mass system, of the analysing power of ^4He calculated using the phase shifts of Hoop and Barschall [12] for 3 MeV neutron energy. Fig.(3) and fig.(4) show the angular distribution in the centre of mass system of the analysing power of ^{12}C calculated using the phase shifts of Wills et al [13] for 3.05 MeV and Meier et al [19] for 3.10 MeV neutron energy, respectively.

The earliest reported polarization measurements for this reaction below 500 keV were performed by Pasma [14]. For deuteron energies ranging from 200 to 500 keV, he found that for reaction angle $\theta_1 = 47^\circ$ in the laboratory system the neutron polarization increased from 6% at 200 keV to about 9.5% at 500 keV. He used ^4He as polarization analyser and recorded the scattered neutrons in coincidence with the helium recoil nuclei. A thin heavy ice target of 50 keV thickness was used in the experiment. The analysing power of helium was obtained from the calculation of van Wageningen [16] which was based on the phase shift data of Seagrave [17]. Due to a background effect in the measurements, which was not taken into account in the analysis,

Figure 2. Angular dependence of the analysing power of ^{4}He in the centre of mass system for 3.0 MeV neutrons as calculated using the phase shifts of Hoop and Barschall [12].

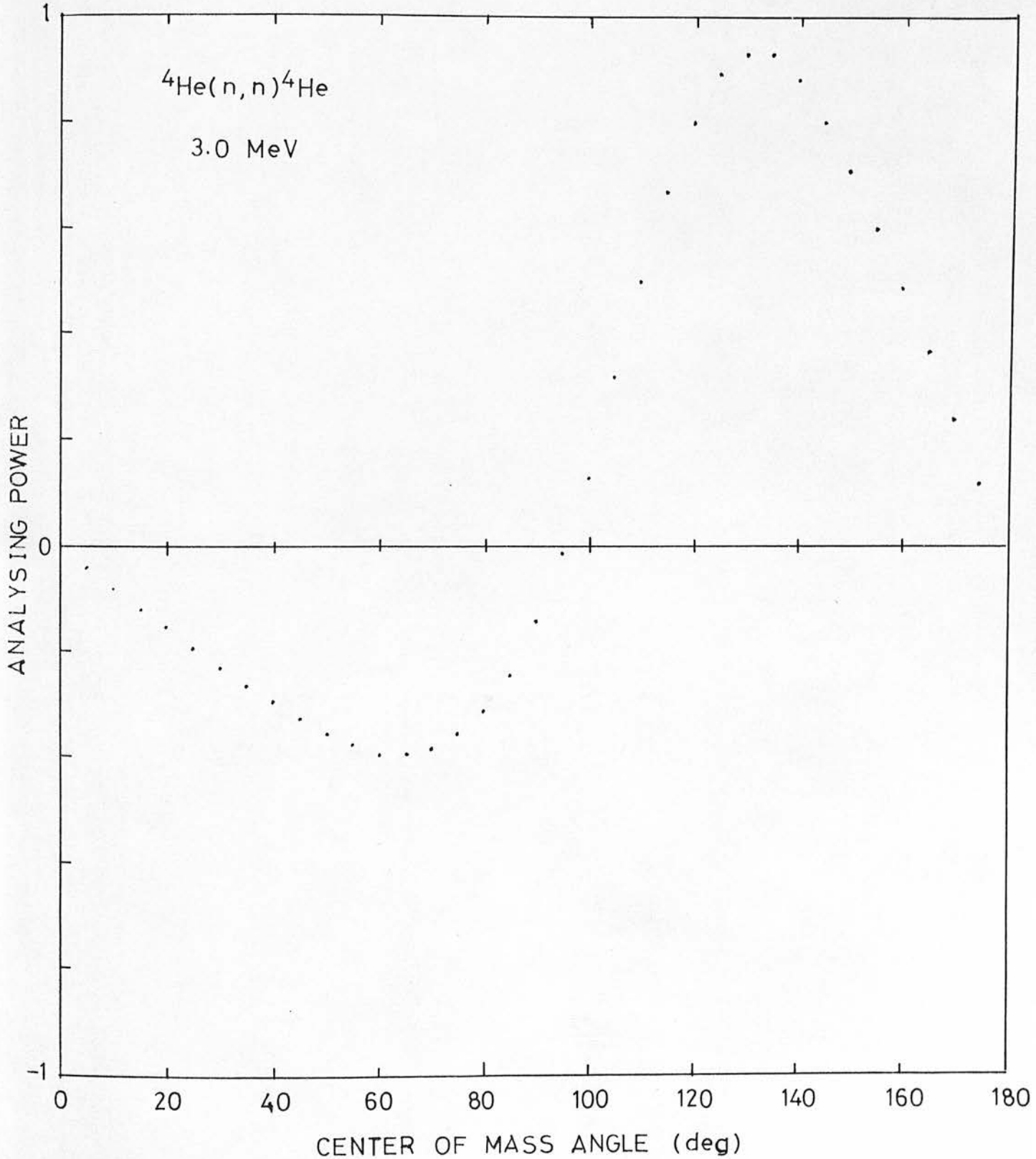
^{4}He(n, n)^{4}He
3.0 MeV
ANALYSING POWER
1
0
-1
0
20
40
60
80
100
120
140
160
180
CENTER OF MASS ANGLE (deg)

Figure 3. Angular dependence of the analysing power of ^{12}C in the centre of mass system for 3.05 MeV neutrons as calculated using the phase shifts of Wills et al [13].

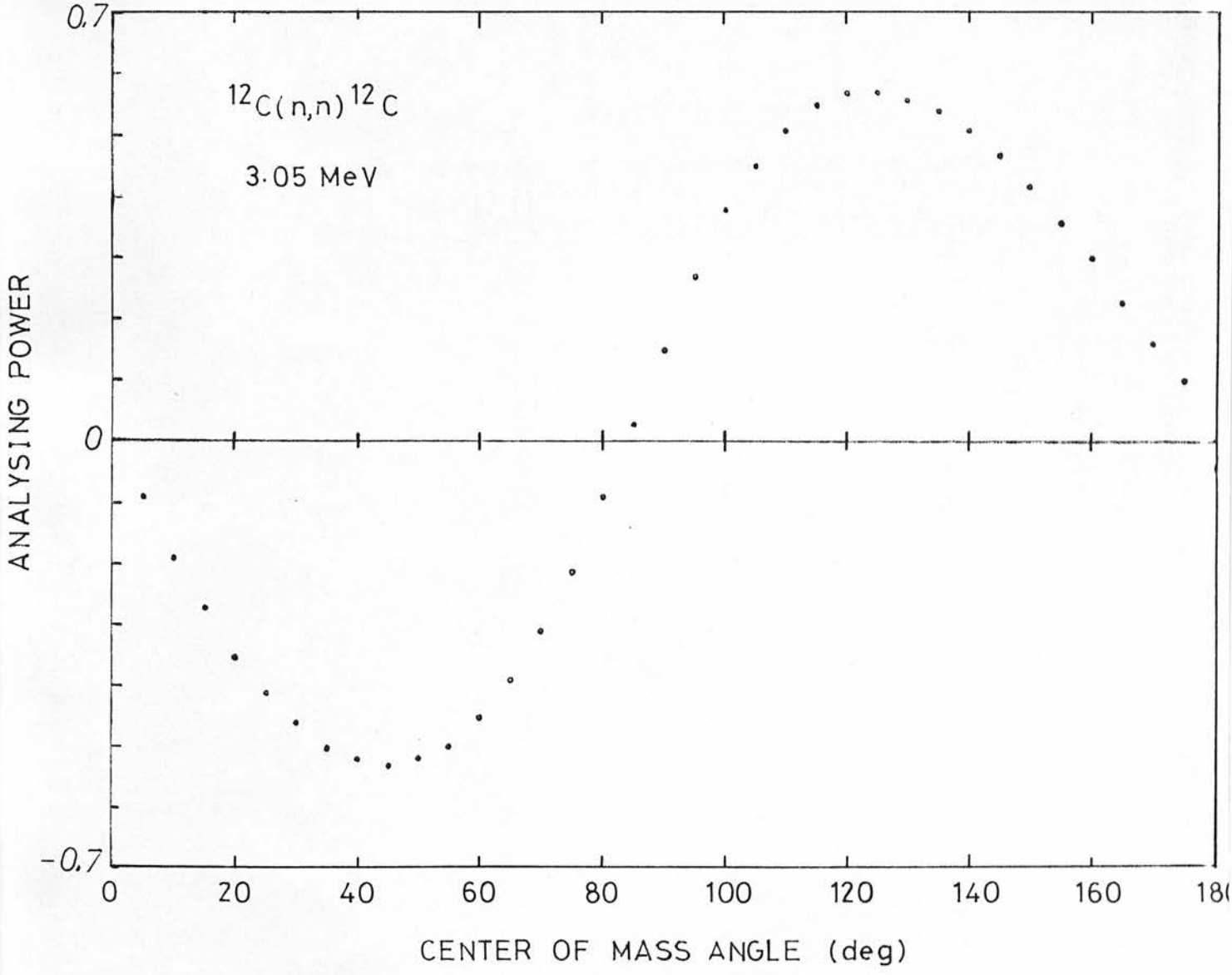
0.7
0
-0.7
$^{12}C(n,n)^{12}C$
3.05 MeV
ANALYSING POWER
0
20
40
60
80
100
120
140
160
CENTER OF MASS ANGLE (deg)

Figure 4. Angular dependence of the analysing power of ^{12}C in the centre of mass system for 3.10 MeV neutrons as calculated using the phase shifts of Meier et al [19].

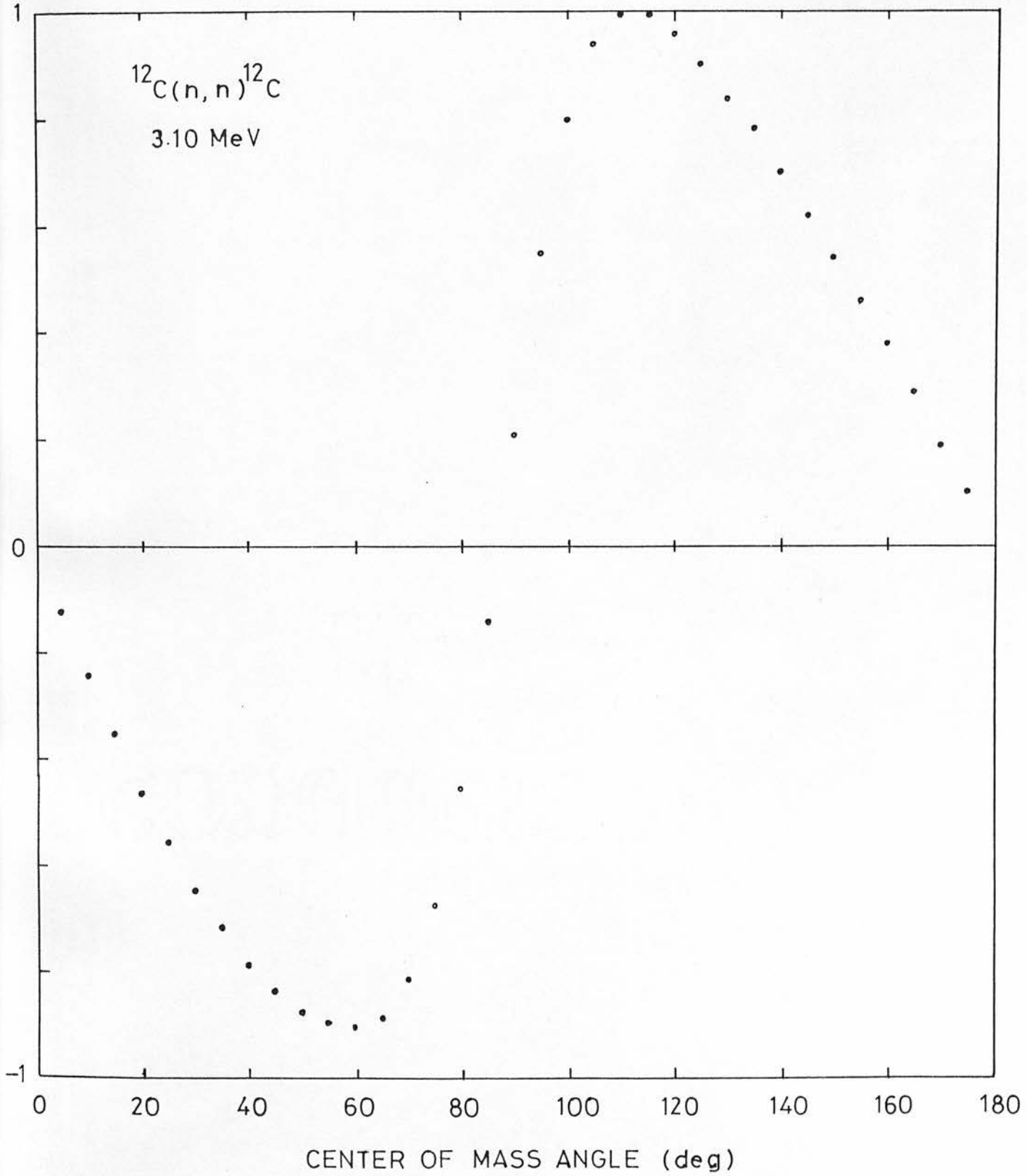
$^{12}C(n,n)^{12}C$
3.10 MeV
1
0
−1
0
20
40
60
80
100
120
140
160
180
CENTER OF MASS ANGLE (deg)

Boersma [15] recomputed these results, and used phase shift data of Austin et al [20] to calculate the analysing power. These new values are represented in fig.(5).

Kane [18] reported an experiment for an average deuteron energy of 93 keV and emission angles of 43° and 53° Lab. His results showed that the polarization values at these angles are -10.6% ± 2.3% and -9.5% ± 3.7% respectively. He has used scattering from carbon for asymmetry measurements. A thick drive-in aluminium target was used in the experiment. One detector was employed in the left-right asymmetry evaluation. The analysing power of carbon was calculated using the phase shifts data of Meier et al [19].

Boersma et al [15] performed an experiment to measure the polarization of D-D reaction neutrons for deuteron energies of 375 keV at ten different angles between 0° and 80° (Lab.) and for deuteron energies of 275 keV and 450 keV at 50° (Lab.). They used a target of 50 keV thickness. ^{4}He was used as polarization analyser and the scattered neutrons were recorded in coincidence with the helium recoil nuclei. A pulse shape discrimination technique was used to reject gamma rays. In order to cancel the instrumental asymmetry the neutrons were allowed to pass through a solenoid placed between the target and the scatterer, to turn their spins 90° to the right or to the left, according to the direction of the current through the solenoid. Therefore asymmetry measurements were determined in the plane

Figure 5. Polarization of neutrons emitted at a laboratory angle of about $45^{\circ} \pm 5^{\circ}$ from the $^{2}H(d,n)^{3}He$ reaction as a function of average deuteron energy. Key in table 1.

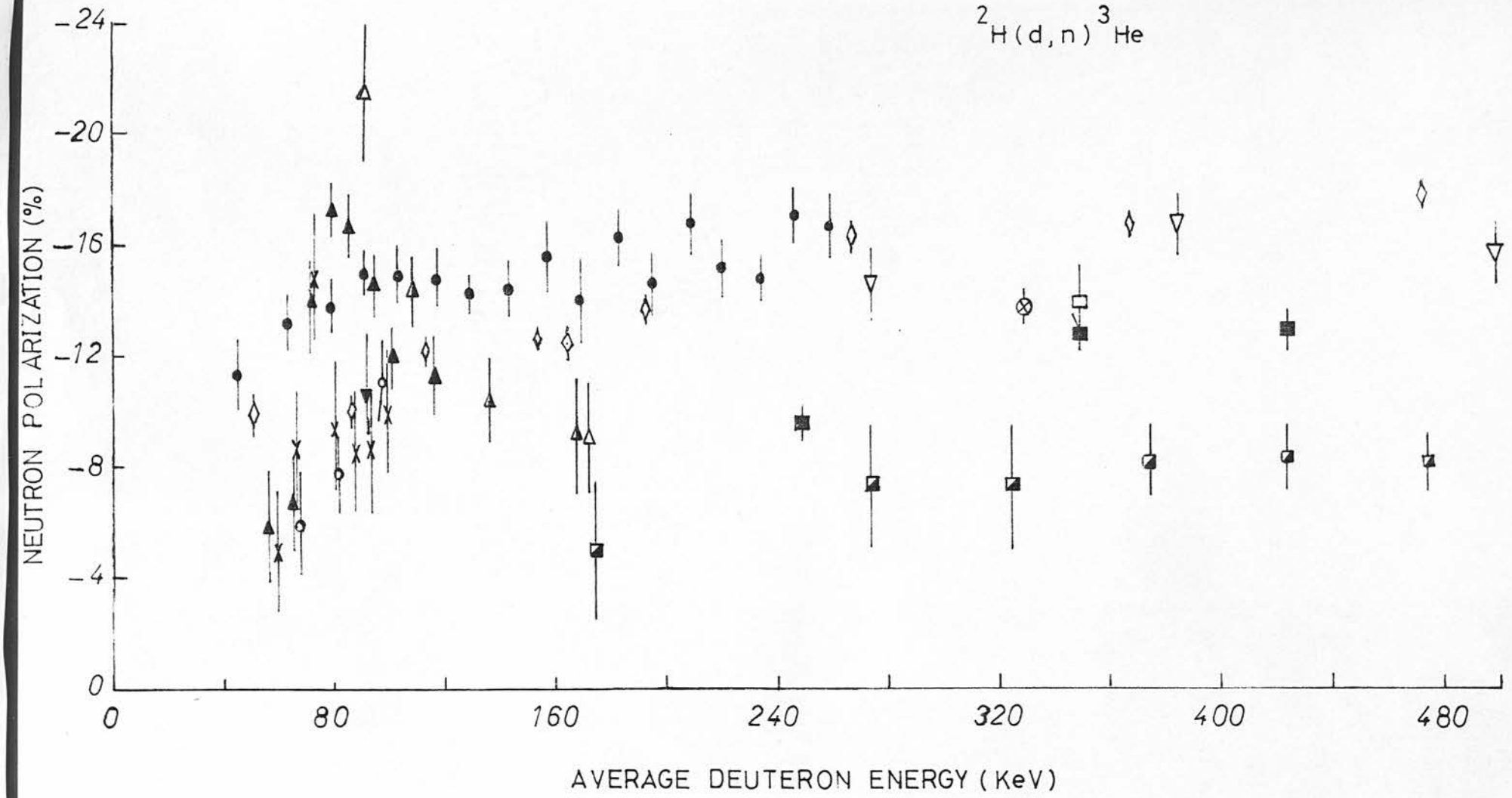
$^{2}H(d,n)^{3}He$
NEUTRON POLARIZATION (%)
-24
-20
-16
-12
-8
-4
0
0
80
160
240
320
400
480
AVERAGE DEUTERON ENERGY (KeV)

Table 1. Key to figure 1.

Symbol	Reference	Angles	Analyser
◪	Pasma [14]	47° Lab	^{4}He
▽	Kane [18]	43° Lab	^{12}C
○	Rogers and Bond [21]	45° Lab	^{12}C
△	Hansgen et al [22]	50° Lab	^{12}C
■	Boersma et al [15]	53°, 45.8°, 51° Lab	^{4}He
●	Behof et al [28]	47° Lab	^{4}He
□	Mulder [31]	46.5° Lab	^{4}He
-	Stoppenhagen & Finlay [32]	50° Lab	^{12}C
X	Thomas & Hofmann [33]	50° Lab	^{4}He
△	Prade & Csikai [36]	49°-54° Lab	^{4}He
▲	Prade & Csikai [36]	49°-54° Lab	^{12}C
▽	Davie & Galloway [37]	46° Lab	^{4}He
⊛	Maayouf & Galloway [38]	47°-50° Lab	Pb, U, & ^{4}He
◇	Sikkema & Steendam [55]	47°-50° Lab	^{4}He

normal to the reaction plane. The analysing power of ^{4}He was calculated using the phase shifts of Austin et al [20]. Their polarization values which were measured at approximately 50° (Lab.) are represented in figure 5.

Rogers and Bond [21] have measured the polarization of neutrons emitted from the D-D reaction at an angle of 45° (Lab.) and average deuteron energies of 99 keV, 81.5 keV and 67.5 keV. A thick heavy ice target was used and carbon was used as a polarization analyser. The phase shift data of Meier et al [19] were used in the carbon analysing power calculation. An un - analysed deuteron beam which contained both atomic and the lower energy molecular components was used in their experiment. The average deuteron energies were calculated in terms of the stopping power of the target material and the energy dependance of the D(d,n)^{3}He cross section.

Hansgen et al [22] performed an experiment to measure the neutron polarization at an angle of 50° (Lab.) for eight average deuteron energies from 57.3 keV to 116.8 keV using a thick heavy ice target. Carbon was used as polarization analyser. Two detectors were used to measure the left - right asymmetry of the scattered neutrons. The phase shifts of both Meier et al [19] and Wills et al [13] were used to calculate the analysing power of carbon. The polarization values obtained by using the phase shifts of Wills et al [13] are represented in fig. 5.

Their results indicated a resonance-like behaviour with peak polarization at an average deuteron energy of 80 keV and a width of approximately 30 keV. The peak polarization was attributed to a virtual level in the ^{4}He compound nucleus. Such a level if present would be at nearly 24 MeV excitation and would be very narrow compared to previously observed excited states in ^{4}He [23,24]. In 1969, Boersma [27] first suggested that the resonance was due to the levels at 7.50 and 7.55 MeV in ^{13}C [25,26] and not due to a level in ^{4}He compound nucleus. Hansgen and Nitzche [48] in 1971, reported the results of a new experiment which was performed to measure the left-right asymmetry of D - D neutrons by scattering from carbon in the deuteron energy range from 150 to 420 keV. The polarization data of Behof et al [28] for the D - D neutrons was used to obtain the analysing power of carbon. From the results they confirmed the influence of the two levels (7.50 and 7.55 MeV) in ^{13}C on the analysing power of carbon in this energy region.

It appears that unexplained anomalies exist in this energy region and these are not associated with the properties of a particular polarization analyser, as will be shown in section 1.5.

Behof et al [28] performed an experiment to measure the polarization of neutrons produced from the D - D reaction at deuteron incident energies between 60 and 380 keV in 20 keV intervals. The measurements were performed at a neutron emission angle of 47° (Lab). The angular distribution of polarization was

determined at 340 keV incident energy. A thick heavy ice target was used in the experiment. ^{4}He was employed as a polarization analyser and as a detector. The neutrons scattered to two interchangeable liquid scintillator neutron detectors placed to the left and to the right of the gas scintillator detector, were recorded in coincidence with the corresponding helium recoil nuclei. In the electronic circuit employed [30] gamma rays were rejected by measuring the flight time of neutrons and gamma rays over the distance between the gas scintillator and the two liquid scintillators. The analysing power of helium was calculated using the phase shift data of Dodder and Gammel [29] which has been published by Seagrave [17].

To compare the data of Behof et al [28] with the other published results, their polarization values are plotted in fig. 5 against the weighted mean energies as calculated instead of the reported incident deuteron energies. No sign of the peak polarization observed by Hansgen et al [22] appears in these results, and the polarization ranges between - 0.14 and - 0.16 from 280 keV down to 80 keV and then drops gradually with energy.

One polarization value was measured by Mulder [31]. A cloud chamber filled with helium was used as polarization analyser in the experiment. At a reaction angle of 46.5° Lab and a mean deuteron energy of 350 keV a polarization value of (- 13.8 ± 1.4)% was obtained. This value is in good agreement with that of

Boersma et al [15] at the same deuteron energy. Thin heavy ice was used as a target with a thickness of 50 keV. The analysing power of helium was calculated from the phase shifts data of Austin et al [20].

Stoppenhagen and Finlay [32] have measured the neutron polarization in the region from 80 to 120 keV incident deuteron energy at a neutron emission angle of 50° Lab. A thick titanium deuterium target was used in the experiment. An associated particle time-of-flight spectrometer was employed to reduce the background effect. Two neutron detectors were used to measure the right-left asymmetry and a spin-precession magnet was used to eliminate any false asymmetry. The polarization analyser was carbon and the analysing power was calculated from the phase shifts of Wills et al [13]. The polarization values were reported to be ranging between - 11% and - 15% and in good agreement with the data of Behof et al [28] in the same energy region. The disagreement between these results and those of Hansgen et al [22] is significant since both experiments have used carbon as polarization analyser and no peak in the polarization was observed in this measurement. This adds more confusion to the present situation of the neutron polarization in this energy region.

Thomas and Hofmann [33] performed an experiment to measure the neutron polarization in the energy region from 80 to 140 keV at a neutron emission angle of 50° Lab. Their polarimeter

consisted of a helium gas sample as a scintillation detector and as a polarization analyser, and two plastic scintillation neutron detectors. The scattered neutrons were detected in coincidence with the helium recoil nuclei. A titanium - deuterium target of 400 $\mu g/cm^2$ thickness was used in the experiment. The analysing power of helium was calculated using the phase shift data of Hoop and Barschall [12]. A peak polarization of $(-14.9 \pm 2.3)\%$ was found at an average deuteron energy of 74 keV with a width of 10 keV. This resonance-like behaviour was attributed to an excited level in ^{4}He at nearly 24 MeV as explained by Fick [34]. But these results were criticised by several authors [27,35] since the width of the peak is much narrower (10 keV) than the target thickness used (50 to 80 keV).

Prade and Csikai [36] have measured the neutron polarization for five average deuteron energies between 92 and 173 keV at a reaction angle of 50° Lab. A thick titanium - deuterium target was employed. Some measurements were performed with a cloud chamber filled with helium as a detector and polarization analyser, and others with an associated - particle method where the neutrons scattered by carbon were detected by one side detector in coincidence with ^{3}He nuclei. The analysing power of helium was calculated using the phase shift data of Austin et al [20] and that of carbon using the phase shift data of both Meier et al [19] and Wills et al [13]. The polarization values obtained by using the phase shifts of Wills et al [13] are represented in fig. 5. These values show a rapid decrease in the

region from 92 to 173 keV. The maximum polarization was obtained at an average deuteron energy of 92 keV with helium serving as polarization analyser.

Davie and Galloway [37] reported on D - D neutron polarization measurements in the deuteron energy range from 300 to 900 keV at a reaction angle of 46° Lab. The polarimeter used in the measurements is the same one used by the author for preliminary measurements and described in chapter 2. A thin Ti - D target was used. The analysing power of helium was calculated using the phase shift data of Austin et al [20]. The polarization values below 500 keV are represented in fig. 5. These results show good agreement with those of Behof et al [28], Mulder [31] and the recent results of Sikkema and Steendam [55].

Maayouf and Galloway [38] reported on measurements at a mean deuteron energy of 330 keV and reaction angle of 47° and 50° Lab. Two techniques were used in the measurements; small angle scattering [39] from Pb and U and scattering from helium. A thin titanium - deuterium target was employed in the experiment. The phase shift data of Satchler et al [40] was used in the calculation of the analysing power of helium. The helium polarimeter employed in the experiment is the same as used by Davie and Galloway [41] and used initially by the author in the present experiment. An excellent agreement between the results of the two experiments was obtained (13.7 ± 1.5)% using small angle scattering and (13.7 ± 0.7)% using scattering from helium ,

and the value agrees with those of Mulder [31] and Boersma et al [15] at 350 keV.

Sikkema and Steendam [55] reported recently while the present work was in progress a new set of neutron polarization results covering the energy range from 50 to 700 keV of average deuteron energy at a neutron emission angle of 46° - 50° in the laboratory system. A multiwire proportional chamber filled with helium, which was used as polarization analyser, was employed as a new type of helium recoil polarimeter. The asymmetry was measured by recording the number of recoil helium nuclei scattered at several scattering angles simultaneously, into equal azimuthal intervals to the left and to the right of the incident neutron beam. The polarization value was obtained by fitting the function $P_n P_{He}$ to the measured asymmetry. The analysing power P_{He} was obtained using the phase shift data of Hoop and Barschall [12]. The measurements were performed using Ti - D target of 220μg/cm^2 thickness. Their results show a monotonic increase of polarization values with increasing deuteron energy. Their results were compared with the theoretical prediction of polarization as given by Blin-Stoyle [58] and Boersma [27] and show reasonable agreement in the energy range from 50 to 350 keV, Their results in this energy range are represented in fig. 5.

1.5 The Resonance, the Ratio (A_2/A_0) and the Predicted $P_n(\theta)$.

The resonance-like behaviour observed in some experiments for both the $^2H(d,n)^3He$ and the $^2H(d,p)^3H$ reactions at a bombarding energy of about 100 keV is still experimentally rather confusing. The neutron polarization measurements of Hansgen et al [22], Thomas and Hofmann [33] and Prade and Csikai[36] and the angular distribution measurements of the D - D reaction products of Franz and Fick [44] and Ying et al [45] support the existence of such a resonance. In contrast, the neutron polarization measurements of Behof et al [28], Stoppenhagen and Finlay [32] and the recent measurements of Sikkema and Steendam[55] and the angular distribution measurements of the D - D reaction products of Theus et al [46], Guckel and Fick [56] Ad'Yasevich et al [57] and Pospiech et al [47] do not show such resonance.

Hansgen et al [22] first suggested an explanation of their polarization peak in terms of a virtual level in the ^4He compound nucleus. Then, Boersma [27] and Hansgen and Nitzsche [48] suggested that the two levels at 7.50 and 7.55 MeV in ^{13}C might be the cause of the resonance, since carbon was used as polarization analyser in the experiment of Hansgen et al [22]. But lately, Knox et al [49], using an experiment somewhat similar to that of Hansgen et al [22] demonstrated that the two levels in ^{13}C are not responsible for the existence of such a resonance at an incident deuteron energy of 100 keV. So the question regarding the resonance observed by Hansgen et al [22] is still unsolved.

The peak polarization observed by Thomas and Hofmann[33] is doubtful because the width of the peak is considerably less than the energy spread of the deuterons reacting in the target.

The rapid variation of polarization with energy reported by Prade and Csikai [36], where carbon and helium were used as polarization analysers, is still unexplained.

The proton angular distribution measurements of Franz and Fick [44] using a polarized deuteron beam exhibit a resonance at 105 keV deuteron energy. Their results have been corrected by Pospiech et al [47] for target thickness, multiple scattering and target contamination effects. The new corrected data show a resonance behaviour around 60 keV deuteron energy.

Ying et al [45] have measured the angular distribution of neutrons and protons from the D - D reaction in the energy range from 300 to 700 keV. In order to explain the difference, they found in the anisotropy coefficients of the $^{2}H(d,n)^{3}He$ and the $^{2}H(d,p)^{3}H$ reactions, they have to assume a resonance in the ^{4}He compound nucleus near 100 keV above the deuteron threshold.

The anisotropy coefficient A_n can be obtained by fitting the expression, used to describe the angular distribution of the D - D reaction products which is an expansion in terms of even Legendre polynomials i.e. :

$$\sigma(\theta) = \sum_{n=0} A_{2n} P_{2n}(\cos\theta) \qquad (1.5.1)$$

to the measured data. The expression can alternatively be written by means of the anisotropy coefficients A and B as :

$$\sigma(\theta) = \sigma(90°)\,(1 + A\cos^2\theta + B\cos^4\theta + \cdots\cdots)$$

For incident deuteron energies below 500 keV, terms higher than $\cos^4\theta$ can be neglected. The relation between A_n and A is given by Boersma [27] in his analysis of the D - D reaction for deuteron energies below 200 keV as :

$$A_2 / A_o = \frac{2A}{3 + A} \qquad (1.5.2)$$

This relation has been used to calculate the ratio A_2/A_o from A values obtained from the angular distribution of the $^2H(d,n)^3He$ reaction products as measured by Booth et al [50], Preston et al [52], Eliot et al [51] and Fuller et al [53]. The anisotropy coefficient ratio A_2/A_o is plotted in fig. 6 versus the average deuteron energy as given by several authors. Several results have not been included in the figure due to the poor statistical accuracy or because they are far away from the general trend of the other data points. The solid curve and the dashed curve have been obtained from the expression given by Boersma [27] for energies below 200 keV as :

$$A_2 / A_0 = \beta \frac{E + 0{\cdot}05}{1 + \alpha\,(E + 0{\cdot}05)} \qquad (1.5.3)$$

where E is the deuteron energy and the quantities α and β are constants which were fitted to the previous existing experiments and take the mean values of 1.9 and 4.2 as given by Boersma [27] (solid curve) and 3.2 and 4.9 as given by Fick and Weiss [54]

Figure 6. The anisotropy coefficient A_2/A_o for $^2H(d,n)^3He$ reaction as a function of the average deuteron energy.

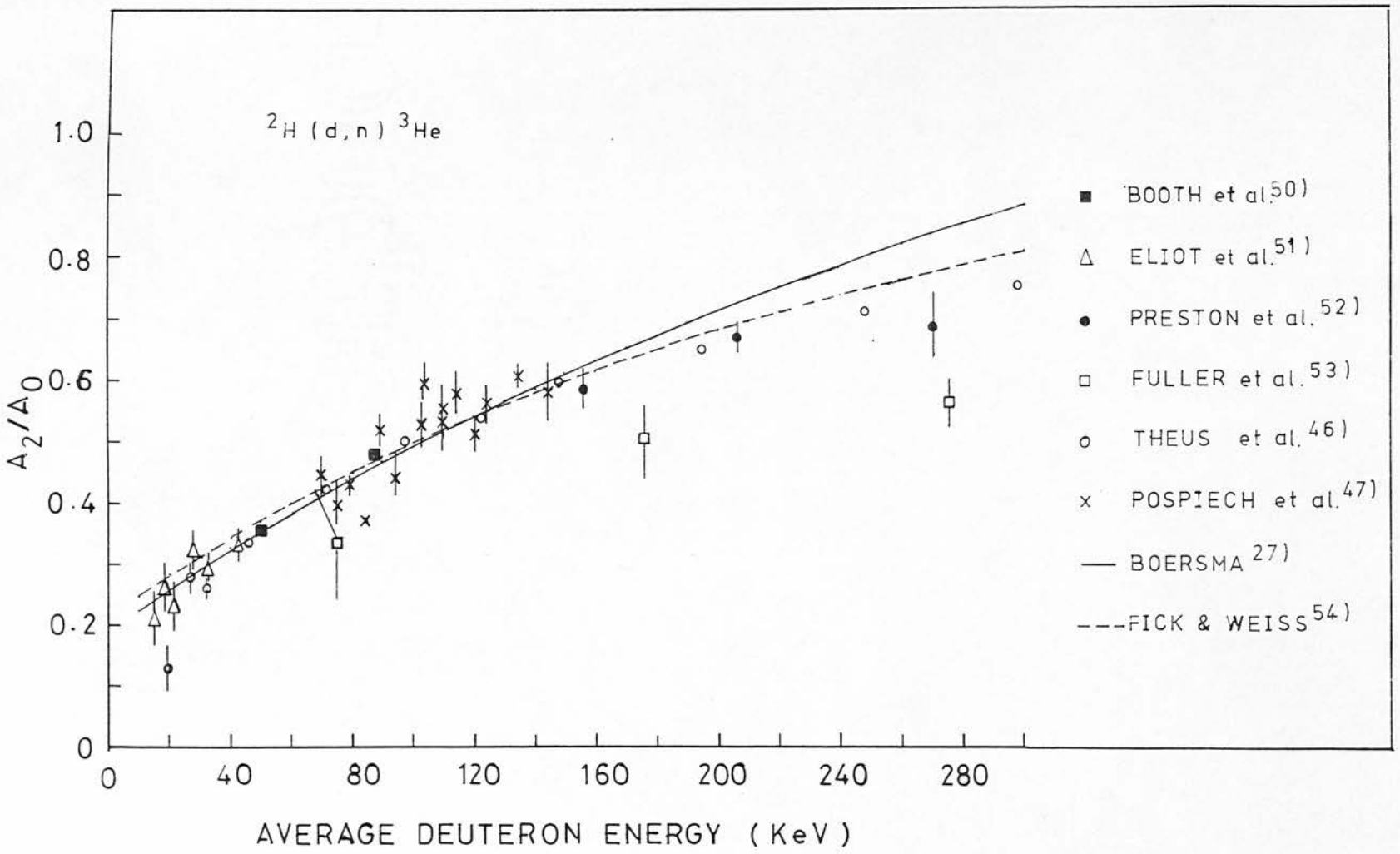
^2H (d, n) ^3He
1.0
0.8
0.6
0.4
0.2
0
A_2/A_0
0
40
80
120
160
200
240
280
AVERAGE DEUTERON ENERGY (KeV)
BOOTH et al.[50]
ELIOT et al.[51]
PRESTON et al.[52]
FULLER et al.[53]
THEUS et al.[46]
POSPIECH et al.[47]
BOERSMA [27]
FICK & WEISS[54]

(dashed curve), respectively. It is very clear from fig. 6 that the anisotropy coefficient ratio A_2/A_o obtained from the angular distribution of the $^2H(d,n)^3He$ reaction does not exhibit a resonance in this energy range. Furthermore, the angular distribution measurements of the $^2H(d,p)^3H$ reaction of Pospiech et al [47], Theus et al [46], Guckel and Fick [56] and Ad'Yasevich [57] do not show such a resonance.

From the theoretical point of view, several authors have extended the theoretical analysis of the D - D reaction by Konopinski and Teller [1] and Beiduck, Pruett and Konopinski [11], to include the polarization of the outgoing nucleon. Fierz [43], Blin-Stoyle [58], Cini [59] and Rook and Goldfarb [60] gave theoretical expressions for the angular distribution of polarization. A general expression for polarization $P(\theta, E)$ when both the bombarding particles and the target nuclei are unpolarized was given as :

$$P(\theta, E) = \frac{1}{\sigma(\theta,E)} \sum_{n=0} a_{2n} P'_{2n} (\cos\theta) \qquad (1.5.4)$$

where P'_{2n} is the associated Legendre polynomial. For incident energies below 300 keV, Blin-Stoyle obtained the expression :

$$P(\theta, E) = c \frac{A \sin 2\theta}{1 + A\cos^2\theta} \qquad (1.5.5)$$

which is seen to be the n = 1 term from expression (1.5.4). Here θ is the nucleon emission angle in the centre of mass

system, c is an energy independent factor and $\sigma(\theta, E) \propto 1 + A \cos^2\theta$ where A is the anisotropy coefficient obtained from the angular distribution measurements. This expression has been used in the early measurements of neutron polarization, for comparison with the experimental results.

In 1969, Boersma [27] analysed the existing data on the D - D reaction and criticised the assumption of Konopinski and Teller [1] and gave an alternative approach. As he assumed that only S and P waves are effective in the reaction, his approach can be applied only for deuteron energies of a few hundred keV. Expressions (1.5.1) and (1.5.4) for the differential cross section and polarization respectively were used in his analysis. So only the n = 1 term can be applied i.e. :

$$\sigma(\theta, E) = A_0 + A_2 P_2(\cos\theta) \qquad (1.5.6)$$

$$P(\theta, E) = \frac{1}{\sigma(\theta, E)} a_2 P_2'(\cos\theta) \qquad (1.5.7)$$

As the coefficients A_2 and a_2 differ by an energy independent factor [1,27], then $P(\theta, E)$ can be rewritten :

$$\begin{aligned} P(\theta, E) &= \frac{a_2 P_2'(\cos\theta)}{A_0 + A_2 P_2(\cos\theta)} \\ &= c \frac{A_2 P_2'(\cos\theta)}{A_0 + A_2 P_2(\cos\theta)} \\ &= c \frac{(A_2/A_0)[P_2'(\cos\theta)]}{1 + (A_2/A_0)[P_2(\cos\theta)]} \end{aligned} \qquad (1.5.8)$$

where c is a constant which can be obtained by fitting the measured polarization values to the expression (1.5.8). Expression (1.5.8) is similar to that given by Blin-Stoyle in equation (1.5.5) except that the anisotropy coefficient A is replaced by A_2/A_0. The relation between the coefficient A and A_2/A_0 is given, by Boersma [27] in the low energy range, in equation (1.5.2).

The dependence of A_2/A_0 on deuteron energy is given in equation (1.5.3) and the dependence of $P(\theta, E)$ on energy can be written, by using equation (1.5.8) as :

$$P(\theta, E) = c \frac{(0{\cdot}05 + E_d) P_2^1(\cos\theta)}{1 + \alpha (0{\cdot}05 + E_d) + \beta (0{\cdot}05 + E_d) P_2(\cos\theta)} \qquad (1.5.9)$$

This expression agrees with Guckel and Fick's [56] expression but it differs from that obtained by Blin-Stoyle [58]. Boersma [27] has emphasised the fact that both A_2/A_0 and $P(\theta, E)$ do not vanish at zero deuteron energy. This fact was already noted by Konopinski and Teller [1] in regard to A_2/A_0.

The comparison of the existing polarization data with the theoretical expressions (1.5.8) and (1.5.9), even if we normalise to the data of Boersma et al [15] at higher energy, was found difficult since several experiments exhibit a resonance near 100 keV and the measurements of Behof et al [28] were done with thick targets and show disagreement with the theory in the low energy range.

1.6 Conclusion.

In the present measurement of polarization of neutrons emitted from $^{2}H(d,n)^{3}He$ reaction in the low energy range, several facts have been taken into account. These facts are summarized as follows:

1. The large discrepancies in the existing neutron polarization measurements.
2. Thick targets were used in all the experiments in the energy range below 200 keV.*
3. Most of the results were obtained with poor statistical accuracy.
4. Resonance-like behaviour was observed by several authors and has not been confirmed by others.
5. A marked disagreement as to the magnitude and energy of the peak polarization in the different experiments.
6. The existence or non-existence of a such resonance is important from the theoretical point of view.
7. The disagreement of all the existing polarization measurements with the theoretical prediction of polarization by Blin-Stoyle [58] and Boersma [27].*

Such facts indicate the need for neutron polarization measurements of as great accuracy as possible which would help in resolving the existing problems and to provide further polarization data

* Except the recent measurements of Sikkema and Steendam[55] which were reported while this work was in progress.

in the energy range below 500 keV. An additional incentive for research into this reaction is its practical value as a source of polarized neutrons for users of low energy accelerators.

The present measurements were carried out using a helium scattering neutron polarimeter based on the one designed by Davie and Galloway [61] and modified by the present author for automatic data collection, to determine the polarization of D - D neutrons for deuteron energies from 35 to 275 keV at an emission angle of 45^{o} in the laboratory system, using both thin and thick targets.

The present work will form a continuation of the previous measurements on the same reaction for deuteron energies from 300 keV to 1 MeV [37] and from 1 MeV to 6 MeV [10]. The results of the high energy measurements have proved to be very reliable and in good agreement with most of the accurate measurements in the high energy range.

The continuing use of this polarimeter for the low energy measurements allowed it to be used with confidence as to its reliability and in the knowledge that any false asymmetries were of negligible proportion.

The neutron polarization measurement procedures will be described in the following chapters.

CHAPTER 2.

THE NEUTRON POLARIMETER.

CHAPTER 2.

THE NEUTRON POLARIMETER.

Schematic diagrams of the apparatus used in the measurements of neutron polarization are shown in figs. 7,8 and photograph 1. The deuteron beam from an AN-400 Van De Graaf accelerator bombarded a Ti-D target. Neutrons emitted at an angle θ_1 with respect to the direction of the deuteron beam were incident on a high pressure helium gas scintillator cell, which was used as scattering sample. Those neutrons which were scattered by helium through an angle θ_2 were detected in coincidence with the associated recoil pulses, by a neutron detector placed close to the left of the gas scintillator detector. Those neutrons which were scattered by helium through an angle $-\theta_2$ were detected in coincidence with the recoil helium pulses, by a neutron detector placed to the right of the gas scintillator detector. The three detectors were mounted upon a rig which could be rotated about the axis joining the centre of the reaction target to the centre of the scattering sample.

The pulses from the three detectors were processed in an arrangement of electronic circuits before sending to the scalers and 400 channel analyser or computer.

Figure 7. The fast neutron polarimeter.

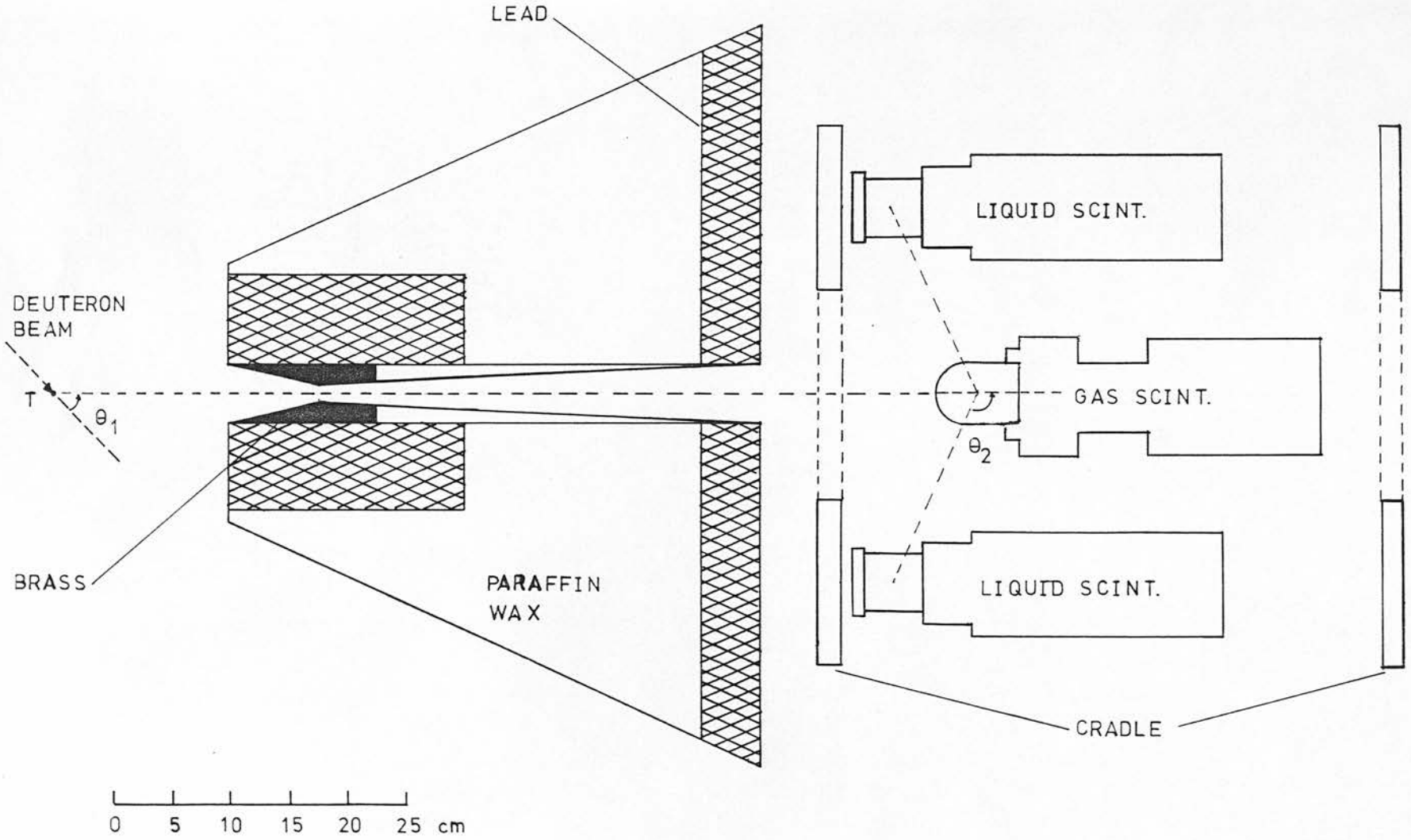
LEAD
DEUTERON
BEAM
T
θ_1
BRASS
PARAFFIN
WAX
LIQUID SCINT.
GAS SCINT.
θ_2
LIQUID SCINT.
CRADLE
0 5 10 15 20 25 cm

Figure 8. The modified fast neutron polarimeter.

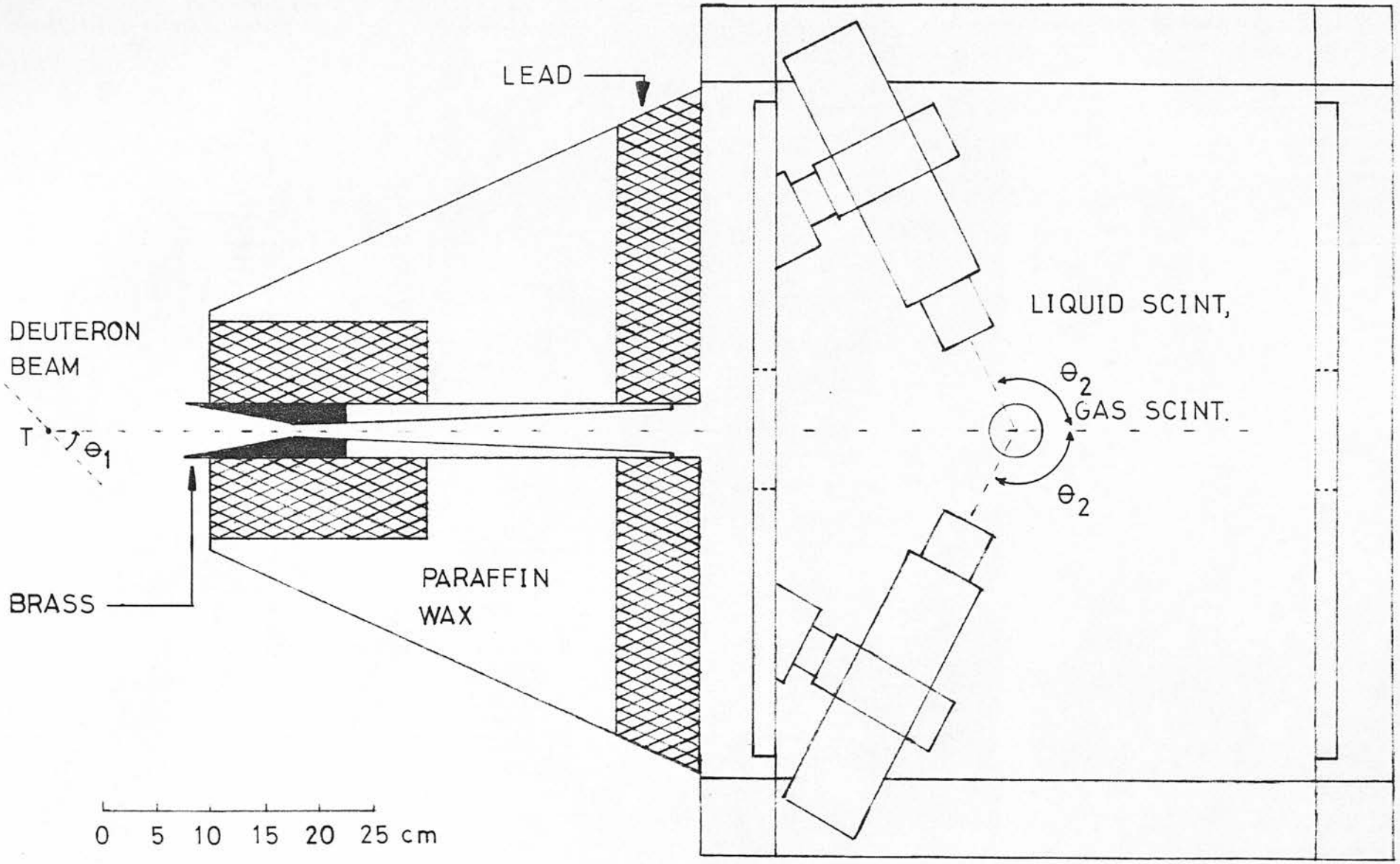
LEAD
DEUTERON
BEAM
T
θ1
BRASS
PARAFFIN
WAX
LIQUID SCINT,
θ2
GAS SCINT.
θ2
0 5 10 15 20 25 cm

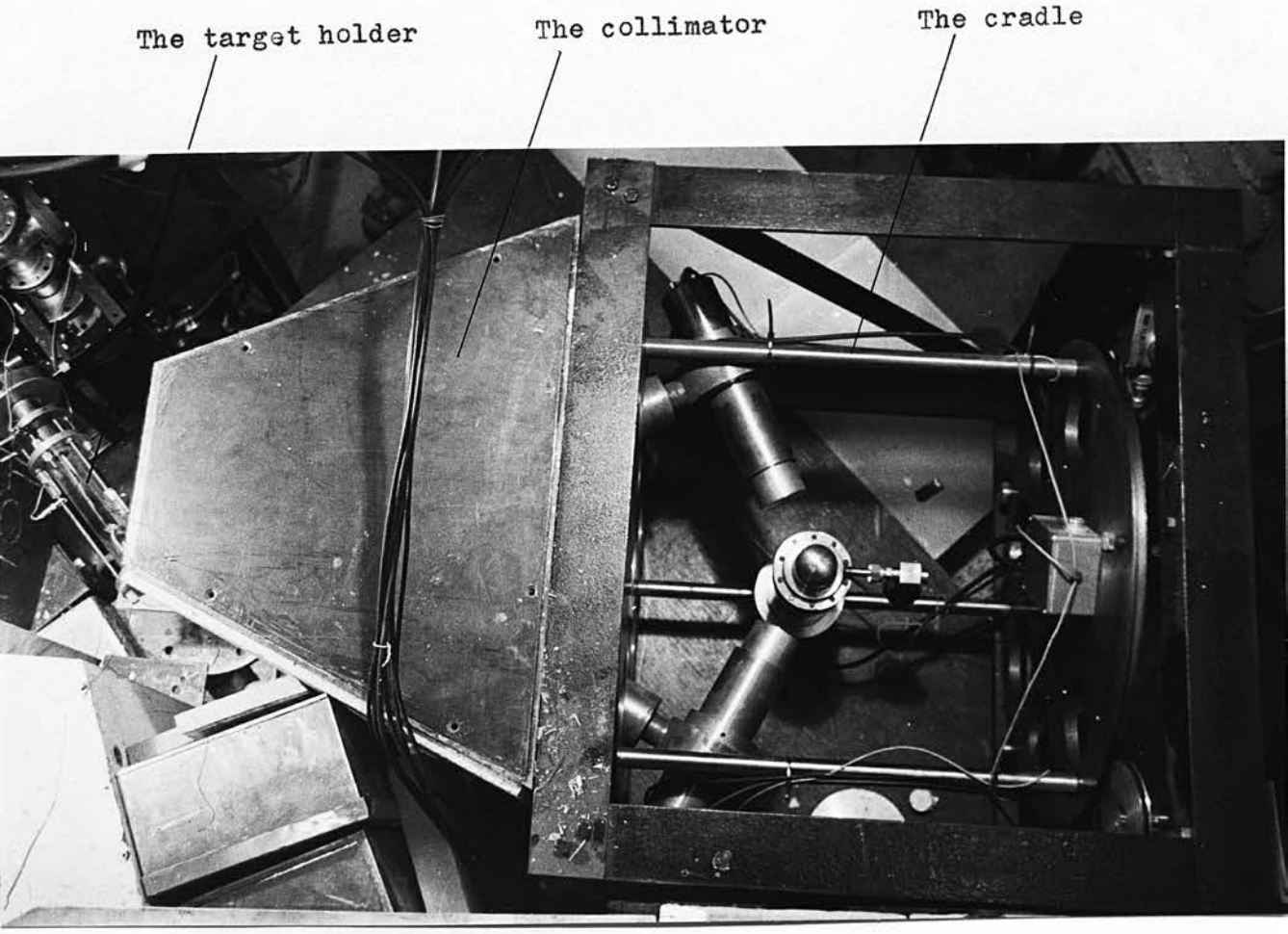

Photograph 1. The modified fast neutron polarimeter

Two polarimeters were used in the present experiment. Both polarimeters consist of a gas helium scintillator detector and two liquid scintillator neutron detectors mounted on a rotatable cradle.

In the original polarimeter (fig. 7) the gas scintillator detector was mounted axially along the direction of the collimated neutron beam. The two side detectors were mounted so that their axes were parallel to the axis of the gas scintillator detector.

In the modified polarimeter (fig. 8 and photograph 1) the helium gas scintillator detector was mounted so that its cylindrical axis was normal to the reaction plane, and the two side detectors were mounted so that their axes were normal to the axis of the gas scintillator detector.

The present chapter describes the different elements involved in the measurements of neutron polarization : the target system, the helium gas scintillator detector, the neutron detectors, the shielding and the electronics.

2.1 The Target System.

The neutrons used in the present experiment were produced by means of the reaction:

$$^{2}H_{1} + {}^{2}H_{1} \longrightarrow n + {}^{3}He + 3.269 \text{ MeV}$$

The incident deuteron beam was produced by a radio frequency ion source and accelerated in a Van De Graaff accelerator to energies from 50 to 350 keV. After acceleration, the beam was magnetically analysed and either the atomic component or the molecular component of the beam was deflected through 15° to impinge upon the target.

The deuterium target used in the present experiment consisted of a copper disk coated with a titanium layer containing absorbed deuterium gas in a near one to one atomic ratio. The targets were supplied by the Radiochemical Centre, Amersham, in the shape of a disk 1" in diameter and 0.01" in thickness. These disks were cut into strips of different sizes according to the target holder to be used and soft soldered to the target holder. Since as much as 20 watts of power were dissipated in the target, a water cooling arrangement was employed, so that the water can pass beneath the copper surface to which the target was soft soldered.

Photograph 2 shows the target assembly and the target holders. Three target holders were used in the present experiment. The most used one was a target of 3 mm width normal to the reaction plane and 2 cm long in the reaction plane. The target was inclined at 45° to the incident beam direction and hence the target spot was an ellipse with semimajor and semiminor axes of approximately 4 mm and 2 mm respectively. A straight target of 3 mm width in the reaction plane and 1.4 cm long normal to the reaction plane

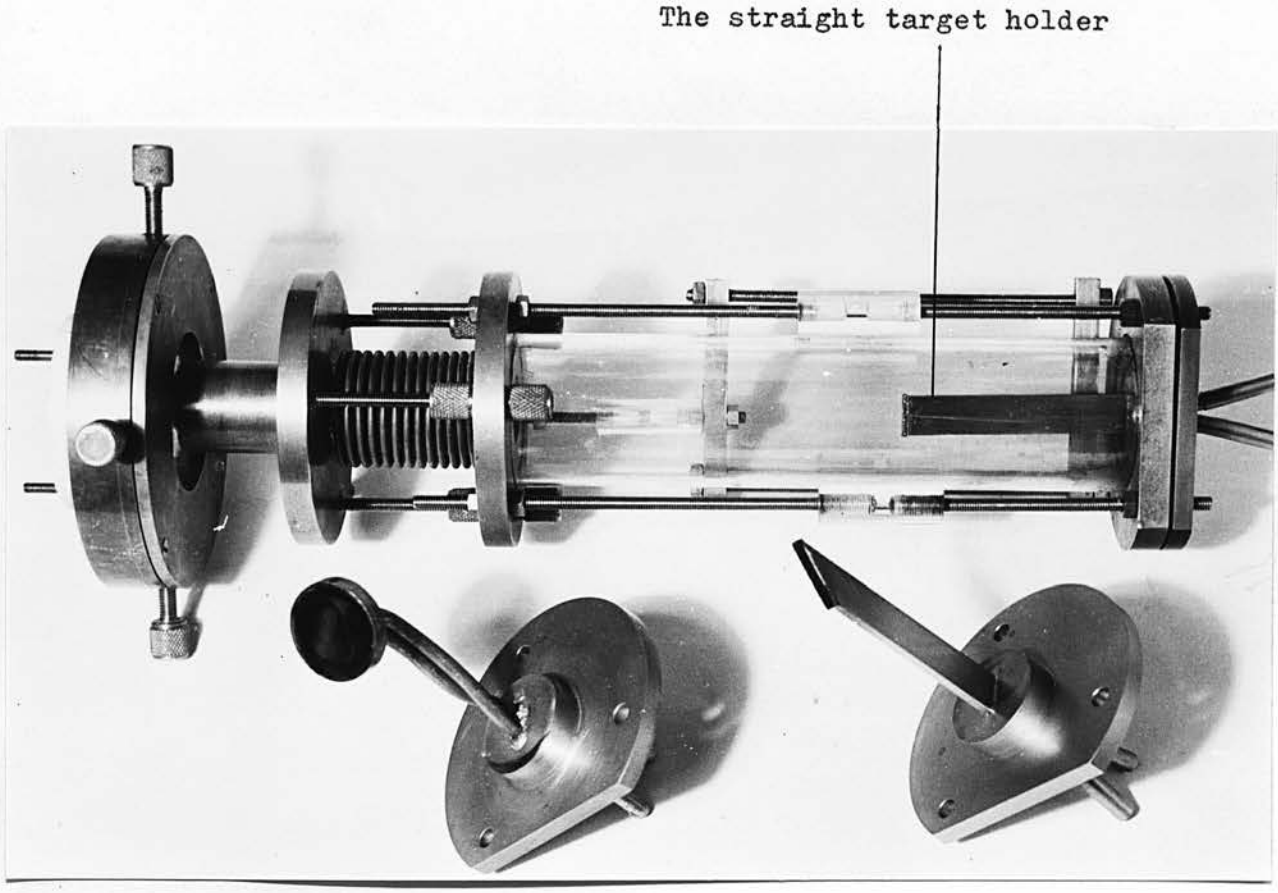

Photograph 2. The target assembly and the target holders.

was used sometimes, either to reduce the target thickness by a factor of ~1.4 or when both the present experiment and a small angle experiment [64] were running simultaneously. The third target was used to overcome the difficulty in focussing the deuteron beam in the low energy range below 100 keV. The target was 1" in diameter, a complete target disk being soft soldered to it. The target was inclined at 45° to the incident beam direction so that most of the beam spot was used thereby considerably increasing the neutron yield.

The target system as a whole was designed so that the target can be accurately located relative to the accelerator beam tube and the collimator axis. Once the target system had been aligned, the target holder can be removed for replacing the target material without the need to realign the system when it is fitted again.

2.2 The Helium Gas Scintillator Detector.

The helium gas scintillator detector, fig. 9, consists of a high pressure helium gas scintillator cell optically coupled to a photomultiplier with a quartz window. The photomultiplier type EMI 6255B is used.

The helium gas scintillator cell is made of a stainless steel cylinder with a wall thickness of 2 mm. The cylinder is closed at the front by a hemisphere. The axial length is 6 cm and the diameter is 5 cm. The cylinder is closed at the rear by

Figure 9. The helium gas scintillator detector.

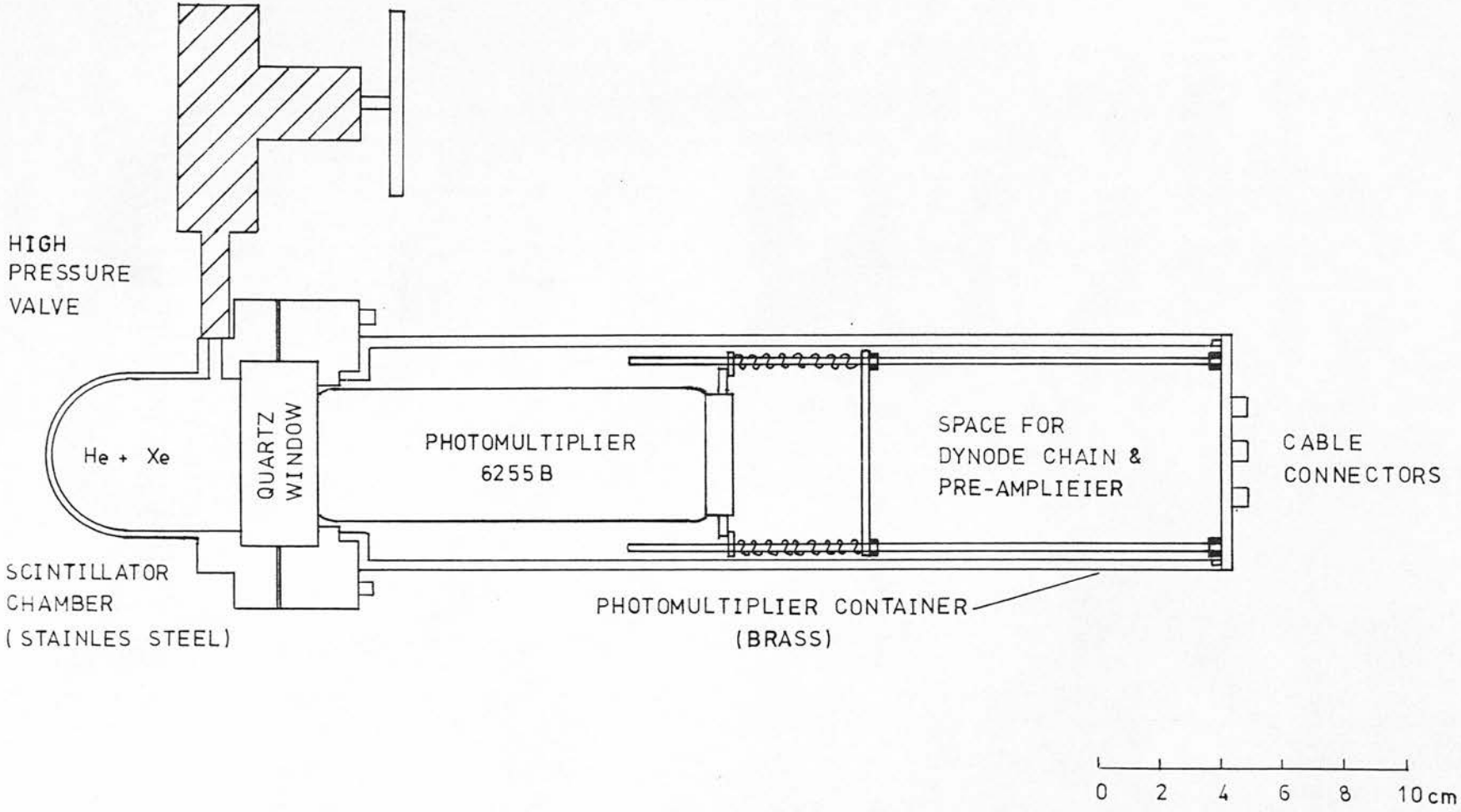
HIGH
PRESSURE
VALVE
He + Xe
QUARTZ
WINDOW
PHOTOMULTIPLIER
6255 B
SPACE FOR
DYNODE CHAIN &
PRE-AMPLIEIER
CABLE
CONNECTORS
SCINTILLATOR
CHAMBER
(STAINLES STEEL)
PHOTOMULTIPLIER CONTAINER
(BRASS)
0 2 4 6 8 10 cm

a 2.5 cm thick quartz window, seated on a P.T.F.E. 'O' ring seal, and held in position by a stainless steel surround clamped with ten bolts. Into this surround screws the brass case which contains the photomultiplier tube and the pre-amplifier circuitry.

The inside wall of the cell is coated with a reflector and with a wavelength shifter. After polishing the steel, the surface is coated with a vacuum deposited layer of aluminium, then with a layer approximately 2 mm thick of electrostatically deposited magnesium oxide. The wavelength shifter is a vacuum deposited film of Diphenyl stilbene (D.P.S.) varied in thickness from 300 $\mu g/cm^2$ on the walls close to the viewing window to 100 $\mu g/cm^2$ on the area of the hemispherical end [65]. The quartz window is also coated with D.P.S. as recommended by Jenkins and Shamu [65].

The helium cell is filled with a mixture of helium and xenon to a pressure of 70 atmospheres.

The filling system has an oil diffusion pump with liquid nitrogen trap and a roughing pump connected to one outlet, and a cylinder of xenon and another of helium connected to two inlets.

The helium cell is generally cleaned and filled by the following process. The roughing pump evacuates the helium cell and is valved off. Helium is then admitted to about 10 atm. and allowed to settle for a few minutes before being let out to atmospheric pressure. The system is then pumped down to 10^{-5} torr.

Flushing with helium and pumping down is repeated several times, to eliminate any contamination from the atmospheric gases. Finally, the helium cell is filled with xenon gas to a pressure of 5 atmospheres and the helium added to bring the total pressure to 70 atmospheres. Then the helium cell is valved off and fixed to the photomultiplier tube to be used in the measurements.

It is found that a gradual drop in the gas pressure occurred due to the gas leakage and is accompanied by a loss in the light output within a few months. To regain the maximum light output the filling procedure has to be repeated nearly every six months.

2.3 The Neutron Detectors.

Two side detectors are used to detect the neutrons scattered from helium in the helium gas scintillator detector. The scintillators used are bubble free encapsulations of a liquid organic material type NE213 supplied by Nuclear Enterprises, Edinburgh. The cells dimensions are 5 cm in diameter and 5 cm long. The scintillator has excellent pulse shape discrimination properties. These properties are used in this experiment to discriminate against gamma rays. The scintillator cell is optically coupled to an EMI 9814 photomultiplier tube. A schematic diagram of the neutron detector is shown in fig. 10.

Figure 10. Liquid scintillation neutron detector.

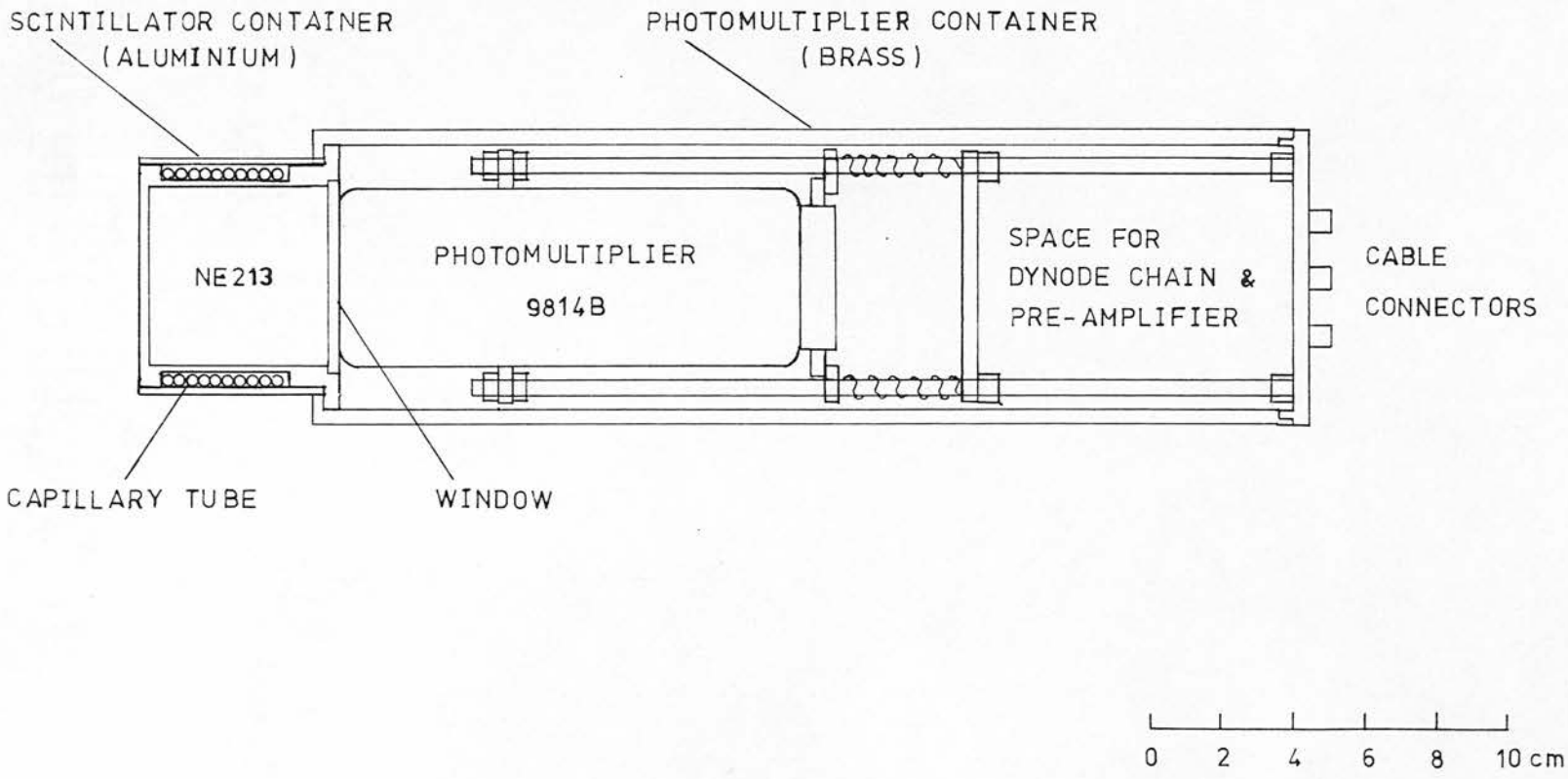
SCINTILLATOR CONTAINER
(ALUMINIUM)
PHOTOMULTIPLIER CONTAINER
(BRASS)
NE213
PHOTOMULTIPLIER
9814B
SPACE FOR
DYNODE CHAIN &
PRE-AMPLIFIER
CABLE
CONNECTORS
CAPILLARY TUBE
WINDOW
0
2
4
6
8
10 cm

The two side detectors and the helium gas scintillator detector are mounted on a rotatable rig. The detectors are accurately mounted so that the axis joining the centre of the side detector cell to the centre of the high pressure helium chamber make a laboratory angle of 117° with the collimated neutron beam. The distance between the gas scintillator chamber and the liquid scintillator cells is 4.75".

For monitoring the neutron yield at the target a NE400 grooved disc of boron polyester with ZnS(Ag) as scintillator is used. The disc is 25 mm in diameter with an active layer of 1.2 mm, obtained from Nuclear Enterprises, Edinburgh. The scintillator is insensitive to gamma rays and it is sensitive only to thermal neutrons. Paraffin wax of 10 cm thickness has been used around the scintillator to moderate the fast neutrons. The detector is located approximately 60 cm from the neutron producing target, making an angle of $\sim 140^{\circ}$ with the incident deuteron beam direction. Pulses from the scintillator detector are amplified and fed to two scalers. The number of counts in the first scaler is displayed every second which is very useful during the focussing of the deuteron beam on the target. Maximum counts indicate that most of the beam spot is hitting the target. Any changes in the counting rate are noticed and the setting of the accelerator controls are adjusted by the operator to maintain maximum counting rate.

In the second scaler the number of counts is given after every data accumulation period, usually 1000, 2000 or 4000 seconds.

In this scaler the change with time of the reaction yield for a given bombarding energy can be observed. Any noticeable drop in the reaction yield indicates a target deterioration which leads to replacing the target material. Usually the target is changed every time the scaler reaches two thirds of its maximum counting rate.

2.4 The Shielding.

To reduce the number of background pulses due to scattered neutrons from the surrounding materials and to gamma rays, the side detectors are shielded in the following way.

A collimator situated in front of the polarimeter is used as shield to eliminate any direct neutron flux from the neutron producing target from reaching the side detectors. The collimator is 46 cm long, narrower at the front close to the target, than the back. It was designed in this shape and fitted with three wheels to permit rotation of the collimator to which the polarimeter is attached, around the centre of the target, for angular distribution measurements. The collimator rests on a very heavy steel table and is fixed to it with two G-clamps. The collimator contains a cylindrical layer of lead close to the target, 20 cm in diameter and 20 cm long, to degrade the neutron energy by inelastic scattering and to attenuate the annihilation gamma ray flux produced from the deuteron reaction with any carbon contamination on the target. The main volume of the

collimator is filled with paraffin wax to slow down and capture the neutrons. Finally a layer of lead 7.5 cm thick is used to prevent the gamma ray flux produced by neutrons captured in the paraffin wax from reaching the side detectors. The collimator aperture is throated by using several inserts each of 5 cm long. They are made from brass and from polythene. Brass is used for the inserts around the throat and polythene for the rest. The inserts are tapered by increasing their diameter in the direction of the neutron beam to reduce neutron scattering from the wall of the collimator aperture.

By varying the number of the inserts and the position of the throat, the area of the helium scintillator illuminated by the neutron beam can be altered. Usually the distance between the target and the collimator is selected so that the solid angle subtended by the helium gas scintillator at the target allows complete illumination of the helium cell by the collimated neutrons. If the diameter of the collimated neutron beam is smaller than the diameter of the helium cell, a false asymmetry can be created due to accelerator voltage fluctuation which may shift the position of the beam spot on the target and, consequently the neutron beam position on the helium cell. But, if the dimension of the collimated neutron beam is bigger than the diameter of the helium cell, neutrons will be scattered from the surrounding materials and increase the background.

More shielding materials are placed around the polarimeter to reduce the background counting rate. Concrete blocks of 45 x 15 x 15 cm are built beneath and around the table carrying the polarimeter to about its height. Then paraffin wax contained in cartons 50 x 24 x 30 cm are placed around the sides of the polarimeter. On the top of it metal boxes filled with either paraffin wax or polythene bags filled with borated water provide 25 cm thickness of shielding. These available shielding materials are built all around the polarimeter and found very effective in reducing the background ratio to a negligible value.

2.5 The Rig Rotation.

The rig is basically a rotating cradle seated in a frame behind the collimator. The cradle consists of two accurately turned discs of 2.5 cm thickness with central holes to allow the passage of neutrons and cables. These discs are held parallel and 50 cm apart by three steel rods of 2.5 cm diameter. The rig is mounted in an angle iron frame with the end plates of the cradle resting on four ball bearings. Thus the rig can be accurately rotated around the axis joining the centres of the two end plates. A pin on the rear end plate and four microswitches attached to the frame allow the rig to be rotated under remote control to any one of the desired positions.

Two accurately machined detector holders are mounted on the front (i.e. close to the target) disc of the cradle. Each of the

two side detectors can be tightly fitted in one of these holders and secured by three bolts. The gas scintillator detector holder is an integral part of the third steel rod. Thus the detector can be fitted in the holder and be accurately perpendicular to the axis of rotation. Collars are provided for setting the position of the two detectors and for fixing the height of the gas scintillator. After adjusting the distances between the side detectors and the gas scintillator the collars are secured to their detectors. Thus any detector can be removed and fitted back in position without need for readjustment. The axial alignment of the polarimeter is performed using cylindrical alignment inserts which fitted the central holes, of the two end plates, and a telescope optically aligned with the axis of the collimator. The method of alignment will be described in chapter 4.

2.6 The Electronics.

A block diagram of the electronics used in the present experiment is shown in figure 11. All the circuits were designed and developed by Davie [66]. The circuit diagrams of the individual components are given in more details in ref. 66.

Each side detector is coupled to photomultiplier tube type EMI 9814B which is connected to its recommended dynode chain circuit. The linear signal from the 11th dynode was found not to be affected by the rotation of the detectors during the

Figure 11. Block diagram of electronic circuitry used with polarimeter.

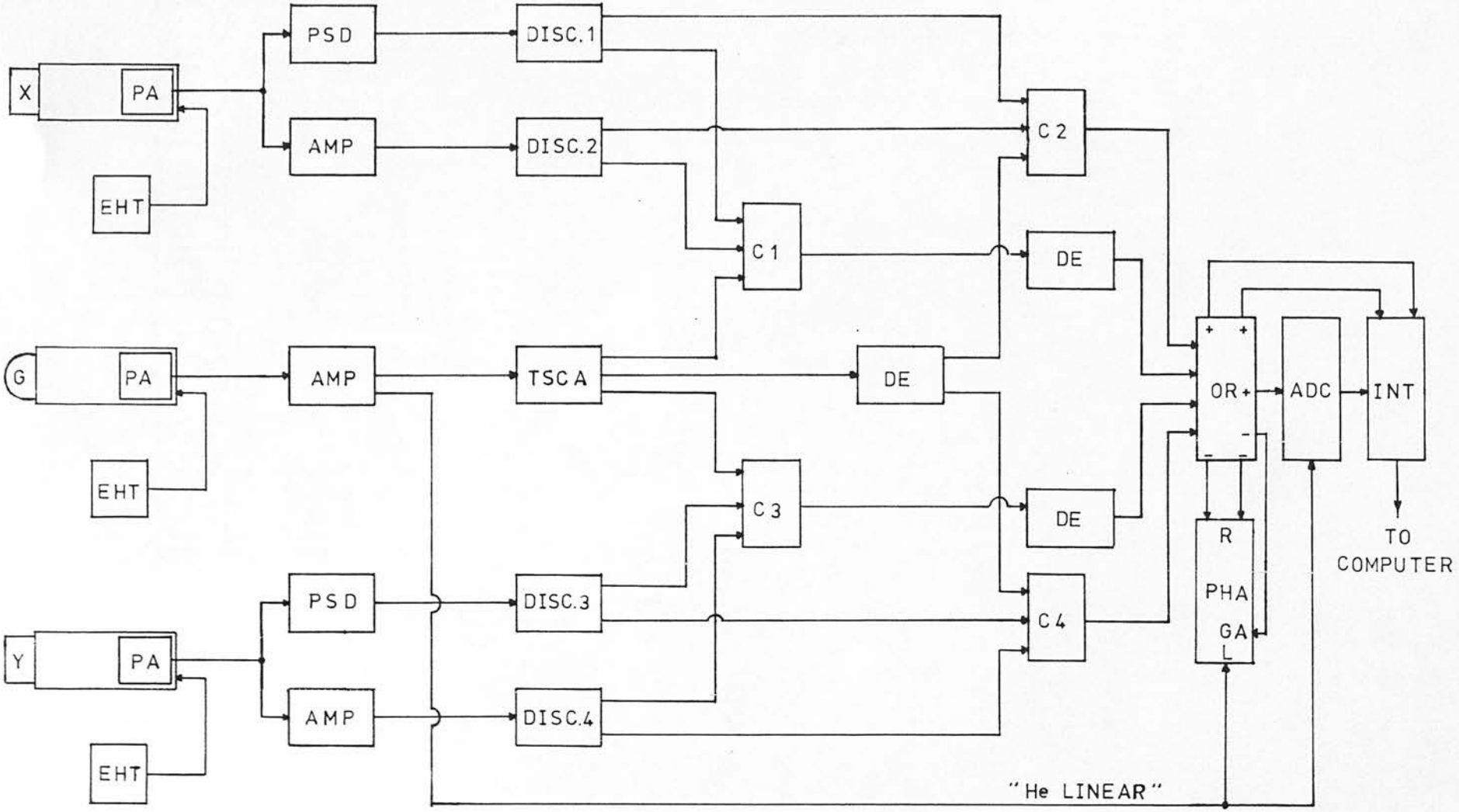
X
PA
EHT
PSD
AMP
DISC.1
DISC.2
C 1
C 2
DE
G
PA
EHT
AMP
TSC A
DE
C 3
DE
Y
PA
EHT
PSD
AMP
DISC.3
DISC.4
C 4
OR
ADC
INT
TO
COMPUTER
R
PHA
GA
L
"He LINEAR"

Table 2. Key to figure 11.

Designation	Description
X	Liquid scintillator 'X'
G	Gas scintillator
Y	Liquid scintillator 'Y'
EHT	EHT power supply
PA	Pre-Amplifier
AMP	Linear amplifier
PSD	Pulse shape discriminator
D	Integral discriminator
TSCA	Timing single channel analyser
C	Triple coincidence unit
DE	Delay
OR	Coding unit
ADC	Analogue to digital converter
INT	Interface
PHA	Multi channel analyser
R	Routeing input
GA	Gate input
L	Linear input

interchanging procedure in the measurements of left-right asymmetry. This linear signal is fed to a pre-amplifier then to a pulse shape discrimination unit similar to the one developed by Roush et al [67]. The pulse shape discrimination output is fed to an integral discriminator which was set to reject gamma rays. So, logic pulses are produced only for neutrons. In addition the pulses from the pre-amplifier are fed to a linear amplifier, then to an integral discriminator. The discriminator is set to allow pulses, due to events above a certain selected energy (usually set at 100 keV electron energy) to generate logic output pulses. The output of the integral discriminators 1 and 2 in fig. 11 are fed to two coincidence units, coincidence unit 1 for real plus random events and coincidence unit 2 for random events. The third input to each coincidence unit is derived from the discriminator of the linear amplifier of the gas scintillator detector output. The input to coincidence unit 2 from the gas scintillator is delayed by 3 μs, so that this coincidence unit output can be triggered only by random events. To the output of coincidence unit 1 a delay of 3 μs is added to bring the two coincidence outputs into the same time relation with respect to the 'He linear' output. Coincidence units 3 and 4 operate as unit 1 and 2 respectively, but for the second side detector Y.

Hence any pulse which appears at the output of one of the four coincidence units indicates that, within the coincidence circuit resolving time of 1 μs, a neutron is detected in the

gas scintillator and in a neutron detector and the signal from the neutron detector satisfies certain pulse height requirements.

The four coincidence units outputs are used to gate a multichannel analyser employed to pulse height analyse the linear output from the gas scintillator amplifier.

Four pulse height spectra of the helium recoil linear pulses are stored in the memory of the multichannel analyser, each one containing only events recorded in association with one of the four gating outputs.

The contents of the memory of the analyser can be recorded by a teletype attached to it, or on paper tape by means of a high speed tape punch, which is attached to the analyser as well. These paper tapes can be read by the teletype reader and their content can be obtained as print out from the teletype. Alternatively, these tapes can be fed to the computer to be compiled and then analysed.

The electronics as described above was used with the original polarimeter. More improvements and modifications were applied to the electronics with the new modified polarimeter as shown in figure 11. A direct interface to the PDP11/45 digital computer was achieved by using the available interface circuit after modification and an analogue to digital converter type (256 ADC MOD 8213) made by Laben.

The integral discriminator of the gas scintillator has been replaced by a timing single channel analyser type (ORTEC MOD 488) which has a better response to zero cross-over pulses of the helium recoil linear amplifier output. The resolving time of the coincidence circuits was improved to about 0.65 μs.

The outputs of the four coincidence units are fed to four scalers which give the number of counts from each coincidence unit output, at the same time these four outputs are fed to a coding unit and pulse shaping unit to provide a coincidence pulse for the ADC to permit analysis of the 'He linear' output. The coding unit is designed to route the real plus random pulses to the desired group of channels in the memory of the computer.

The content of the memory of the computer can be recalled and displayed in a video display unit during or after the collection of data. Fig. 12 shows typical spectra recorded during measurements for an incident deuteron energy of 300 keV and for neutrons emitted at a laboratory angle of 45°, where both spectra related to the same side detector, are overlapped.

The new method of direct interface to the computer has speeded up the data collection and data analysis time which is particularly important in this low energy range.

The polarimeter was modified to allow automatic data collection to be employed. Logic circuitry was designed and

Figure 12. Typical recoil spectra recorded during measurements for an incident deuteron energy of 300 keV and for neutrons emitted at 45° Lab., where both spectra related to the same side detector are overlapped.

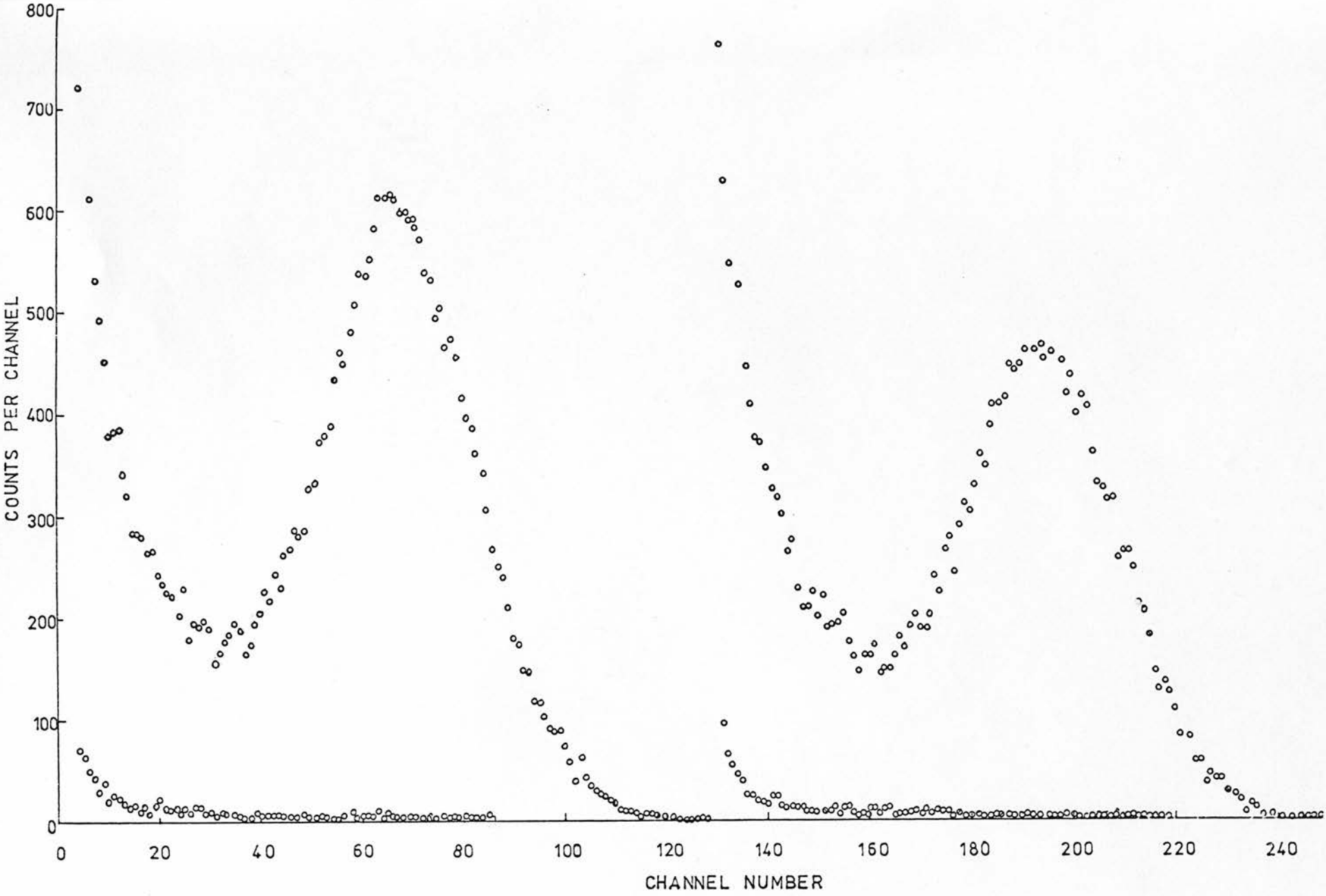
800
700
600
500
400
300
200
100
0
COUNTS PER CHANNEL
0
20
40
60
80
100
120
140
160
180
200
220
240
CHANNEL NUMBER

constructed for rotating the polarimeter. In the measurements of the left-right asymmetry the polarimeter is set to a certain position and the computer starts to accept data for a selected counting time. After completing the counting time, the computer stores the data and sends a signal to the logic circuitry to rotate the polarimeter to the next position. After reaching the desired position the computer starts accepting the new data, and the procedure continues until the end of running at a certain energy.

The racks of electronics, including the automatic data collection system, multichannel analyser and the H.S.T.P. are illustrated in photograph 3.

The automatic system circuitry is described in detail in chapter 3.

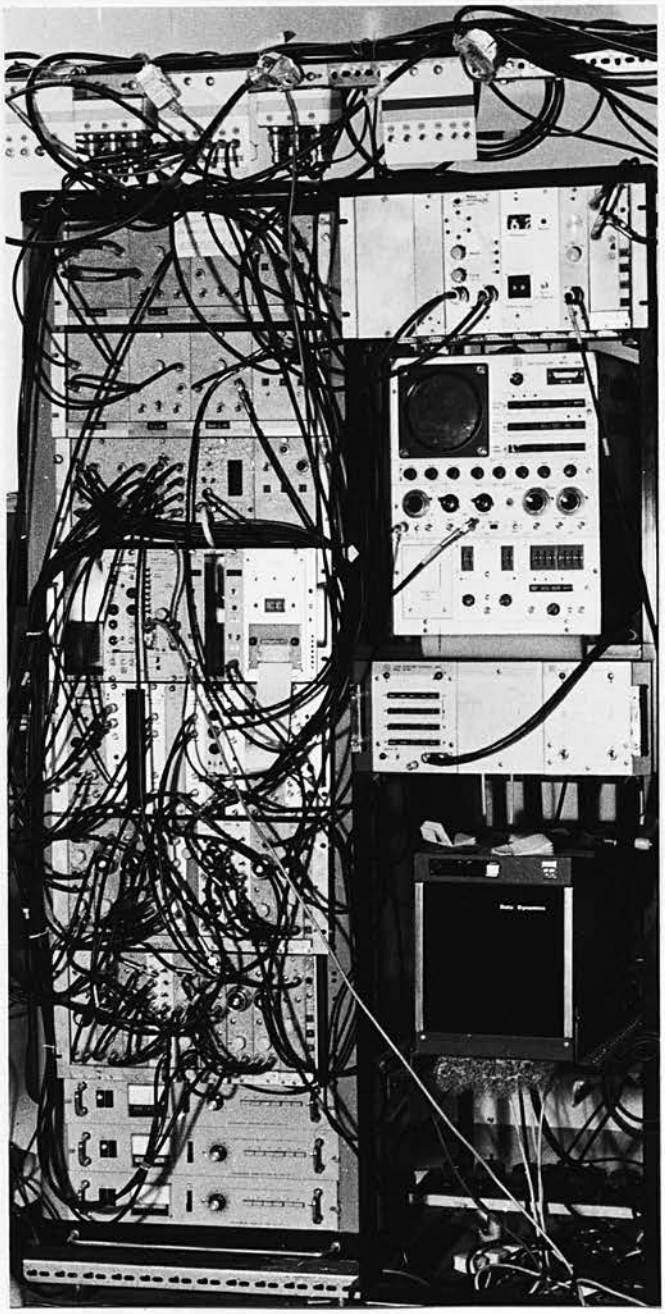

Photograph 3. The racks of electronics, multichannel analyser, H.S.T.P. and the automatic data collection system.

CHAPTER 3.

THE AUTOMATIC DATA COLLECTION SYSTEM.

CHAPTER 3.

THE AUTOMATIC DATA COLLECTION SYSTEM.

3.1 Introduction.

Having been convinced of the reliability and appropriateness of the previously described polarimeter for the present measurements, it was decided to modify it for automatic data collection. This modification was found especially necessary in this low energy range where the D-D reaction neutron yield drops considerably with energy in the range from 500 to 50 keV, as can be seen from the curves published by Seagrave [68]. These curves indicate the need for longer time measurements to obtain a polarization value with good statistical accuracy. For example, if 240 hours of running time is needed to obtain a polarization value with statistical accuracy of 1%, then by dividing by eight hours (the normal running time each day with the unmodified polarimeter) we need 30 days of continuous running to achieve that accuracy. Because of the other users of the machine, only ten days can be used each month, which means that three months are required to complete the measurement of one polarization value. That is assuming that the machine is in good working condition and only routine servicing is required, i.e. the changing of the ion source or the filling of the deuterium gas cylinder which normally takes at most four days each month.

From this example one can see the importance of having an automatic data collection system to allow the measurements to be done for 24 hours per day, thereby completing such a measurement in 10 days rather than extending over more than three months. In addition, by using the automatic system the measurement can be done with the same machine conditions, target alignment and electronic settings. More difficulty arose as additional experiments were set up within the laboratory and the shielding they required increased the difficulty of access to the polarimeter for manual rotation. At one stage, five experiments were set up in the laboratory; three small angle scattering experiments, the associated particle technique experiment and the present experiment all with heavy shielding surrounding each experiment. One can imagine the difficulty in passing through the limited space to the polarimeter every 30 minutes for manual rotation. So the building of the automatic system has reduced the amount of inconvenience and delay and speeded up the measurement time by a factor of three.

In the following sections the operation of the individual units and their functions will be described.

3.2 The Automatic System Arrangement.

The automatic data collection system is designed and constructed using integrated circuits of the TTL 74 series. A block diagram of the circuitry used in the system is shown in

fig. 13. Each unit was built in a plug-in module which fits into a 19" rack mounting frame as shown in photograph 4. Double width plug-in modules were used to accommodate the switches, sockets and display on some of the units. The transformers and capacitors of the power supplies are mounted into the back of the rack.

It may be seen from fig. 13 that three operations are controlled automatically by the system. First is to switch on the High Speed Tape Punch (H.S.T.P.), the mains for which passes through relay 1. This is enabled 40 seconds before the completion of a preselected counting time by means of a preset scaler, (4000 max.). This scaler may be set for data collection periods of 1, 2, 4 thousand seconds; the scaler is zeroed on receipt of a pulse derived, via pulse shape 2, from the stop/start level transition of the data analysis system (Pulse Height Analyser or Computer). This same transition is used via nor gate 2 to disable the m ains relay 1 to the H.S.T.P. The counting time scaler receives its one second clock pulses from the P.H.A. via pulse shaper 1.

The second operation is the stopping of the P.H.A. after the end of a selected number of runs. The output of pulse shaper 2 feeds a pulse for every run to a two digit scaler (99 count maximum). The output of the scaler is fed to a drive then to a "Nixie" display, to display the run numbers. A thumb switch is used to select the total number of runs required. When a selected number of runs is reached, a level is produced and used to stop

Figure 13. Block diagram of the automatic data collection system.

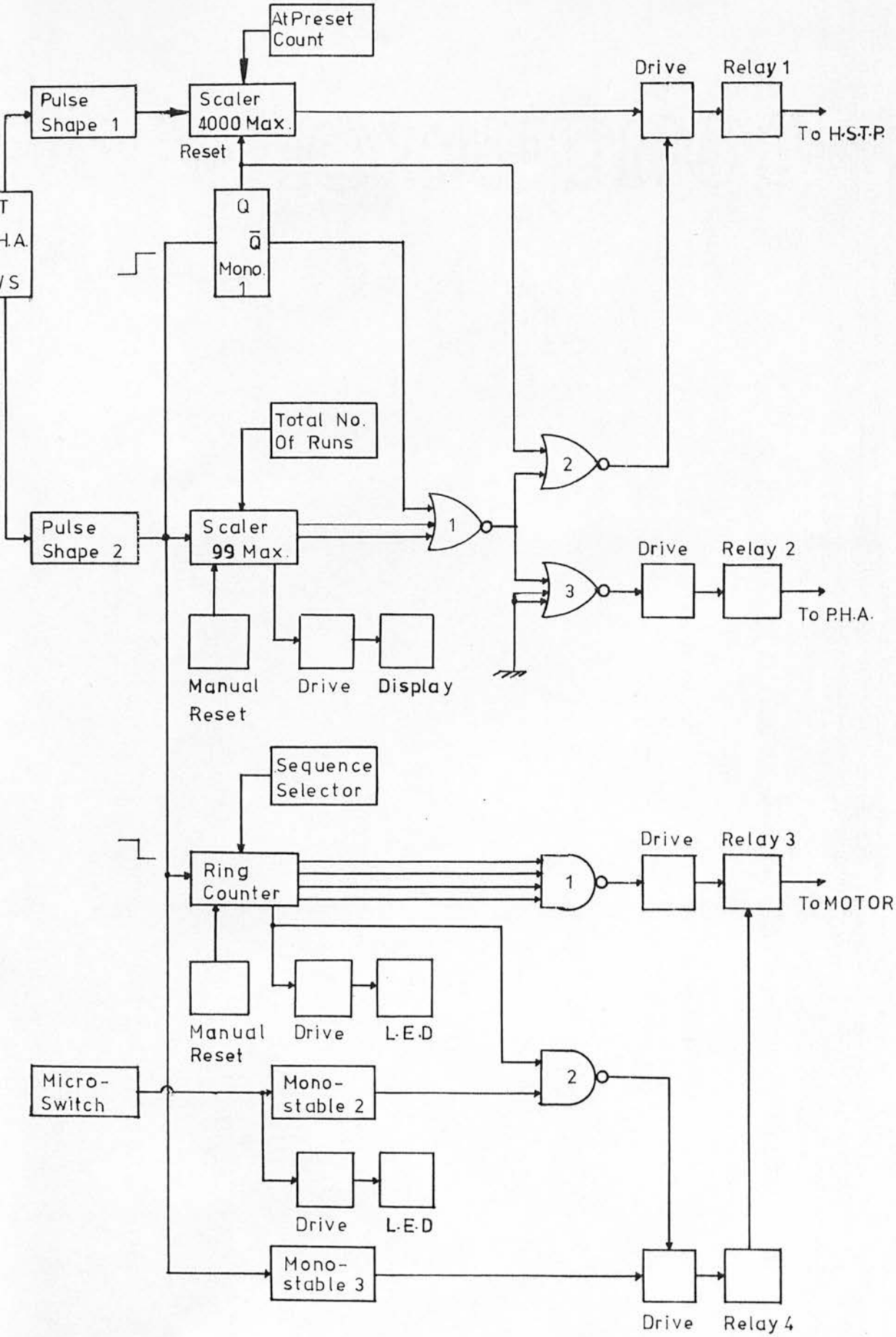
At Preset Count
Pulse Shape 1
Scaler 4000 Max.
Reset
Drive
Relay 1
To H.S.T.P.
Q
$\bar{Q}$
Mono. 1
Total No. Of Runs
Pulse Shape 2
Scaler 99 Max.
1
2
3
Drive
Relay 2
To P.H.A.
Manual Reset
Drive
Display
Sequence Selector
Ring Counter
1
Drive
Relay 3
To MOTOR
Manual Reset
Drive
L.E.D
Micro-Switch
Mono-stable 2
2
Drive
L.E.D
Mono-stable 3
Drive
Relay 4

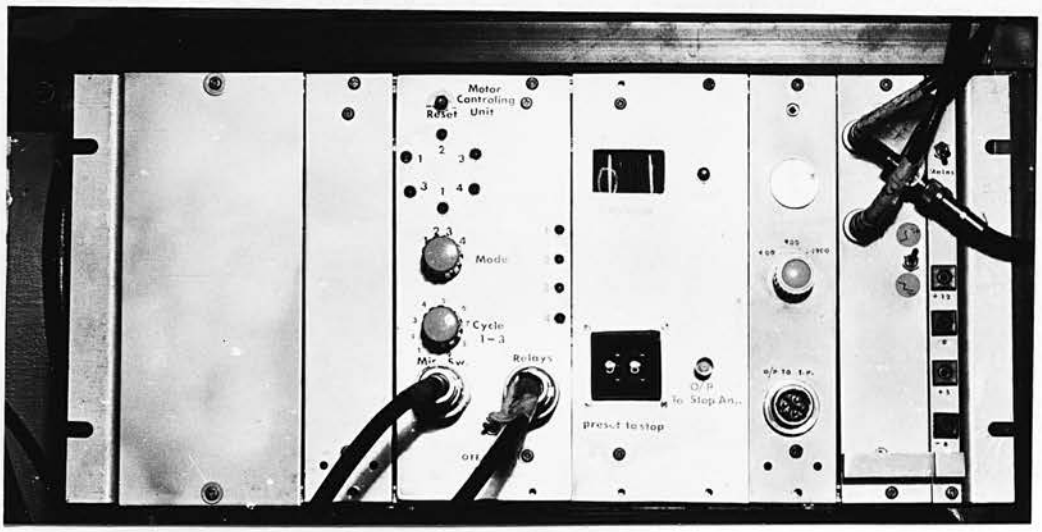

Photograph 4. The automatic data collection system as mounted on the rack.

the P.H.A. through nor gate 3 where its second input is either connected to earth or can be connected to other equipment (e.g. the accelerator control system) to stop the experiment. The output of nor gate 1 is also fed to nor gate 2 to stop the H.S.T.P. at the end of this selected number of runs. Scaler 1 (99 max.) is provided with manual reset, usually used when starting a new series of measurements.

The third operation is the control of the motor to rotate the polarimeter. The rotation in the appropriate direction and the stopping at the desired position are controlled by means of a ring counter and microswitches. The polarimeter can be stopped at four positions. Two positions with the two side detectors in a horizontal plane (reaction plane) and the other two in a vertical plane (normal to the reaction plane) as shown in fig. 14.

The stop level from the P.H.A. after convertion to a logical level by the pulse shaper 2 is used to operate a ring counter of six counts. This ring counter can be used in four different modes by means of a sequence selector switch. These modes will be described in the following sections. The $\bar{Q}$ outputs from the ring counter (J.K. flip flops are used in the design of the ring counter) are fed to nand gate 1 which energises the direction of rotation relay (3) if one of those $\bar{Q}$'s goes high, and de-energises it if all $\bar{Q}$'s are low. The leads from the motor are connected to relay (3) in such a way that if relay 3 energises, the motor can be rotated clockwise, and anticlockwise if the relay (3)

Figure 14. The orientation of the neutron detectors by the rotation of the polarimeter.

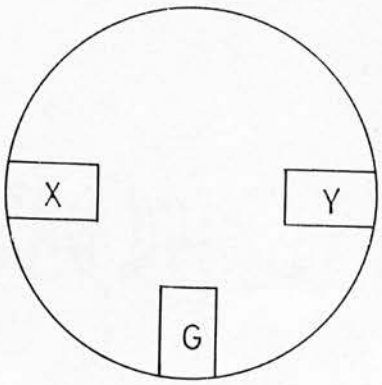

POSITION 1

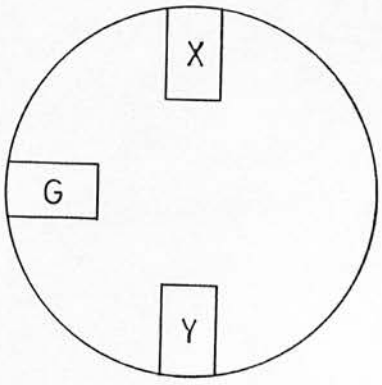

POSITION 2

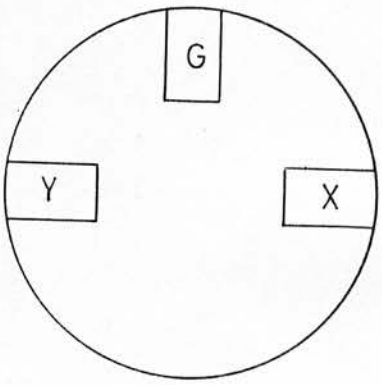

POSITION 3

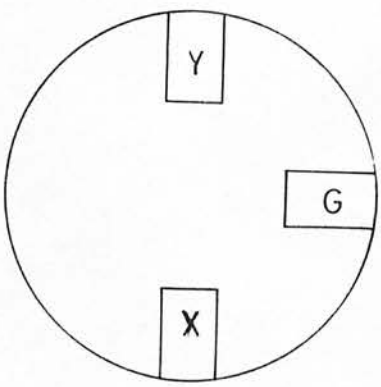

POSITION 4

de-energises. The same stop level is used to energise the mains relay (4) after a delay of 700 ms, by means of monostable 3. This delay allows relay (3) to settle before relay (4) provides the mains through it to the motor. To ensure that the polarimeter stops at a particular position, the Q outputs of the ring counter are used and fed to nand gate (2) e.g. associated with the microswitch shown in the figure. The microswitch associated with this position of the polarimeter will provide a pulse from monostable (2) on arrival. If this agrees with the code of Q outputs, nand gate (2) will disable the mains relay (4) drive. Similar circuits serve the other three microswitches. The four microswitches are mounted on the frame of the polarimeter, two in the horizontal plane and the other two in the vertical plane (photograph 5). Each Q output of the ring counter is fed to drive Light Emitting Diodes (L.E.D.) to indicate the direction of rotation, while the L.E.D.'s from the microswitches indicate the position of the polarimeter. The ring counter is provided with manual reset switch which is normally used when selecting another mode of sequence.

The details of the individual circuits are given in the following sections.

3.3 The Pulse Shaper.

Most digital integrated circuits use positive supply voltages in the range of 3.6 to 7.0 volts. As TTL 74 series integrated

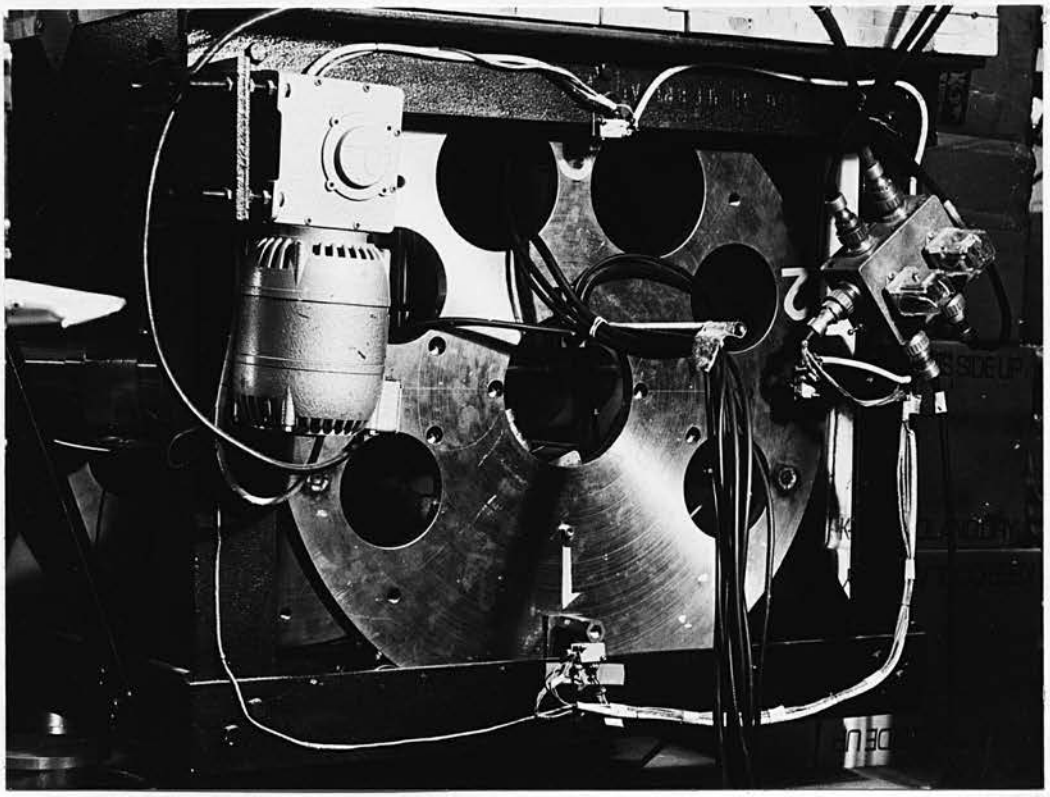

Photograph 5. The rear end of the polarimeter, the motor, relays, microswitches and the central hole.

circuits are used in the design of the present system, these require a positive supply voltage of 5 volts, and also require positive logical inputs. The time pulses and the stop/start outputs from the P.H.A. have negative polarity. These two outputs are used to operate the automatic system, so they have to be converted to positive logical signals. Fig. 15 shows the circuit diagram of the pulse shaper used to convert the negative polarity signals to positive logical signals. This circuit is modified from the circuit given by D'cunha [69] where the available transistors 2N1132 and 2N1711 are used instead of the given transistors and different values of resistors are used to suit the requirement of the present system.

The circuit operates when a negative pulse or transition is delivered to the input, all transistors are switched on, and the inverted signal then appears at the output. In the absence of an input, the transistors are turned off and only negligible leakage currents are drawn by the circuit from the transistors.

Two of these circuits have been built in one plug-in module as shown in photograph 6 where one is used to convert the time pulse output and the other to convert the stop/start level output to a logic signal. The output of these two circuits is connected internally through the back of the rack to the corresponding inputs of the other units.

Figure 15. Circuit diagram of the pulse shaping unit.

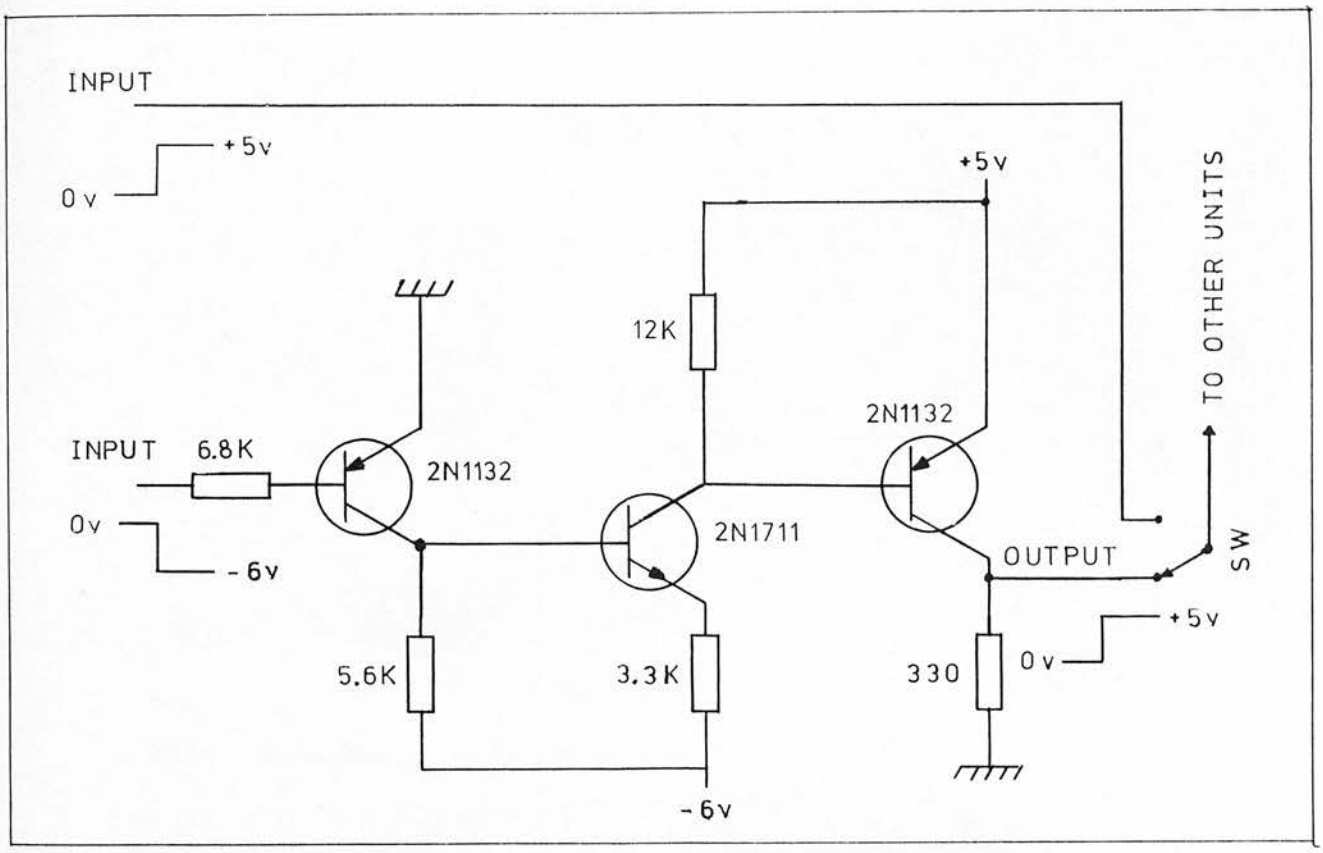

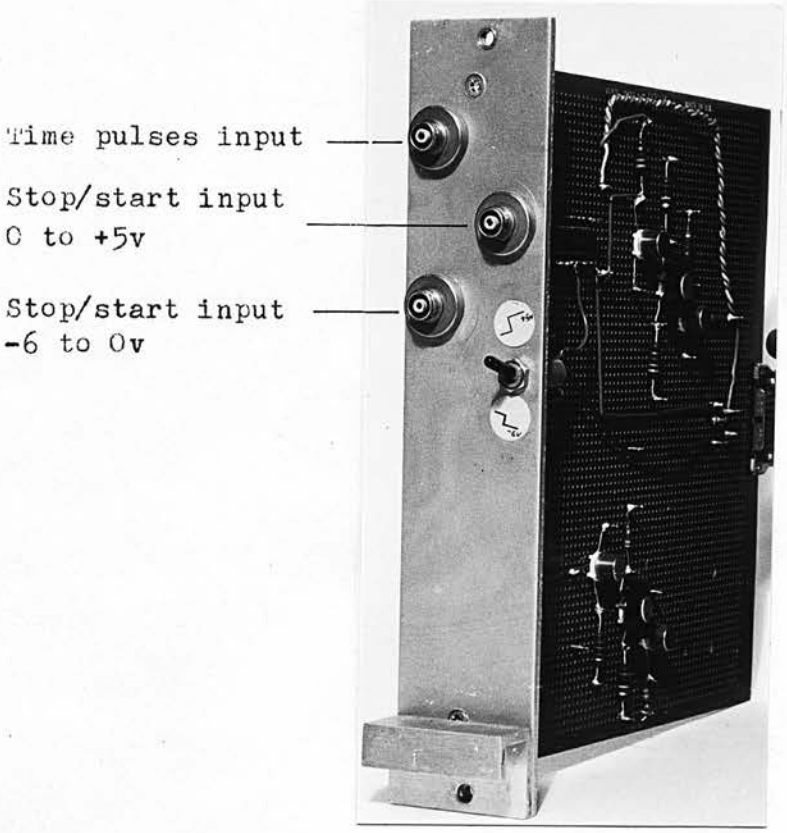

Photograph 6. Layout of the pulse shaping unit.

When the computer is used in the data collection, the start/stop logical level from it is used to operate the automatic system. This level can be fed directly to the other units without need to be converted by the pulse shaper. For that reason a two way switch (SW) is used to select either the start/stop level from the P.H.A. which has to be converted to a logic level, or the logic start/stop level from the computer, to operate the system.

3.4 The Tape Punch Control Unit.

Fig. 16 shows the tape puncher control circuit. It is to switch on and off the H.S.T.P. at a preselected time. The circuit is built in a plug-in module as in photograph 7. The circuit is operated by the time pulse output from the P.H.A. which provides a pulse every second. These pulses are of negative polarity and they are converted to logic pulses by means of the pulse shaper described in the previous section. The system is built around a scaler of 4000 counts maximum. The scaler is built from three decade counters (2, 3 and 4 in figure 16) and two J.K. flip flops (1 and 5) in the same figure.

With an input of one pulse every second from the time pulse output of the P.H.A., each counter output will change at the times shown in table 4. Usually these outputs start from the reset condition where all the outputs are zeroed.

Figure 16. Circuit diagram of the H.S.T.P. control unit. Each IC is connected to earth and to + 5V supply from the corresponding pins. In the figure CL is clear, CP is clock pulse and R is zero reset. List of components is in table 3.

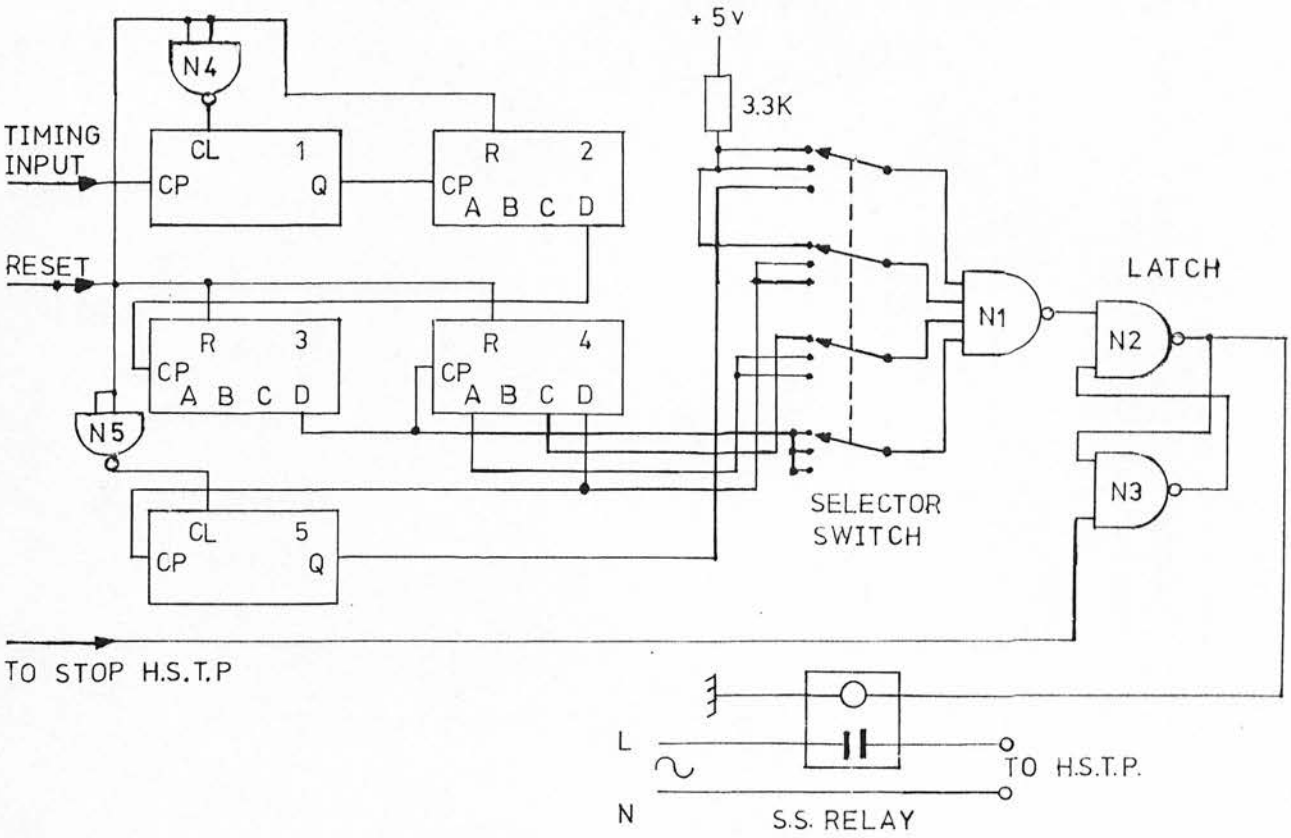
+ 5 v
3.3K
N4
TIMING INPUT
CL 1
CP Q
R 2
CP A B C D
RESET
R 3
CP A B C D
R 4
CP A B C D
N5
CL 5
CP Q
N1
N2
N3
LATCH
SELECTOR SWITCH
TO STOP H.S.T.P
L
N
TO H.S.T.P.
S.S. RELAY

Table 3. List of components of figure 16.

Designation	Description	Type
1 and 5	J.K. flip flop	SN7476N
2, 3 and 4	decade counter	SN7490N
N1	4-input nand gate	½SN7420N
N2, N3, N4 and N5	2-input nand gate	½SN7400N
Selector switch	rotary switch 4 pole 3 way	Min. Maka
S.S. relay	solid state relay	D2425

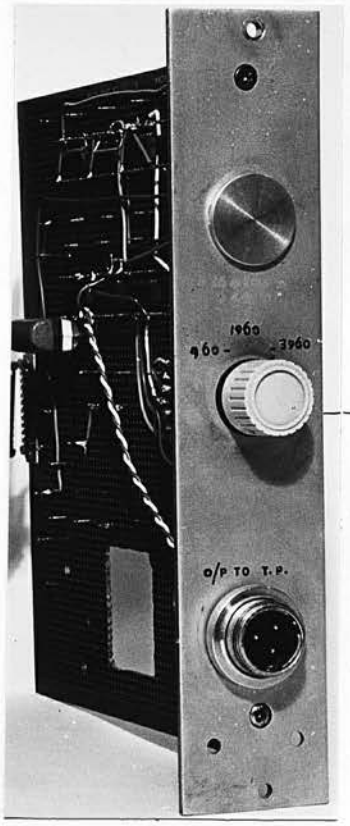

Photograph 7. Layout of the H.S.T.P. control unit.

Table 4. The counter outputs at different times.

Q_1	output	every	1	seconds
A_2	"	"	2	"
B_2	"	"	4	"
C_2	"	"	8	"
D_2	"	"	16	"
A_3	"	"	20	"
B_3	"	"	40	"
C_3	"	"	80	"
D_3	"	"	160	"
A_4	"	"	200	"
B_4	"	"	400	"
C_4	"	"	800	"
D_4	"	"	1600	"
Q_5	"	"	2000	"

A combination of the outputs can be selected by gating so that a signal is obtained at a predetermined time after the start of the count. For the present experiment, output signals from the scaler obtained at one of three predetermined times can be selected by means of a rotary switch leading to a nand gate (N1). The three predetermined times are 960, 1960 and 3960 seconds. The signals obtained at any one of these preselected times are used to switch on the H.S.T.P. 40 seconds before the end of the preselected measuring time. The measuring time can be selected from the P.H.A. as 1000, 2000 or 4000 seconds, respectively. The scaler outputs required to trigger the 4 input nand gate (N1) at each predetermined time are taken according to table 4 as follows:

C_4D_3H H changes the 4 input nand gate output after 960 seconds from start.

$D_4A_4D_3H$ changes the 4 input nand gate output after 1960 seconds from start.

$Q_5D_4A_4D_3$ changes the 4 input nand gate output after 3960 seconds from start.

Here H indicates a high level input to the nand gate which is usually taken as + 5V through a 3.3 kΩ resistor to the input of any gate. The four outputs of the scaler selected as before are connected to a 4 pole, 3 way rotary switch. The 4 poles are leading to the 4 input nand gate (N1). The output of this gate is fed to a latch made of two nand gates (N2 and N3) connected as in the figure. Its output drives a solid state relay type no. D2425 supplied by International Rectifier, England.

This relay when energised, allows the mains to pass through to the H.S.T.P. The H.S.T.P. can only be switched off by de-energising the relay which can be done by resetting the latch. The reset signal is taken from the start/stop transition output from the P.H.A. through monostable 7 in figure 17. The monostable can be triggered only with the start signal from the P.H.A. Its Q output is connected internally through the back of the rack to the reset input of this circuit to reset the latch through nor gate N2 as well as resetting all the scaler outputs to zero.

The solid state relay is mounted in a diecast box to keep the source of e.m. fields shielded and remote from the logic circuits. Experience with electro-mechanical relays to control the H.S.T.P. showed the noise generation and interference with data outputs that can be incurred. The use of a solid state relay incorporating zero switching and opto-isolation overcame most of these problems. Further discussion appears in section 3.6.

3.5 The P.H.A. Stopping Unit.

The circuit employed to stop the P.H.A. is shown in figure 17. It is built in a double width plug-in module as shown in photograph 8. The circuit is designed to stop the P.H.A. at the end of a preselected number of runs required to do certain neutron polarization measurements. The running time is usually 2000 seconds interspersed with 300 seconds intervals and is repeated several times. These intervals allow for the rotation of the polarimeter

Figure 17. Circuit diagram of the P.H.A. stopping unit. Each IC is connected to earth and to + 5V supply from the corresponding pins. In decade counter 1 and 2, CP represents clock pulse input and R zero reset input. The list of components is in table 5.

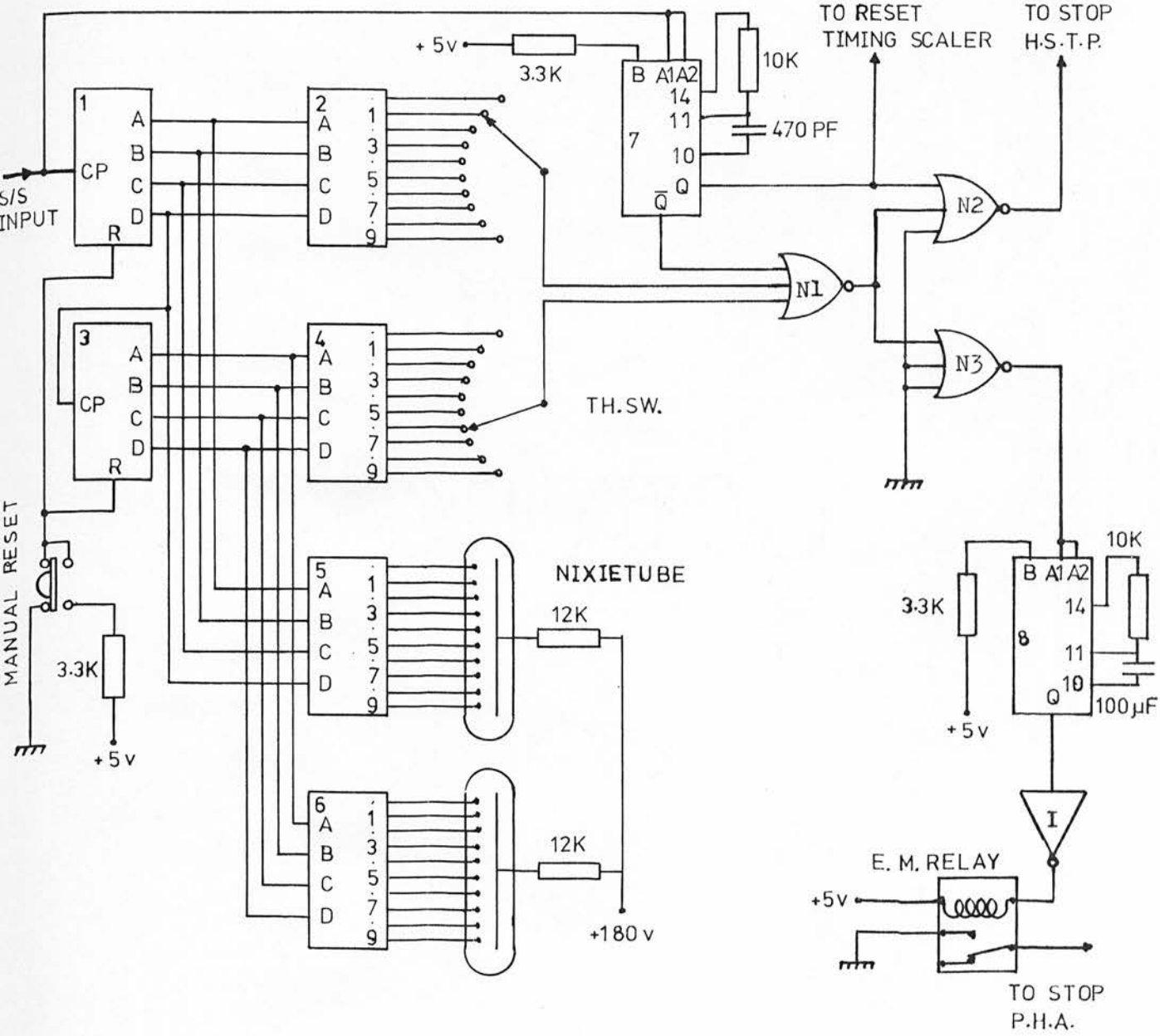
TO RESET
TIMING SCALER
TO STOP
H.S.T.P.
+5v
3.3K
10K
470 PF
S/S
INPUT
CP
R
N1
N2
N3
TH.SW.
MANUAL RESET
NIXIETUBE
12K
12K
+180v
100μF
E. M. RELAY
TO STOP
P.H.A.

Table 5. List of components of figure 17.

Designation	Description	Type
1 and 3	decade counter	SN7490N
2 and 4	BCD to decimal decoder	SN7442N
5 and 6	BCD to decimal decoder driver	SN74141N
7 and 8	Monostable multivibrator	SN74121N
N1, N2 and N3	3-input nor gate	$\frac{1}{3}$SN7427N
I	inverter driver	$\frac{1}{6}$SN7406N
Th. Sw.	thumb switch	D Edge SW
Nixie Tube	numerical indicator tube	Num. Tube
Manual reset	push-button switch	Min. push
E.M. Relay	elect. mechanical relay	Relay 15

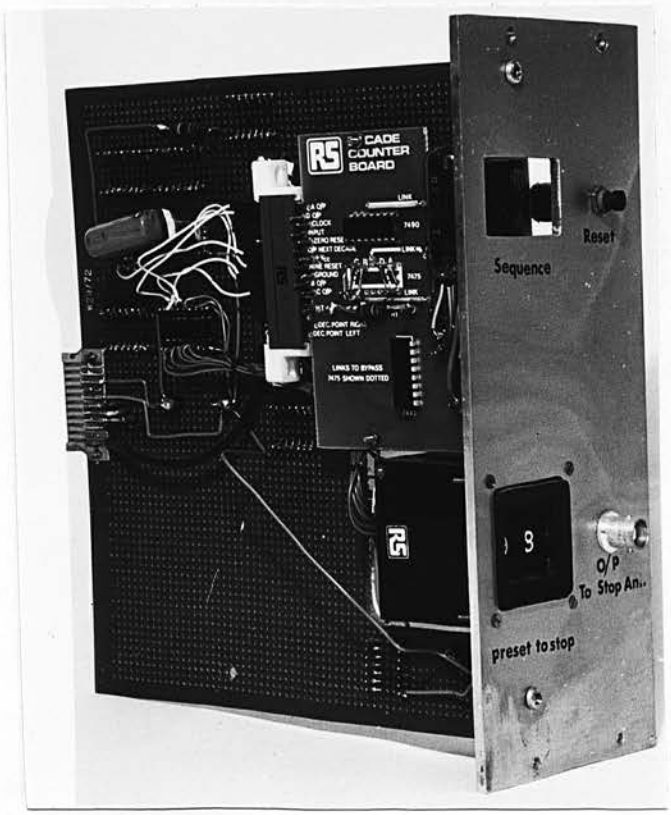

Photograph 8. Layout of the P.H.A. stopping unit.

and the printing out of the contents of the memory of the analyser at the end of each measurement.

The circuit is built around a scaler of 99 counts maximum operated by the start signal from the start/stop output of the P.H.A. The scaler is built with two decade counters 1 and 3 in figure 17. The start signals are supplied to the clock input of the first decade counter 1 at a rate of one signal per run. The outputs of counter 1 are connected to the inputs of two decoders (decoder 2 and decoder driver 5). Each decodes the BCD number to produce a count up to nine in one count increments. Decoder 2 outputs are connected to a thumb switch with 10 ways and one pole. Decoder driver 5 outputs drive a 'nixie' tube to indicate the number of runs.

The D output of decade counter 1 is fed to the clock input of decade counter 3 at a rate of one signal per 10 runs. The output of I.C.3 is decoded by I.C.'s 4 and 6. Their outputs produce an increase of one count every ten runs. Decoder 4 outputs are connected to another thumb switch and decoder driver 6 drives a 'nixie' tube to indicate number of tens of runs.

The outputs of decoders 2 and 4 which correspond to the maximum number of runs required to complete a certain measurement can be selected by means of the two thumb switches, and can be used to stop the P.H.A. and the H.S.T.P. The two thumb switches pass the signals to a three input nor gate 1.

Its output is fed to both nor gate 2 and nor gate 3. Nor gate 2 output is used to stop the H.S.T.P. as described in the previous section, and nor gate 3 output is used to stop the P.H.A.

The start/stop input to A_1 and A_2 of monostable 7 are used with B input kept at a high level by connecting it to + 5V through a resistor of 3.3 kΩ, so that the monostable can only be triggered with negative going inputs associated with the start signal from the P.H.A.

With each start signal the Q output of monostable 7 is produced and used to reset the timing scaler, described in the previous section, and through nor gate 2 to reset the latch controlling the running of the H.S.T.P. (figure 16).

The $\overline{Q}$ output of monostable 7 is connected to the third input of nor gate 1 so that a pulse can be produced at the end of the preselected number of runs and fed to nor gate 2 and 3. Nor gate 3 is used as a spare gate so it can be used to stop the experiment by feeding its input with pulses from other equipment. In the present case this has not been required so the two other inputs were tied to earth.

Monostable 8 is used to energise the relay through the inverter driver for about 0.7 seconds. This is achieved by selecting the external resistor and capacitor and connecting them to pins 10, 11 and 14. The monostable produces a pulse with

a width of about 0.7 seconds, if the resistor is 10 kΩ and the capacitor is 100 μF as shown in the figure. The Q output of monostable 8 is fed to the inverter driver I and then to an electro-mechanical relay type 912 supplied by R.S. Components Limited, England. The relay energises when the Q output goes high and de-energises when it goes low. This time was found sufficient to stop the P.H.A.

The power supply to the 'nixie' tubes is connected to the back of the bin and +180V is connected to the anodes of the tubes through resistors of 12 kΩ as recommended by the manufacturer.

Each 'nixie' tube is mounted on a special printed circuit board supplied by R.S. Components. The board also accommodates the decade counter and the decoder driver which reduces the amount of wiring and susceptibility to noise.

3.6 The Rotation of the Polarimeter Control Unit.

Figure 18 shows the circuit diagram of the control unit used for the polarimeter rotation to interchange the positions of the two side detectors. The circuit is basically designed to operate a motor, mounted to the frame of the polarimeter, with a shaft in contact with the rear end plate of the cradle as can be seen from photograph 5. The operation of the motor is controlled by two relays. The first relay R1 is for selecting the direction of rotation (i.e. clockwise or anticlockwise) and

Figure 18. Circuit diagram of the motor controlling unit. Each IC is connected to ground and to + 5V supply from the corresponding input pins. Each monostable is provided with a capacitor connected between pin 10 and pin 11 and a resistor connected between pin 11 and pin 14, to give the desired pulse width as in table 6.

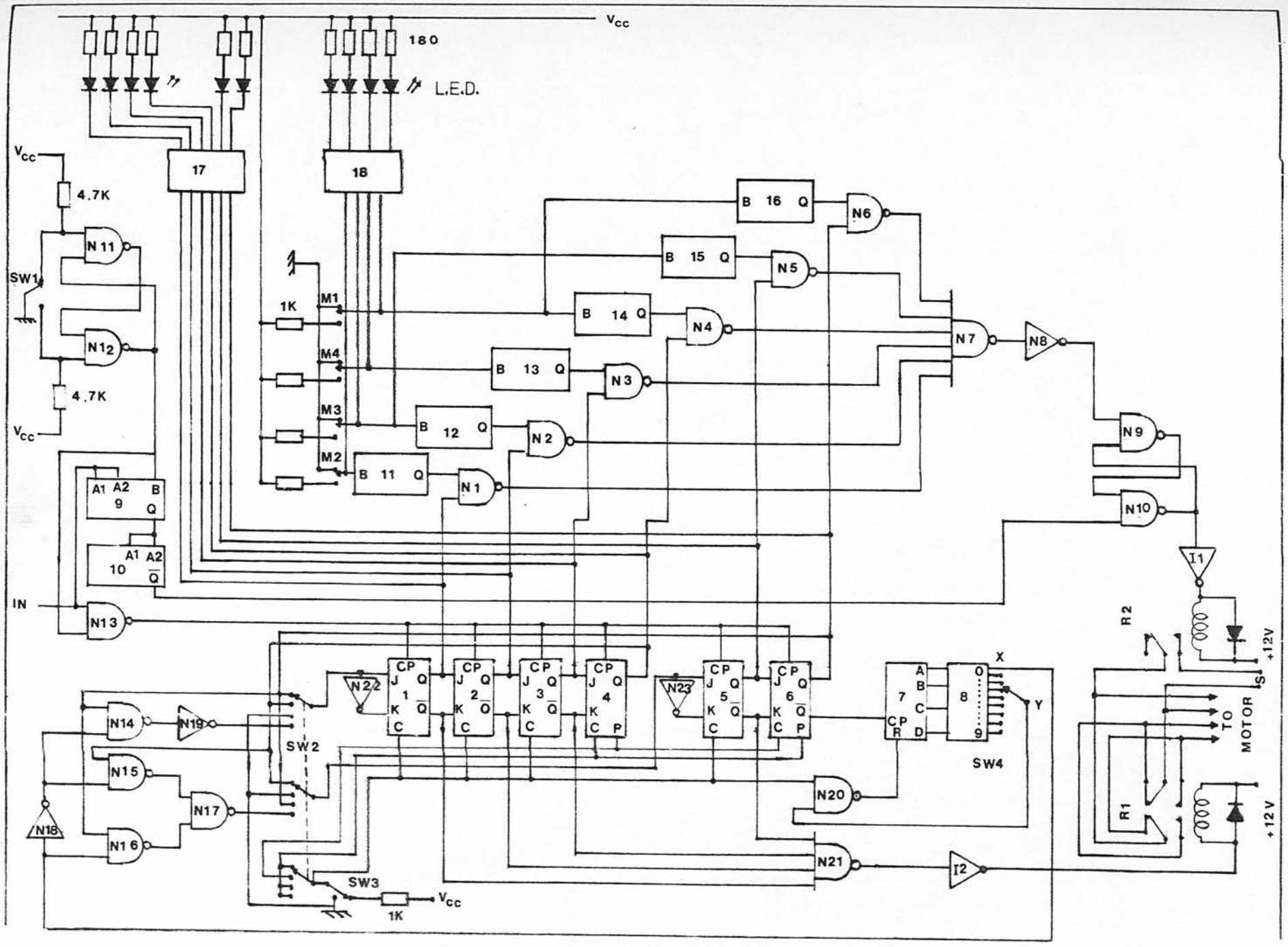
Vcc
180
L.E.D.
17
18
4.7K
N11
SW1
N12
4.7K
Vcc
1K
M1
M4
M3
M2
B 16 Q
B 15 Q
B 14 Q
B 13 Q
B 12 Q
B 11 Q
N6
N5
N4
N3
N2
N1
N7
N8
N9
N10
I1
A1 A2 B
9 Q
10 A1 A2
Q
IN
N13
N14
N19
N15
N17
N18
N16
SW2
N22
N23
CP J Q
1 K Q
C
2
3
4
5
6
P
7 CP R
A
B
C
D
8
0
9
X
Y
SW4
N20
N21
I2
SW3
1K
Vcc
R2
R1
+12V
+12V
TO MOTOR
S

Table 6. Monostable outputs pulse width.

Monostable	Capacitor	Resistor	Pulse width
9	470 μf	10 kΩ	0.7 sec
10	180 pF	10 kΩ	1 μs
11 - 16	18 pF	10 kΩ	0.1 μs

All unused inputs and outputs are connected as recommended by reference 62 .

List of components is in table 7.

Table 7. List of components of figure 18.

Designation	Description	Type
1 to 6	J.K. flip flop	SN7476N
7	Decade counter	SN7490N
8	BCD to decimal decoder	SN7442N
9 to 16	Monostable Multivibrator	SN74121N
N1 to N6	2-input Nand gate	¼SN7400N
N7	8-input Nand gate	SN7430N
N8 to N20*	2-input Nand gate	¼SN7400N
N21	4-input Nand gate	½SN7420N
N22 and N23*	2-input Nand gate	¼SN7400N
I1, I2, I7 and I8	Inverter driver	$\frac{1}{6}$SN7406N
R1 and R2	Electro-mechanical relay	Type 1A
SW1	Switch, 1 pole 2 way	Type M/Toggle
SW2	Rotary switch, 3 pole 4 way	Min. Maka
SW3	Push-button switch	Min. push
SW4	Rotary switch, 1 pole 10 way	Min. Maka
M1, M2, M3 and M4	Microswitch	Micro. Sw.
L.E.D.	Light emitting diode.	

* N8, N18, N19, N22 and N23 each is two-input Nand gate with the two inputs tied together to function as an inverter where each is represented in the figure as an inverter for simplicity. All IC's are supplied by Quarndon Electronics, Derby, England and all switches and relays by R.S. Components, London, England.

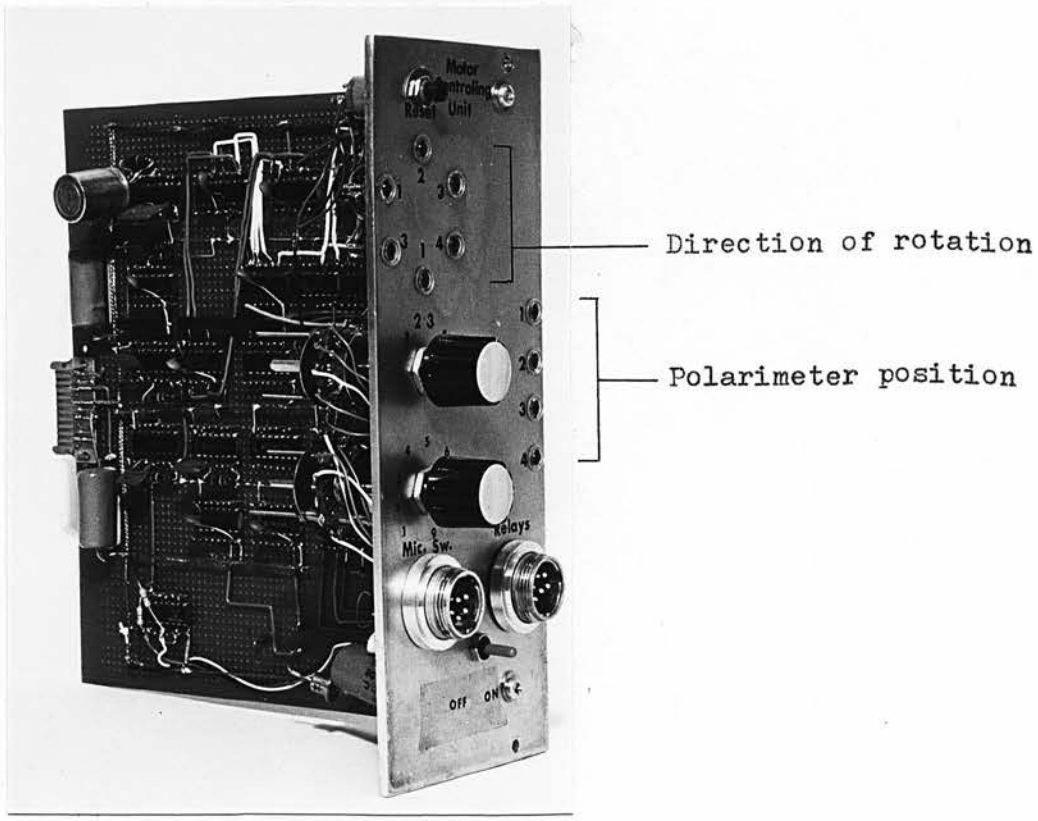

Photograph 9. Layout of the motor control unit.

the second relay R2 is to feed the mains to the motor through relay R1. Both R1 and R2 are initially energised by the stop level from the start/stop level output of the P.H.A. or the computer. To avoid energising both relays simultaneously, which may create a high level of noise due to the feed back of electromotive force from the motor to the circuit, energising relay R2 is delayed by 0.7 seconds so that relay R1 can be energised and settled during this delay time. The 0.7 seconds delay is selected by using monostable 9 where a capacitor of 100 μF is connected between pin 10 and pin 11 and a resistor of 10 kΩ is connected between pin 11 and pin 14 (not shown in the figure for clarity). According to the selected capacitor and resistor the Q output of monostable 9 will be a pulse of 0.7 seconds width. The negative going edge of this pulse triggers monostable 10 and the $\overline{Q}$ output is used to set a latch made of two nand gates N9 and N10 as in the figure which change the output level of an inverter driver I1 to energise R2.

The stopping of the polarimeter at the desired position is controlled by Q outputs of a ring counter of 6 counts made from six J.K. flip flops 1 to 6 as connected in the figure and four microswitches M1, M2, M3 and M4 mounted to the frame of the polarimeter as in photograph 5. The ring counter can be used in four different modes of sequence of rotation according to the setting of rotary switch SW2. For describing the functions of this ring counter let us take the first setting of SW2 as shown in the figure. In this case Q6 output is connected to J1 input

and the same output is inverted and connected to K1 input. Also Q4 output and its inverted output are connected to J5 and K5 respectively. So all the six J.K. flip flops are in use. By pressing the push button reset switch SW3, which is in this case connected to the clear C input of J.K. flip flops from 1 to 5 and to the preset input P of J.K. flip flop 6, the Q1 to Q5 outputs become low and only Q6 output becomes high. So if a stop level is delivered to the input several operations will occur as follows:

a. The level delivered to the clock input CP of each J.K. flip flop will shift the high level from Q6 to Q1.

b. $\overline{Q1}$ output changes the level from the four input nand gate N21 and energises R1 through the inverter driver I2, which sets the required direction of rotation according to the connection of the motor leads to the relay.

c. After 0.7 seconds delay through monostable 9 and 10 the stop level sets the latch (N9 and N10) and energises relay R2 through the inverter driver I1 and allows the mains to pass to R1 and to the motor which starts rotating the polarimeter.

d. When the polarimeter reaches microswitch M2 it triggers monostable 11 and its Q output triggers nand gate N1 then nand gate N7 and the inverter N8 which resets the latch and de-energises R2 and stops the polarimeter rotation at that particular position. The polarimeter does not stop at any other position even if it passes through the other microswitches. This is done by using two input nand gates

N1 to N6 where each microswitch is connected to one input through a monostable and the second input is provided by the Q outputs of the ring counter. As the Q outputs are all, except one, at low level no effect will occur to any output of these nand gates except the one attached to a Q output at a high level. So according to the connection of the circuit:

If Q1 is at high level the polarimeter stops only at M2,
If Q2 is at high level the polarimeter stops only at M3,
If Q3 is at high level the polarimeter stops only at M4,
If Q4 is at high level the polarimeter stops only at M1,
If Q5 is at high level the polarimeter stops only at M3 and
If Q6 is at high level the polarimeter stops only at M1.

Each Q output of the ring counter is connected to an L.E.D. through the Hex inverter driver 17 to indicate the state of the ring counter, direction of rotation and the mode of sequence of rotation in use. Also each microswitch is connected to an L.E.D., through the Hex inverter driver 18, to indicate the position of the polarimeter. Each L.E.D. is connected to the + 5V through a resistor of 180Ω to limit the voltage to be applied across the L.E.D.

The direction of rotation of the polarimeter is controlled by the $\overline{Q}$ outputs of the ring counter. $\overline{Q}1$, $\overline{Q}2$, $\overline{Q}3$ and $\overline{Q}5$ outputs are connected to four input nand gate N21, so when one of these $\overline{Q}$ outputs is at a low level R1 will be energised and the

polarimeter will rotate clockwise and when all these $\bar{Q}$ outputs are at a high level R1 will be de-energised and the polarimeter will rotate anticlockwise. The direction of rotation of the motor can be selected according to the connection of the leads of the motor to the contacts of relay R1. The motor type SD18WS is of ⅛ HP and operates at 1 r.p.m. (Parvalux Electric Motors Ltd., Bournemouth, England). Relays R1 and R2 are electro-mechanical relays with two-pole changeover contacts type 1A supplied by R.S. Components Ltd., London.

Monostables 11 to 16 type SN74121N are used to provide a pulse with 100 n s width selected by connecting a capacitor of 18 pF between pin 10 and pin 11 and a resistor of 10 kΩ between pin 11 and pin 14 (not shown in the figure for clarity). The A_1 and A_2 inputs of each monostable are connected to ground (not shown) so that the monostable triggers only at the positive going edge provided by the microswitches M1 to M4 where each is connected to + 5V through a resistor of 1 kΩ.

3.6.1 Mode of Rotation Selector.

In the neutron polarization measurements a check on the freedom of the system from false asymmetry is frequently required. In the present system the measurement of the asymmetry in the vertical plane can give a good indication on the existence or non-existence of a such false asymmetry (in the vertical plane the asymmetry should be zero). For this reason special arrangement

has been made in the circuit so that the polarimeter can be located at a position to measure the asymmetry in the vertical plane or in the horizontal plane as follows:

Mode 1. Switch SW2 to be connected as in the figure. In this case the polarimeter will be located to measure the asymmetry in the horizontal plane twice as often as in the vertical plane and the sequence of rotation will be as follows:
position 1 - position 2 - position 3 - position 4 - position 1 - position 3, where position 1 and 3 represent the horizontal orientation and position 2 and 4 represent the vertical orientation.

Mode 2. SW2 to be rotated to the second setting. In this case the polarimeter will be located to measure the asymmetry in the horizontal plane as often as in the vertical plane and the sequence of the rotation will be as follows:
position 1 - position 2 - position 3 - position 4.

Mode 3. SW2 to be rotated to the third setting. In this case the polarimeter will be located to measure the asymmetry in the horizontal plane only and the sequence of rotation will be between positions 1 and 3 only.

Mode 4. SW2 to be rotated to the fourth setting. In this case the polarimeter will be located to measure the asymmetry in the horizontal plane several times as much as in the vertical plane according to the setting of SW4 which can be set to make the ratio of the measurement in the horizontal plane to the vertical plane vary from 3:1 to 10:1.

Modes 1, 2 and 3 can be applied by using the six J.K. flip flops as shown in the figure, but for mode 4 several integrated circuits had to be added to achieve this type of sequence. J.K. flip flops 5 and 6 are used for repeating the measurements in the horizontal plane where Q5 is associated with position 3 and Q6 with position 1. Decade counter 7 and decoder 8 are used to select the number of the required repetitions of the measurement in the horizontal plane.

In mode 4 the J1 input is controlled by N14 and N19 where each is a two input nand gate. One input to N14 is the Q6 output and the other input is the inverted X output where X is the 0 output of decoder 8. So J1 input can be given as $Q6.\overline{X}$ where J1 can be at high level when Q6 is at high level and X at low level only. J5 input is controlled by N15, N16, N17, N18 and N20. It can be seen from the figure that J5 input can be given as $\overline{X}Q4 + XQ6$ where J5 can be at high level when either Q4 is at high level and X at low level or both X and Q6 are at high level only. Nand gate N20 is used to reset the decade counter 7 after completing the number of measurements in the horizontal plane selected by SW4 and its output Y. Table 8 shows the sequence of Q outputs of the ring counter, J1, J5 inputs and X output in mode 4 where the number of repetitions of the measurement in the horizontal plane is selected to be four times more than the measurements in the vertical plane.

Table 8. The truth table of the ring counter at mode 4.

	Q1	Q2	Q3	Q4	Q5	Q6	X	J1	J5	Y
Reset	L	L	L	L	L	H	L	H	L	H
1st input	H	L	L	L	L	L	L	L	L	H
2nd input	L	H	L	L	L	L	L	L	L	H
3rd input	L	L	H	L	L	L	L	L	L	H
4th input	L	L	L	H	L	L	L	L	H	L
5th input	L	L	L	L	H	L	L	L	L	H
6th input	L	L	L	L	L	H	H	L	H	H
7th input	L	L	L	L	H	L	H	L	L	H
8th input	L	L	L	L	L	H	H	L	H	H
9th input	L	L	L	L	H	L	H	L	L	H
10th input	L	L	L	L	L	H	L	H	L	⊔
11th input	H	L	L	L	L	L	L	L	L	H

3.6.2 The Operation of the Switch SW1.

The automatic system is usually connected to the start/stop output of the P.H.A. or the computer. Both these data collection systems are periodically used for other experiments and frequently used for testing the electronics of this experiment. To avoid disconnecting the cables every time the P.H.A. or the computer is taken over by another experimenter, a switch SW1 is used to cut off the signals from the P.H.A. to the automatic system. SW1 is connected to the system through nand gates N11 and N12. If SW1 is connected as shown in the figure, N11 output will be high and N12 output will be low. N12 output is connected to B input of monostable 9 and to N13, so keeping B input of 9 at a low level will inhibit any output from 9 and any input to nand gate N13 will not affect its output. But if SW1 is connected to the other side N12 output will be high which enables monostable 9 to be triggered by the stop level to A_1 and A_2 inputs, also N13 can be triggered by the same stop level to operate the ring counter.

3.7 Noise Immunity.

The automatic system circuitry was initially powered by a commercial power supply providing the logic circuitry with + 5V and the relays with + 12V. The former supply was derived by two zener stabilised stages with a current capability of 1 amp. During the testing of the system it was noticed that a high noise

existed on both power and signal lines and falsely triggered the gates thereby introducing errors into the system. Several decoupling capacitors of 2.2 μF were added to the circuits and connected between the + 5V supply line and earth after every 5 IC's on each board. This reduced the noise effect but did not eliminate it. More decoupling capacitors were used especially to each IC of figure 18, where a ceramic capacitor of 0.01 μF was connected between the V_{cc} pin and the earth pin of each IC. It was noticed that most of the noise was created when the H.S.T.P. switched on or when the relays were energised. To start the motor of the H.S.T.P., 10 amps is required from the mains supply; this was the worst source of noise particularly in the early stages when an electro-mechanical relay was in use. The relay was replaced with a solid state relay which has a better performance and high noise immunity. A combination of capacitor and resistor of 0.1 μF and 47 ohms respectively were connected in series accross the mains input of the solid state relay in order to suppress the voltage surges due to the switching of the H.S.T.P. and consequently its effect on the automatic system.

As the problems of the noise created by the H.S.T.P. were solved the noise created by energising of the two relays R1 and R2 of figure 18 still existed so it was decided to build a separate power supply for these relays, and another two power supplies, one to provide the logic circuits with + 5V and the other to provide the shaping unit with - 6V. After designing, constructing and connecting the three new power supplies a very

good performance was achieved and the noise created by the different sources was eliminated completely.

In the design of the power supplies several factors were taken into account; reliability, economy, minimum component count and space. All these factors have been achieved by using the voltage regulator type NE550A supplied by Quarndon Electronics, England, to provide the system with + 5V and - 6V and a voltage regulator type MVR12V supplied by R.S. components, England, to provide the relay with the required + 12V. The transformers, capacitors and rectifiers are mounted on the back of the bin and their outputs are internally connected to the voltage regulator. The three voltage regulators and the associated circuits are built in one plug-in module. The output of each power supply is internally connected to other units through the back of the bin. The circuit diagrams of each power supply with brief descriptions will be given in the following section.

3.8 The Power Supplies.

The circuit diagram for the complete regulated + 5V supply is shown in figure 19. This circuit is based on the voltage regulator NE550A and the power transistor Q. The internal circuit of the voltage regulator NE550A is shown in figure 20. In figure 19 the frequency compensation used 1000 pF to ensure stability of the output. Short circuit protection is provided by R_{sc} and

Figure 19. Circuit diagram of the regulated + 5V supply

Figure 20. Circuit diagram of the IC NE550A

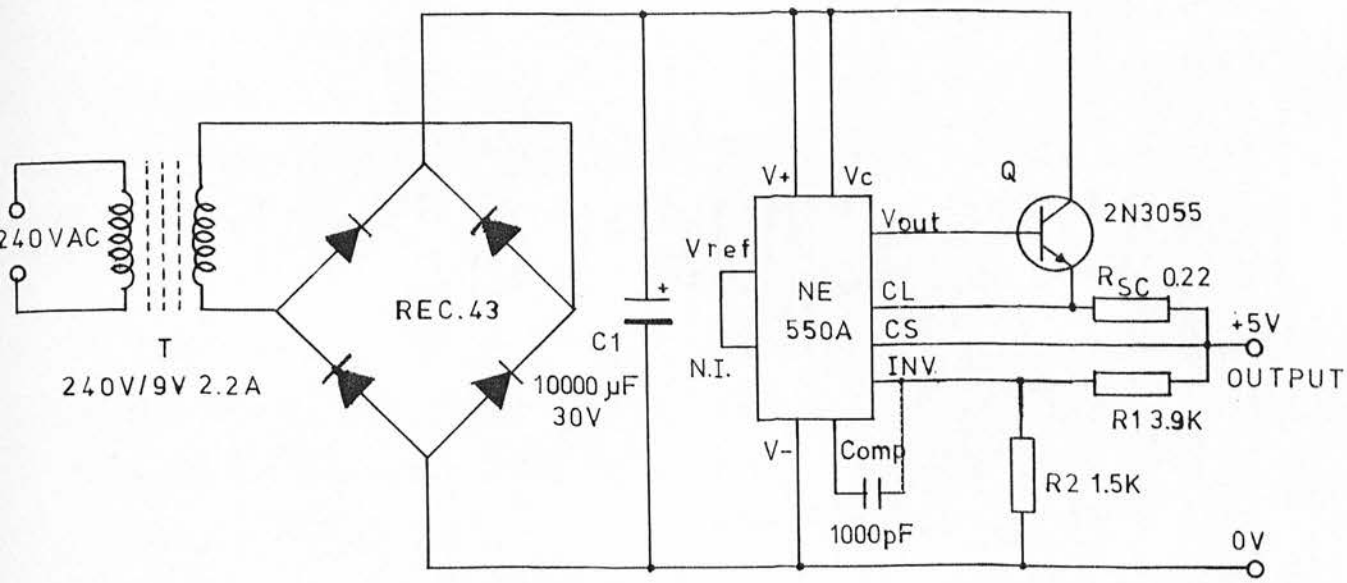
240VAC
T
240V/9V 2.2A
REC.43
C1
10000 µF
30V
V+
Vc
Q
2N3055
Vout
Vref
NE
550A
CL
CS
INV
N.I.
V-
Comp
1000pF
R2 1.5K
R_{SC} 0.22
+5V
OUTPUT
R1 3.9K
0V

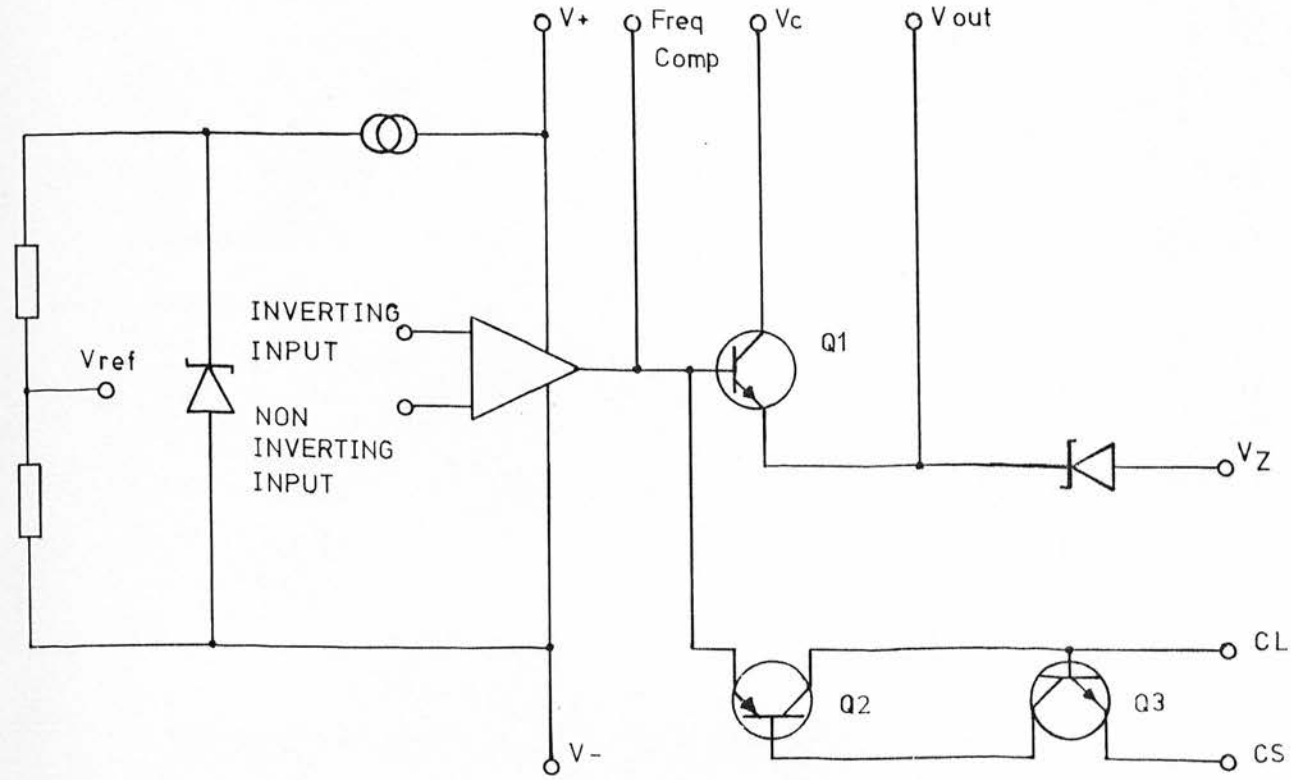
V+
Freq
Comp
Vc
Vout
Vref
INVERTING
INPUT
NON
INVERTING
INPUT
Q1
V_Z
CL
Q2
Q3
CS
V-

the transistor within the voltage regulator Q3 of figure 20. The output voltage and current obtained from the unit is a function of the used components. Using a 9V centre-tapped transformer with 2.2 A capacity and selecting the resistors R1 and R2 the circuit provides 2 A at 5 volts output voltage with a load regulation of 1% of the output voltage.

For the - 6V supply another voltage regulator of the same type is used. The circuit diagram of the complete power supply is shown in figure 21. This supply is used for the shaping unit circuit of figure 15. As only very low current is needed a PNP transistor 2N1132 is used instead of transistor 2N3055 of figure 19. The output voltage of the circuit was - 8V so another stage of transistor T2 and zener diode Z were used to obtain the desired - 6V output.

The + 12V supply is used to operate the relays R1 and R2 of figure 18. Each relay draws 120 mA when energised so the voltage regulator MVR12V, available at the time in this laboratory, was found sufficient to provide the system with the required current and voltage. The circuit diagram of the complete regulated + 12V power supply is shown in figure 22. This type of voltage regulator has a high noise immunity and short circuit protection.

3.9 Conclusion.

The performance of the automatic system became very reliable after removing all sources of noise and it has been used for

Figure 21. Circuit diagram of the - 6V supply

Figure 22. Circuit diagram of the + 12V supply.

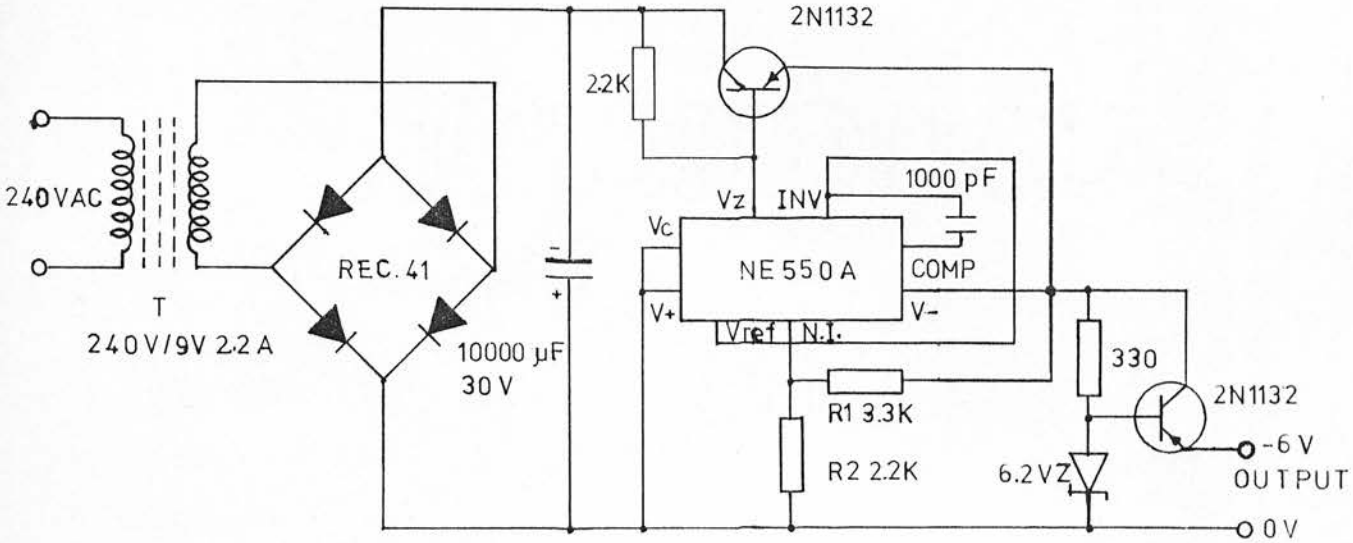
2N1132
2.2K
240VAC
REC. 41
T
240V/9V 2.2A
10000 µF
30 V
1000 pF
Vz
INV
Vc
NE 550 A
COMP
V+
V-
Vref
N.I.
330
2N1132
R1 3.3K
R2 2.2K
6.2VZ
-6 V
OUTPUT
0 V

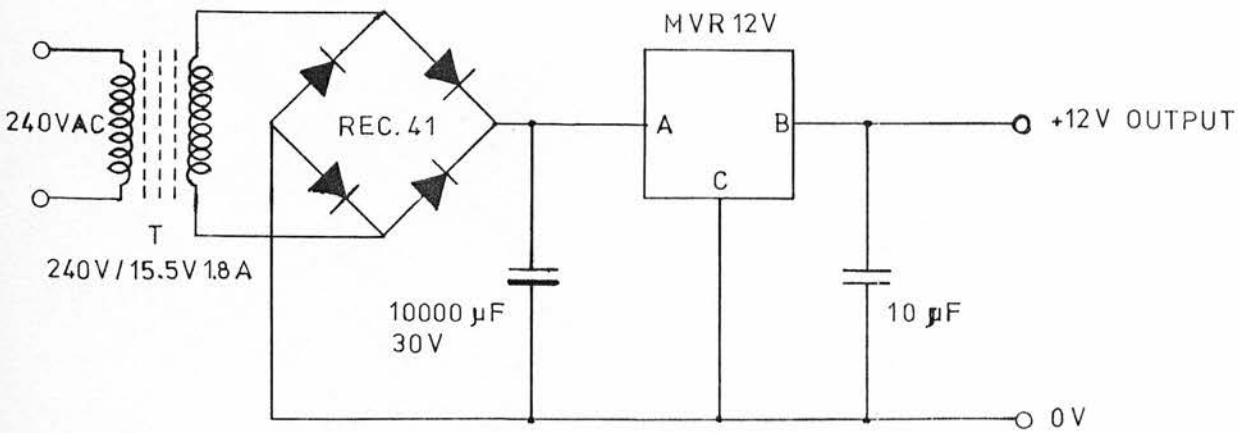
MVR 12V
240VAC
REC. 41
A
B
C
+12V OUTPUT
T
240V/15.5V 1.8A
10000 µF
30V
10 µF
0 V

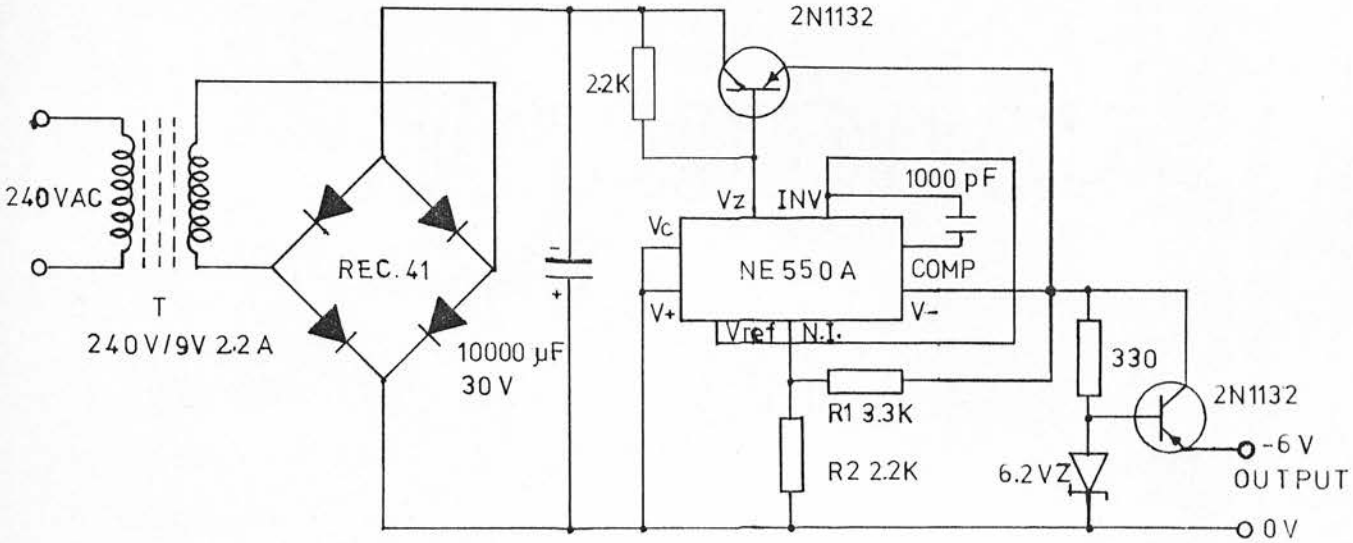
2N1132
2.2K
240VAC
REC. 41
T
240V/9V 2.2A
10000 µF
30 V
1000 pF
Vz
INV
Vc
NE 550 A
COMP
V+
V-
Vref
N.I.
330
2N1132
R1 3.3K
R2 2.2K
6.2VZ
-6 V
OUTPUT
0 V

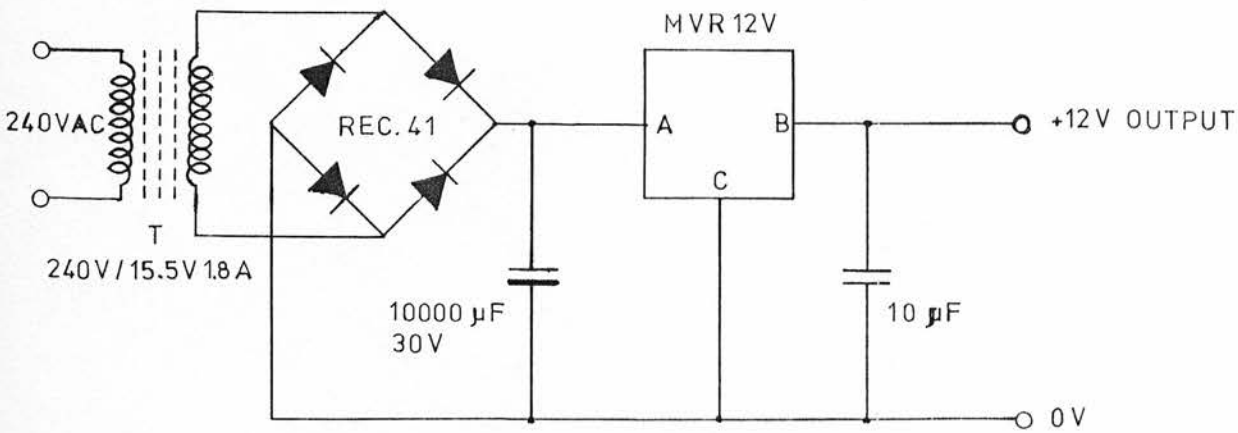
MVR 12V
240VAC
REC. 41
A
B
C
+12V OUTPUT
T
240V/15.5V 1.8A
10000 µF
30V
10 µF
0 V

automatic data collection for very long periods without the need for any external control.

The system was used to run the helium scattering experiment in the high energy region [10] at A.E.R.E. Harwell where it was found very useful in saving time and effort especially for remotely rotating the polarimeter from one position to another; its use has thus reduced the exposure of the operator to high energy radiation.

The system was also used to run the experiment of the associated particle time of flight technique [70] in this laboratory.

The system can be adopted to run any type of experiment involving a motor to be switched on and off at the desired time or location.

CHAPTER 4.

EXPERIMENTAL PROCEDURE.

CHAPTER 4.

EXPERIMENTAL PROCEDURE.

4.1 Introduction.

The experimental procedure used in the present measurement will be described in this chapter. It includes the description of the polarimeter alignment procedure, the set-up of the electronics involved in the measurement, an experimental method to check the interchanging of the two neutron detectors and its effect on their photomultiplier gains, the calibration of the Van de Graaff accelerator by using two different reactions with resonance energies within the limit of the accelerator, the data collection method and the computer programs used in the treatment of the data.

4.2 The Polarimeter Alignment.

In order to make reliable measurements the polarimeter has to be aligned accurately with respect to the collimated neutron beam. The gas scintillation detector has to be centred in the neutron beam to avoid any false asymmetry measurement, which will exist if the gas detector is located asymmetrically with respect to the two side detectors. Also the side detectors have to be located at equal scattering angles and distances from the gas detector to avoid any false asymmetry measurement which will

occur if any change in scattering angles or distances occurs. The detector holders and detector collars were used to locate the detectors at the required scattering angles and distances as described in chapter 2.

The axial alignment of the polarimeter was done by using a telescope and four cylindrical inserts each with an axial hole of 2 mm diameter. Two of these inserts were placed into each end of the collimator tube and the other two into the central hole of each disk of the cradle. The telescope was located to sight down the axis of the neutron collimator at about 2 metres from the back of the polarimeter. The horizontal and vertical positioning of the polarimeter was adjusted so that the centres of the holes of the inserts came into line with cross hairs in the telescope. The accuracy of the alignment of the system using these inserts is achieved to within 0.5 mm. The polarimeter alignment was found unaffected after several months of operation and no further adjustment was needed.

The target alignment was done by the same method using the cylindrical inserts and a fine adjustment to the target assembly was done to locate the target in the right position so that the centre of it came into line with the cross hairs of the telescope. The target assembly design has reduced the need for alignment adjustment since the target holder can be replaced without affecting the alignment.

4.3 The Electronic Set-up.

Before each new measurement, the electronic set-up is checked so that any changes in the detection threshold or the photomultiplier gains can be adjusted to the required setting. The electronic setting is usually done as follows.

Using a ^{22}Na gamma source mounted close to each of the two liquid scintillators, the linear output of the corresponding amplifier is pulse height analysed and the gain of the photomultiplier assessed by finding the Compton edges for the 0.33 and 1.07 MeV recoil electrons. Using this method of gain assessment the photomultipliers are adjusted to have equal gain by varying their high voltages.

To determine the threshold of each side detector, the linear amplifier pulse height spectrum is measured in coincidence with the amplifier discriminator output. This gives a spectrum of the ^{22}Na gammas with a low energy cut-off corresponding to the amplifier discriminator threshold. The cut-off is typically 6 channels wide with the 1.07 MeV Compton edge in channel 60. Using the known proton to electron energy ratio for equal pulse height, this cut-off represents a measure of the neutron detection thresholds of the neutron detectors. The neutron thresholds are then set by adjusting the photomultiplier gains and the amplifier discriminator thresholds. Figure (23) shows the ^{22}Na gamma spectrum with amplifier discriminator in

Figure 23. The ^{22}Na gamma spectrum without coincidence as obtained using a neutron detector.

Figure 24. The ^{22}Na gamma spectrum with coincidence illustrating the threshold determination.

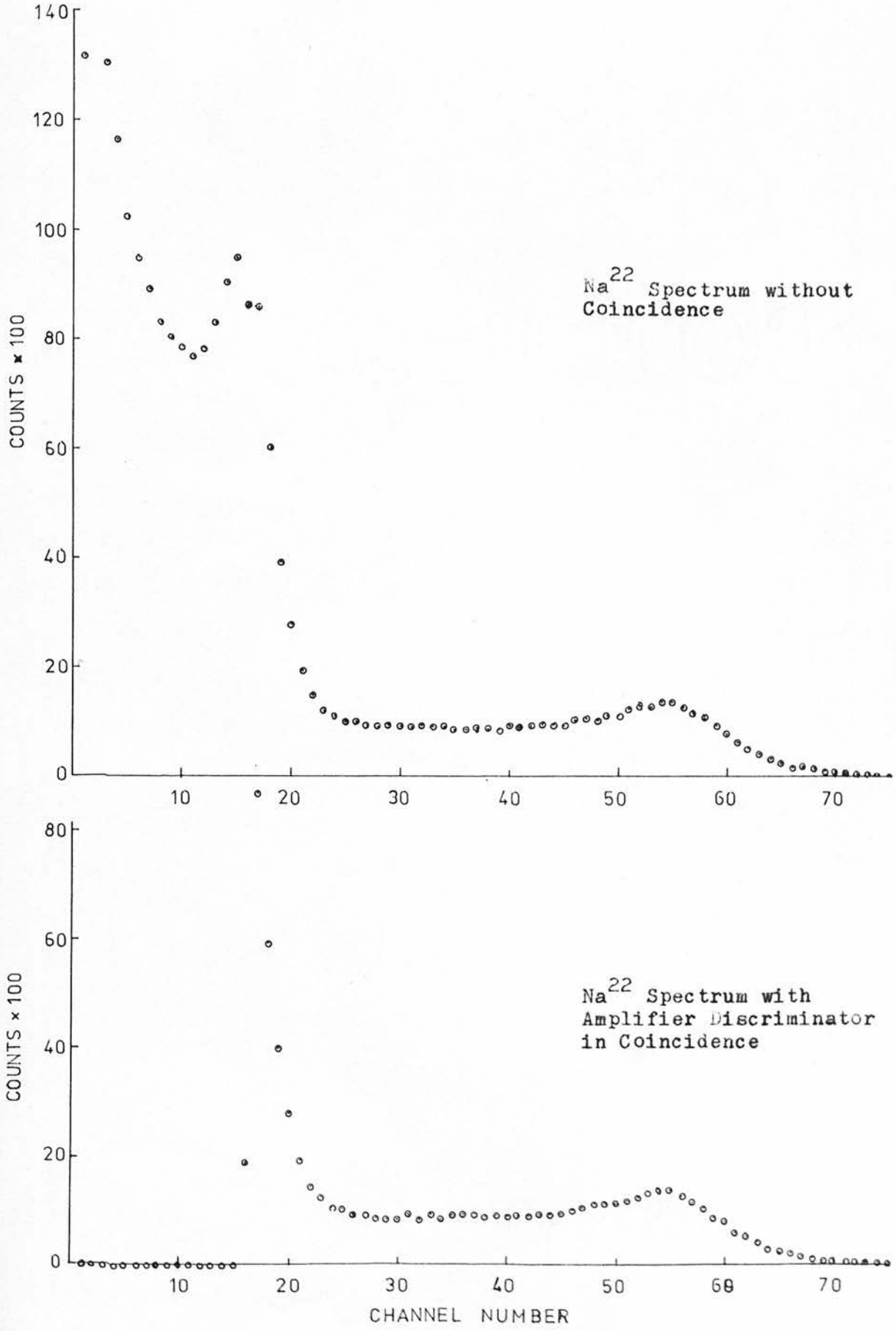
140
120
100
80
60
40
20
0
COUNTS × 100
10
20
30
40
50
60
70
Na22 Spectrum without Coincidence
80
60
40
20
0
COUNTS × 100
10
20
30
40
50
60
70
CHANNEL NUMBER
Na22 Spectrum with Amplifier Discriminator in Coincidence

coincidence where the discriminator is set so that only events higher than 300 keV recoil electrons can be detected and figure 24 shows the ^{22}Na gamma spectrum without coincidence.

To reject events due to gamma rays the pulse shape discrimination technique is used. This method is based on the fact that in some organic scintillators the decay time of the scintillations due to electron recoils from incident gamma rays is different from the decay time of scintillations due to proton recoils from incident neutrons. In the P.S.D. circuit used in the present experiment an RC integration in the pre-amplifier followed by a double RC differentiation is applied to the linear current pulses from the photomultiplier of the side detector. After this shaping the output pulses corresponding to neutron events will have a longer time from the start of the pulse to its crossing the zero amplitude baseline, than for those corresponding to gamma rays. This time interval is converted into a proportional voltage pulse in a time to pulse height converter built within the P.S.D. circuit. Figure 25 shows a ^{252}Cf spectrum obtained from the output of the P.S.D. unit in coincidence with an amplifier discriminator which was set to accept events with a light output greater than that produced by a 300 keV electron recoil in the scintillator.

The P.S.D. pulse height spectrum, using a ^{252}Cf source placed beside the scintillator, is measured in coincidence with P.S.D. discriminator output, so that a threshold may be set to

Figure 25 Relative pulse height spectrum of the output from the pulse shape discrimination unit, only events with a light output greater than 300 keV recoil electrons being recorded. ^{252}Cf source.

Figure 26 Relative pulse height spectrum of the output from the P.S.D. unit with coincidence with the P.S.D. discriminator. Illustrating the γ - rays cut-off. ^{252}Cf source.

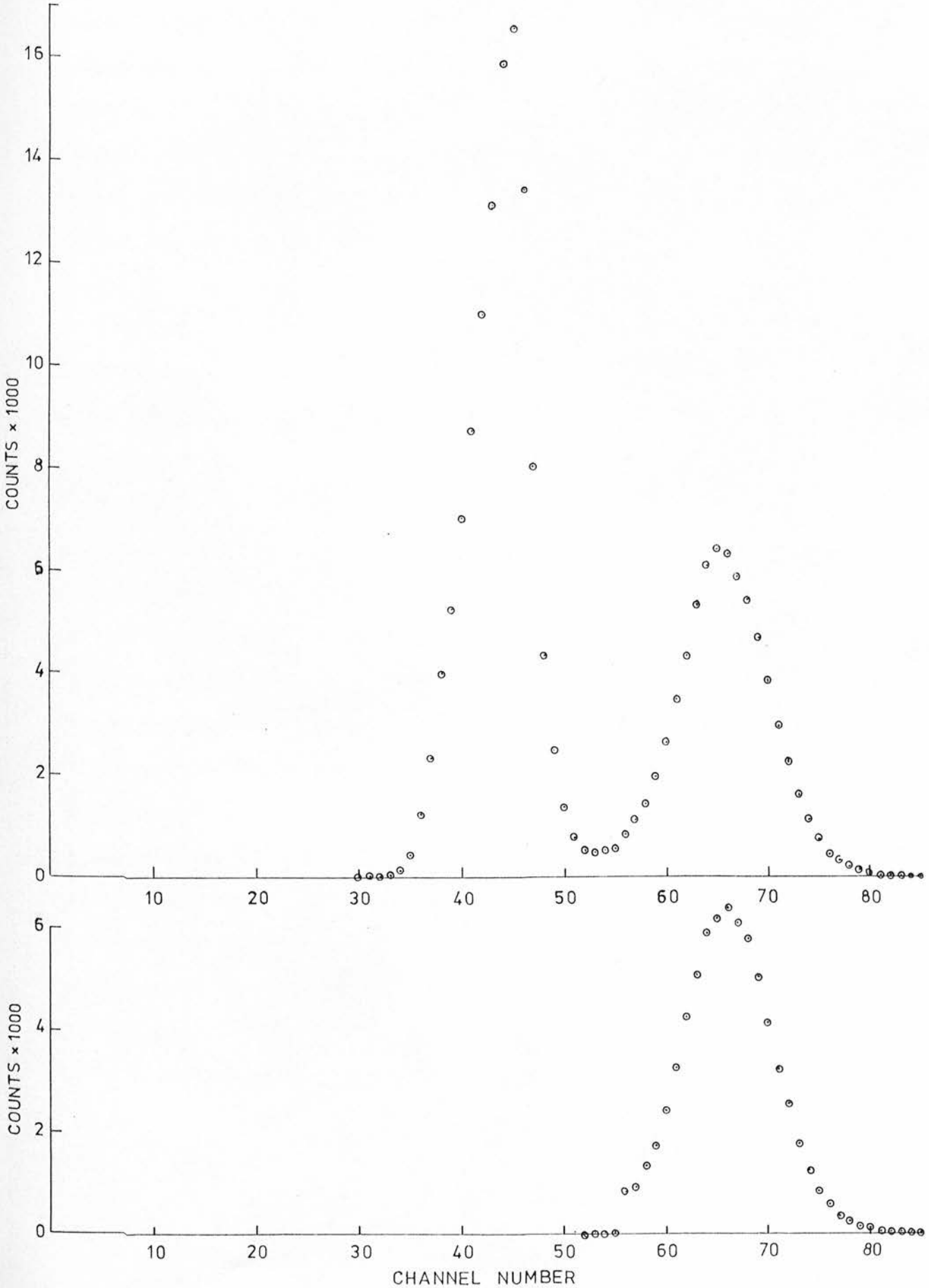
COUNTS × 1000
0
2
4
6
8
10
12
14
16
10
20
30
40
50
60
70
80
COUNTS × 1000
0
2
4
6
10
20
30
40
50
60
70
80
CHANNEL NUMBER

reject gamma rays. This gives a spectrum of the ^{252}Cf neutrons with gamma rays cut-off corresponding to the P.S.D. discriminator threshold. Usually the discriminator is set to cut-off gamma rays at the lowest point in the spectrum in the valley between gamma ray and neutron peaks as can be seen in figure 26.

Using a ^{252}Cf neutron source placed beside the gas scintillation detector the output of its linear amplifier is pulse height analysed and the gain of the photomultiplier adjusted so as to cover the whole 100 channels of the P.H.A. with the recoil helium spectrum. By using this method the detector high voltage is set at the required value. The electronic circuit is then connected as described in chapter 2, and as shown in figure 11. A preliminary measurement with a neutron beam from the D-D reaction is made in order to adjust the gas detector linear amplifier output by recording the gated helium recoil spectrum. Usually the gas detector gain is adjusted so that the helium recoil peak is set between channel 40 and 70. Figure 27 shows a typical gated helium recoil spectrum obtained with a neutron beam emitted from D-D reaction at an incident deuteron energy of 250 keV. The spectrum indicated a peak and low energy tail. The tail and the method used to correct the resulting data for the existence of such tail will be described in chapter 5.

Figure 27 Typical helium recoil spectrum obtained from the reaction at incident deuteron energy of 250 keV and reaction angle of 45^{o} Lab.

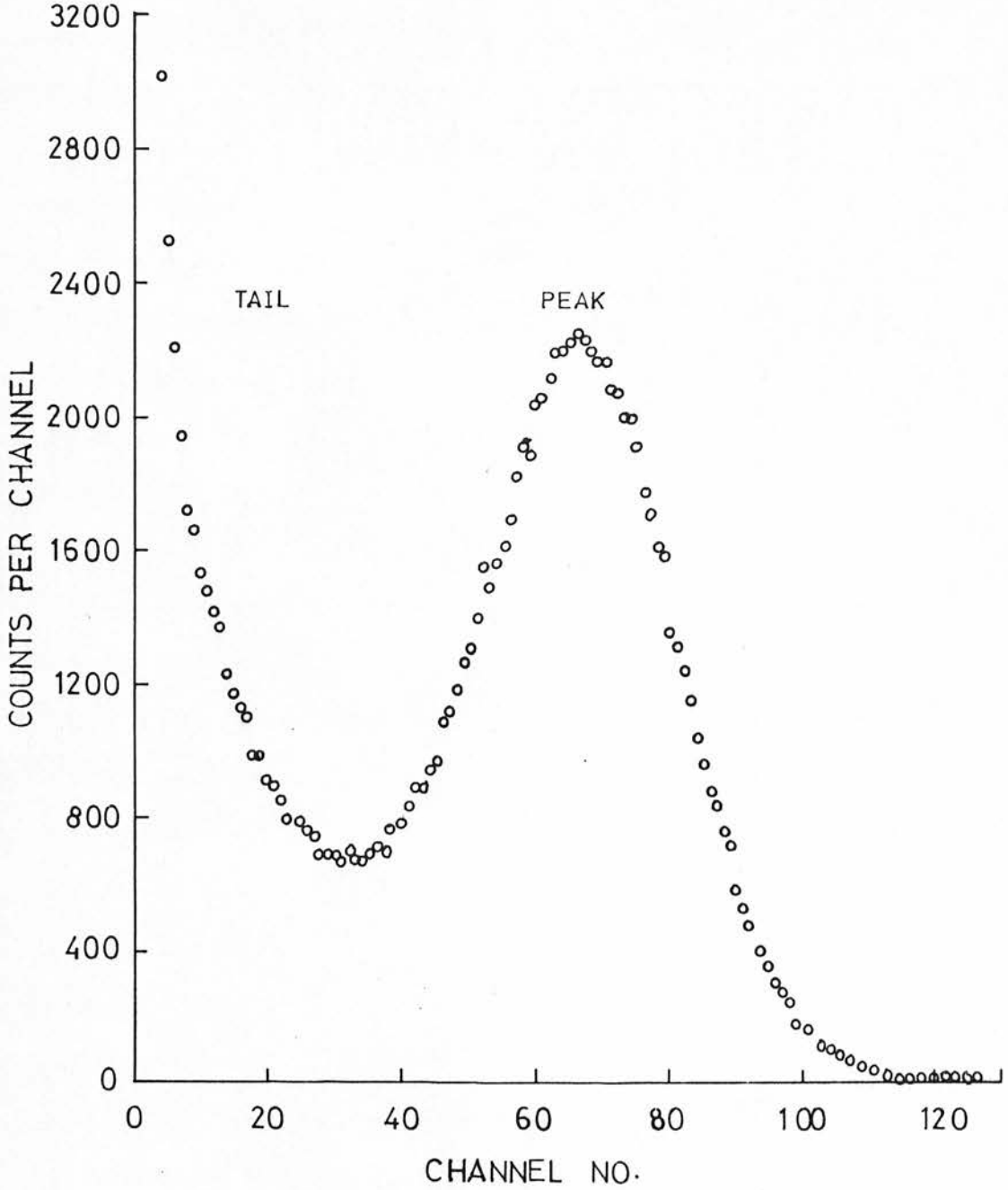
3200
2800
2400
2000
1600
1200
800
400
0
COUNTS PER CHANNEL
TAIL
PEAK
0
20
40
60
80
100
120
CHANNEL NO.

4.4 The Gain Stability Check

When making neutron polarization measurements it is necessary that the detection efficiency of the side detectors does not alter when they are interchanged. Since the detection efficiency is set by the photomultiplier gain and the amplifier discriminator and P.S.D. discriminator thresholds, these are measured periodically to check their stability. A ^{60}Co gamma ray source was used to check the photomultiplier gain stability of each side detector. The source was placed between the two side detectors. The pulses from the linear amplifier were stored in a P.H.A. A spectrum from each detector at position 1 was stored in separate 100 channel groups of the first 200 channels of the P.H.A. The two detectors were then interchanged and the measurement repeated and the spectrum from each detector at position 3 was stored in separate 100 channel groups in the second half of the P.H.A. memory. The spectra were accumulated for 200 seconds using the P.H.A. internal clock pulses as a time reference. The spectra from each detector could then be easily compared by displaying them in an overlapping readout mode. Typical results of such a test are shown in figure 28. In this figure the two spectra corresponding to a given side detector at position 1 and position 3 are overlapped. Figure 29 shows the spectrum which results from the subtraction of the two spectra shown in figure 28. At no time during the course of the experiment was any gain shift observed.

Figure 28 Typical ^{60}Co spectra taken during a test of gain stability. The crosses represent the spectrum obtained with the cradle held at position 1 and the dots represent the spectrum obtained with the cradle held at position 3.

Figure 29 The spectrum which results from the subtraction of the two spectra shown in figure 28. Note the expanded scale used in this figure.

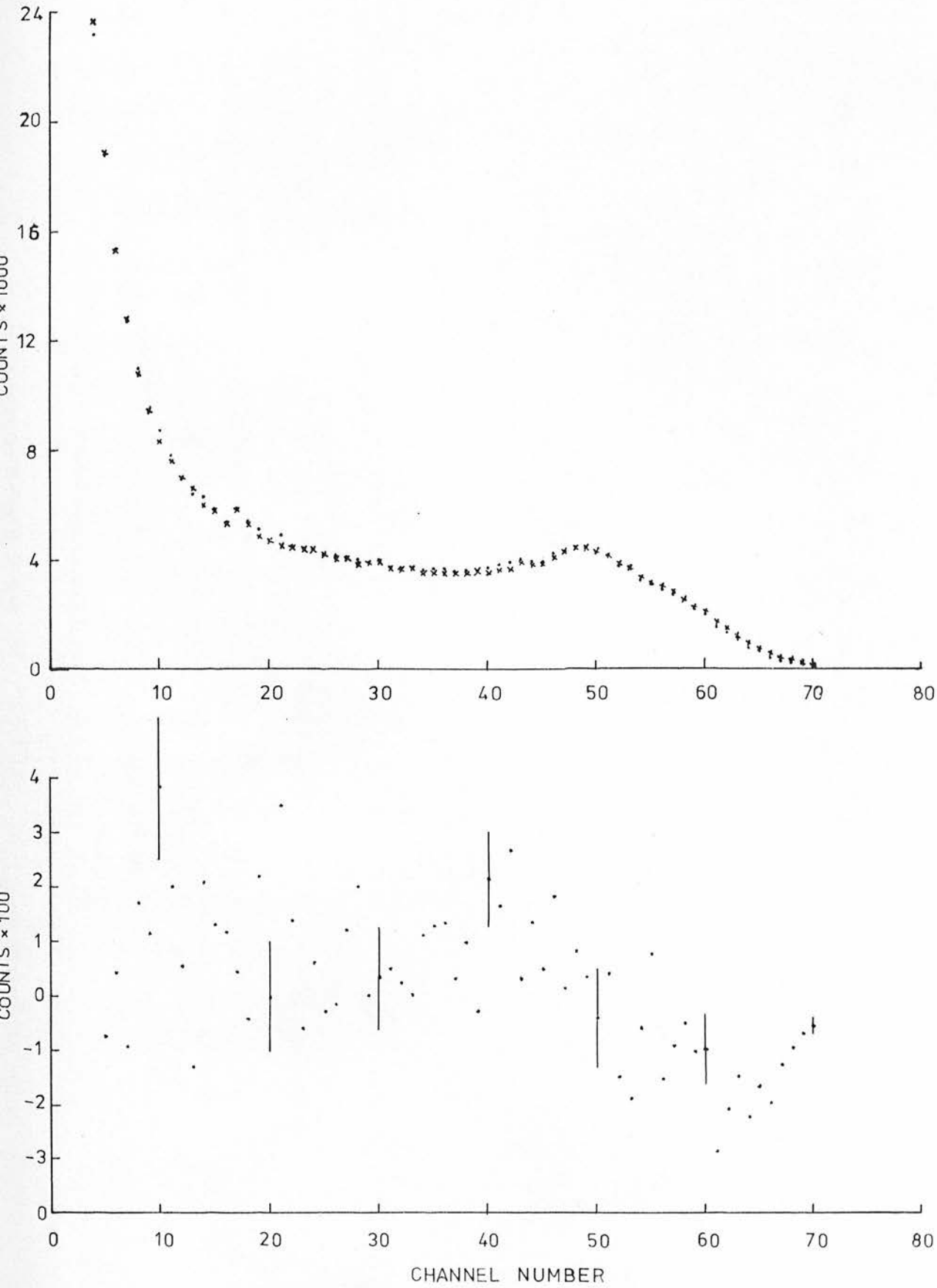
24
20
16
12
8
4
0
COUNTS x 1000
0
10
20
30
40
50
60
70
80
4
3
2
1
0
-1
-2
-3
COUNTS x 100
CHANNEL NUMBER

The test described above also served to show the absence of any systematic drifts in the photomultiplier gain as the spectra did not change in position or shape over the long period of data accumulation.

4.5 The Calibration of the Van de Graaff Accelerator.

At the final stage of the present neutron polarization measurements a special experiment was performed in order to check the reliability of the voltmeter used to record the accelerator potential. As most of the measurements were performed with a target of about 50 keV thickness, the accelerating voltage has to be known to within 10 keV. The Van de Graaff accelerator's potential at the high voltage terminal is measured by a generating voltmeter type D-A-VM-2 supplied by the High Voltage Engineering Corporation. This meter actually generates within its circuit a voltage proportional to the terminal voltage. The voltmeter itself has an accuracy of $\pm$ 0.05%, the meter circuit has an accuracy of $\pm$ 2%. As the voltmeter is sensitive to its geometric relationship to the high voltage terminal and since the only calibration check was made after installing the accelerator in this laboratory, it was felt that some check on the voltage calibration would be appropriate. The calibration was made by studying (P, γ) resonance.

A sodium iodide crystal scintillator was used as a gamma ray detector. The crystal is 5 inches in diameter and 4 inches long mounted on a 58 AVP photomultiplier. In order to detect most of the yield produced from the reaction, the solid angle subtended by the detector at the gamma-producing target was arranged to be as large as possible.

Two (P, γ) reactions were used in the calibration of the accelerator voltage. The first reaction to be studied was $^{19}F(P,\alpha\gamma)^{16}O$. The information about this reaction was taken from Hunt and Jones [71] and Ajzenberg-Selove and Lauritsen [72]. An evaporated layer of zinc fluoride was used as a target. The target holder is provided with a water cooling arrangement and has a vacuum attachment compatible with the beam tube. The gas cylinder used to provide the gas to the ion source was filled with hydrogen to a pressure of a few PSI. Maximum current obtained was about 12 μA on the target. In order to reduce the background gamma rays a thick layer of lead was placed between the detector and the analysing magnet which was the source of most of the gamma ray background.

The fluorine resonances were studied at the three incident proton energies within the limit of the accelerator. The output from the photomultiplier after amplification was pulse height analysed and spectra were stored in the memory of the P.H.A. The first resonance to be studied was that at incident proton energy of 341 keV. A high yield and a photopeak with good

resolution was observed. The integral of the area under the peak proportional to the yield was plotted against the proton incident energy. The yield curve as obtained from this experiment is plotted in figure 30 in the energy range from 300 to 370 keV. The error bars on the yield are an estimate of the effect of the uncertainty in the beam current used in the normalisation of these results. The maximum yield from the corresponding photopeaks recorded in the P.H.A. was used to mark the resonance.

The fluorine resonance which occurs at an incident proton energy of 224 keV was very weak. In order to investigate this resonance, a fresh zinc fluoride target was used and a higher beam current was applied on the target. The yield curve is plotted in figure 30 in the energy range from 200 to 260 kev. Maximum yield from the corresponding photopeak was used as a second calibration point.

The last resonance to be studied from this reaction was that which occurs at an incident proton energy of 484 keV. The emitted gamma ray energy is in the range from 6 to 7 MeV. The yield curve is plotted in figure 30 in the energy range from 420 to 500 keV. Maximum yield from the corresponding photopeak was used as a further resonance point.

The second reaction to be studied was $^{11}B(P, \gamma)^{12}C$. The information about this reaction was taken from Hunt et al [71]

Figure 30. Gamma rays yield as obtained using $^{11}B(P, \gamma)^{12}C$ reaction (+ and ∘) and $^{19}F(P,\alpha\gamma)^{16}O$ reaction (▽).

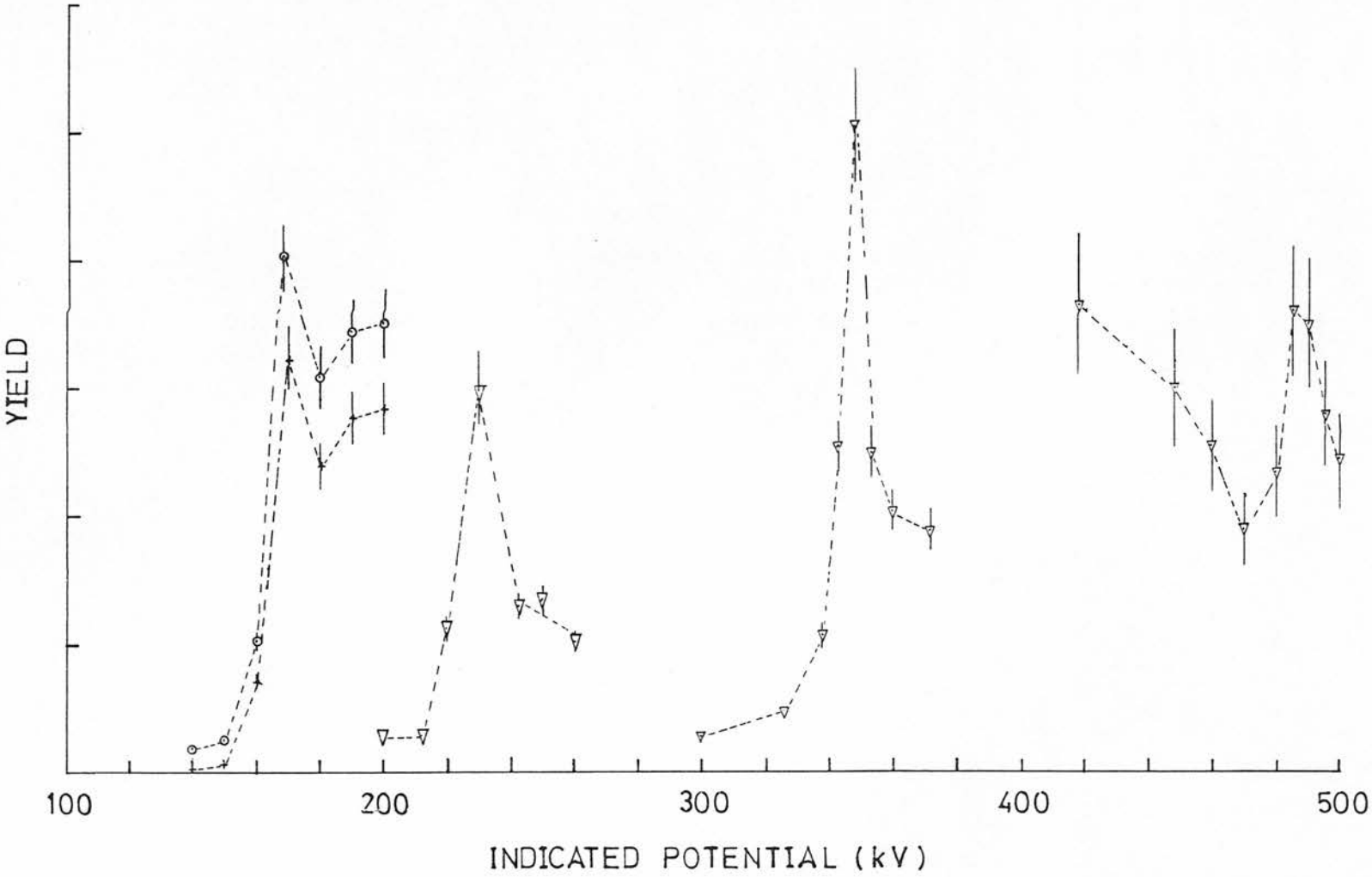
YIELD
100
200
300
400
500
INDICATED POTENTIAL (kV)

and Marion [73]. The boron target was obtained by using a thick evaporated layer of sodium tetra borate. Two photopeaks can be observed in this reaction with about the same yield at an incident proton energy of about 163 keV. The first peak corresponds to gamma ray with energy of about 4 MeV and the second corresponds to gamma ray with energy of about 12 MeV. The two photopeaks of this reaction were observed and taken into account in the calculation. The step in the yield from the corresponding photopeaks recorded in the P.H.A. was used as a further calibration point. The yield curve as obtained from this experiment is plotted in figure 30 in the energy range from 140 to 200 keV.

Figure 31 shows the accelerating potential as recorded by the voltmeter versus the real accelerating potential. The four points were obtained from the resonances observed in the yield of the two reactions. The straight line drawn through these points was then used as a calibration chart. The line indicates an agreement between the potential recorded in the voltmeter and the real potential to within 6 keV which is acceptable in the present measurements.

Figure 31. The indicated potential versus the true potential as obtained from figure 30 and the well known resonances of reaction $^{11}B(P, \gamma)^{12}C$ and $^{19}F(P,\alpha\gamma)^{16}O$.

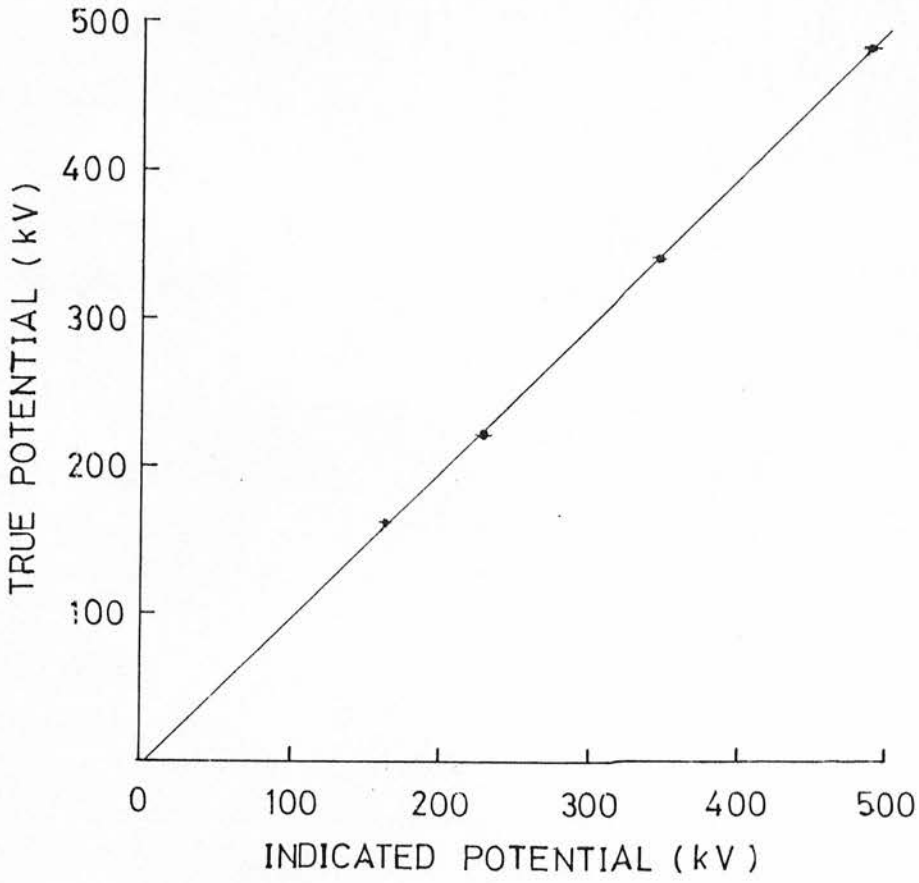
500
400
300
200
100
TRUE POTENTIAL (kV)
0
100
200
300
400
500
INDICATED POTENTIAL (kV)

4.6 Data Collection

The neutron polarization measurements described in the present section were performed using both the original and the modified polarimeters in the incident deuteron energy range from 200 to 350 keV and from 50 to 350 keV respectively. In each case the polarimeter was aligned before every new measurement as described in section 4.2. The measurements were performed at a mean laboratory angle of 45^{o}. Three Ti-D target thicknesses were used in the present experiment. Targets of 14 mg/in^2 thick were used for thick target measurements, targets of 1.5 mg/in^2 thick were used for thin target measurements in the incident deuteron energy range from 200 to 350 keV and targets of 0.5 mg/in^2 thick were used for very thin target measurements in the incident deuteron energy range from 50 to 200 keV. The measurements were performed using the 400 channel analyser or the PDP11/45 computer to pulse height analyse the pulses from the helium scintillator, routing to produce the desired gated recoil spectra being performed into 100 channel or 128 channel section of memory of the analyser or the computer respectively.

In order to determine that there were no false asymmetries introduced due to the experimental arrangements, a measurement of the system asymmetry was made at several deuteron energies. For these tests the asymmetry was measured in the vertical plane where the cradle carrying the three detectors was placed at position 2 and 4 (see figure 14). Due to the factor $P_n(\theta_1).P_s(\theta_2)$

in equation 1.2.7, one would expect no asymmetry to be observed under these conditions. The technique used in these measurements was to intersperse readings with the liquid scintillators in the horizontal plane (position 1 and 3 of figure 14), with those taken in the vertical plane (position 2 and 4 of figure 14). Having verified that the system asymmetry was approximately zero (see the result table in chapter 5) further asymmetry measurements were made in the horizontal plane only in order to save time at the low counting rates obtained at low deuteron energies. Even so, it was found necessary to accumulate data at a given energy for long periods of time. The average length of time during which the data was collected at a given deuteron energy, was approximately 10 days. Thus, it was essential to exercise certain precautions in order to prevent electronic shifts which would distort the data.

For a given incident deuteron energy, the data was accumulated in a sequence of runs each of approximately 60 minutes duration. The spectra were recorded in one of the four selectable cradle positions, then the data collected was punched out (automatically) on the high speed tape puncher coupled to the P.H.A. and the readings of the scalers coupled to the system were noted. The cradle then rotated (automatically) to the next position, the procedure being repeated until all four positions were sampled. Thus a measurement cycle in both horizontal and vertical plane lasted approximately 4 hours and approximately 2 hours in the horizontal plane only. These cycles of

measurements were repeated until the desired statistical accuracy was achieved. If any unexplained systematic drifts or any sudden changes occurred in the scaler readings, data accumulation was stopped until an explanation was found or a malfunction of some component corrected.

The polarization data was taken at several deuteron energies in the energy range from 50 to 350 keV. At a particular energy in the range up to 150 keV the data was obtained as an accumulation of several experimental runs. This was due to the low counting rate at these energies and the desired statistical accuracy which cannot be achieved in one continuous run. Comparison of the results obtained from the several parts of each energy run demonstrated the reproducibility of the measurements within the statistical error. In all cases the reproducibility was such that the results of the several parts of each energy run were combined and a single result quoted for each of the energies.

The treatment of the data will be discussed in the next section and the analysis of the data will be discussed in chapter 5.

4.7 Data Treatment.

Before coupling the polarimeter electronics to the computer through the interface unit, a 400 channel analyser was used to pulse height analyse the pulses from the helium gas scintillation detector and the resulting data were punched out in a paper tape by a high speed tape puncher coupled to the P.H.A.

The treatment of the experimental data tapes was carried out using a Digital Equipment Corporation PDP-11/45 computer which is available in the Department of Physics. Several programs were written in a modified form of 'IMP' language using the Edinburgh Multi Access System, 'EMAS'. These programs were then translated by an ICL 4-75 computer to a machine code to operate the PDP-11/45. The translated programs can be obtained in the form of a paper tape to be fed into the PDP-11/45 and stored in the disk to be used when required.

The first program allows the paper tape produced by the P.H.A. to be read into the PDP-11/45 through its high speed paper tape reader and stores the number of counts from each of the 400 channels in 400 separate stores. Then when a further paper tape produced by the pulse height analyser is fed in, it adds its content to the previous one. By continuing feeding the tapes in this method until the desired number of tapes, resulting with the cradle held at a particular position, has been summed then the content of the 400 channels may be stored

in a file in the disk and can be identified by six figures (usually the cradle position and the incident deuteron energy). This procedure is executed four times, so producing four files each corresponding to a particular cradle position. These four files can be joined together from 1 to 4, respectively in one master file by using a special code developed by Mr S.T. Hayes and available in the disk for the users of PDP-11/45 computer. The master file can be stored in a magnetic 'Dectape' or printed in a line printer or punched out in a paper tape where it can be used when required. Thus for a particular polarization measurement 16 spectra were stored in the computer, 8 of these spectra were (real + random) ones, and the other eight were the corresponding random spectra. The spectra can be displayed through a special code, written by F. Watson [74], in a vidio screen, available in the neutron physics laboratory, and coupled to the PDP-11/45 computer. Such display could help in preliminary judgement about the quality of the measurements.

The second program was used to calculate the measured asymmetry. The code is based on expression (1.3.6). It calls the appropriate keyword to obtain access to the data, contained in the master file and stored in the disk, and then on the selection of two channel numbers from the keyboard, the program sums the counts between the selected channel limits in each of the 16 spectra. It prints out the 16 totals along with the two asymmetries accompanied with their standard errors, one of which corresponds to the horizontal plane and the other to the

vertical plane which should be zero within the limits of statistical accuracy. The method used to obtain the standard error equation of the asymmetry used in this program will be described in chapter 5. Any other two channel limits can be selected and the program will repeat the above calculations for the new limits until it is stopped by the operator. In order to study the behaviour of the asymmetry and the effect of the tail on the results, a special keyword can be applied so that an output file can be obtained which contains the asymmetry as calculated by integrating the whole recoil spectrum including the tail and then increasing the lower limit of integration by four channels. In the same file the resulting asymmetry as calculated over a range of ten channels was also obtained at intervals of 5 channels. The whole procedure does not take more than a few seconds. Fig. 32 shows the behaviour of the asymmetry over the whole recoil spectrum with an increase of 4 channels to the lower limit of integration, and fig. 33 shows the behaviour of the asymmetry in a group of 10 channels with an interval of 5 channels along with the same recoil spectrum resulting with neutrons emitted from the reaction at 45° Lab., and incident deuteron energy of 100 keV. In figure 32 the effect of the tail on the results can be seen from the low asymmetry values under the tail region. In figure 33 the asymmetry values under the same region are compatible with zero within the statistical accuracy, thus the tail can be attributed to unpolarized low energy neutrons scattered from the surrounding materials which agree with the conclusion of references 66 and 78.

Figure 32. The behaviour of the asymmetry along the recoil spectrum obtained with neutrons emitted from the reaction at 45^{o} Lab. and incident deuteron energy of 100 keV. The asymmetry obtained by increasing the lower limit of integration by 4 channels.

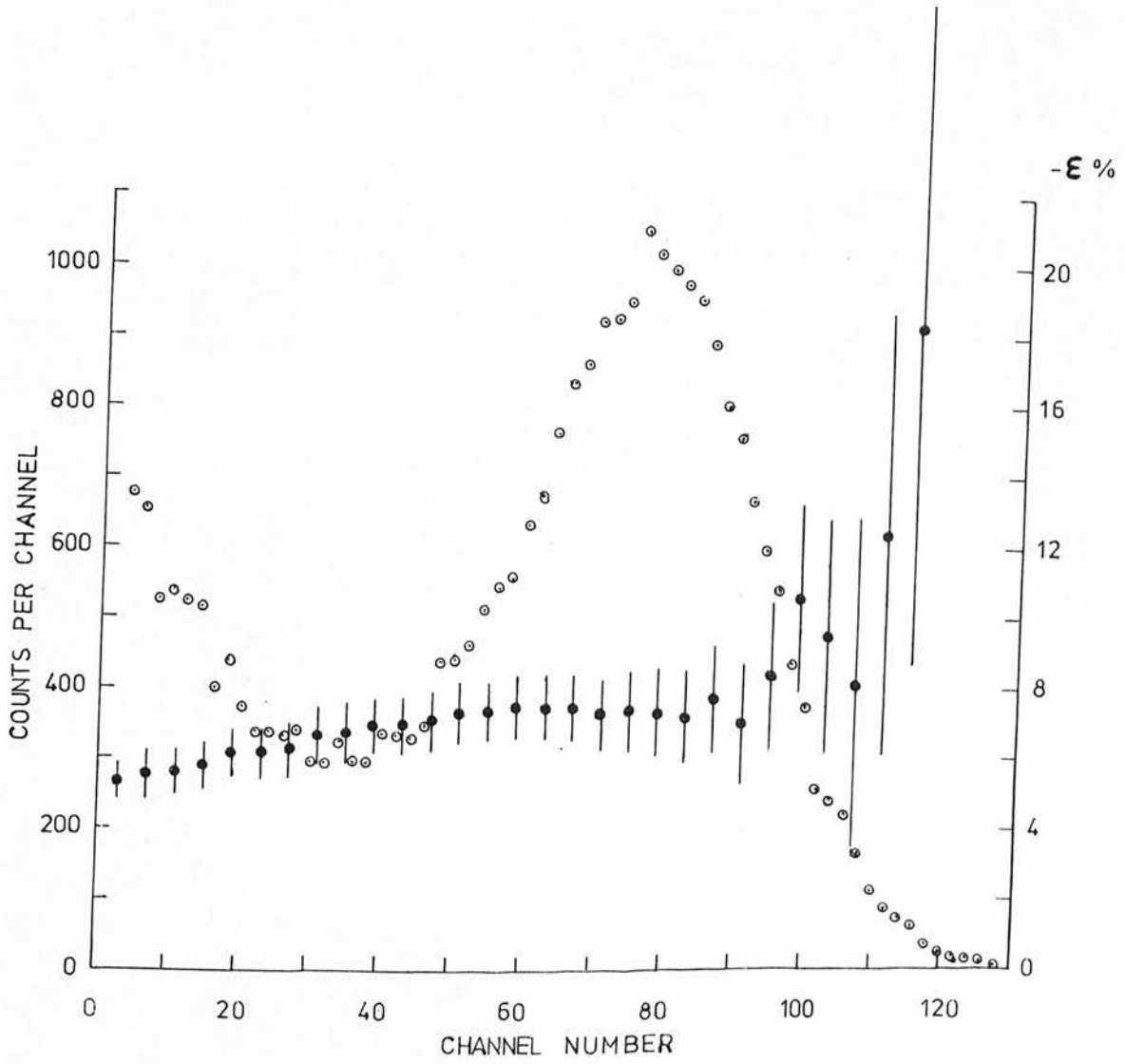
-ε %
1000
800
600
400
200
0
20
16
12
8
4
0
COUNTS PER CHANNEL
0
20
40
60
80
100
120
CHANNEL NUMBER

Figure 33. The behaviour of the asymmetry along the recoil spectrum obtained with neutrons emitted from the reaction at 45^{o} Lab. and incident energy of 100 keV,
The asymmetry obtained by integrating over a group of 10 channels in 5 channels intervals.

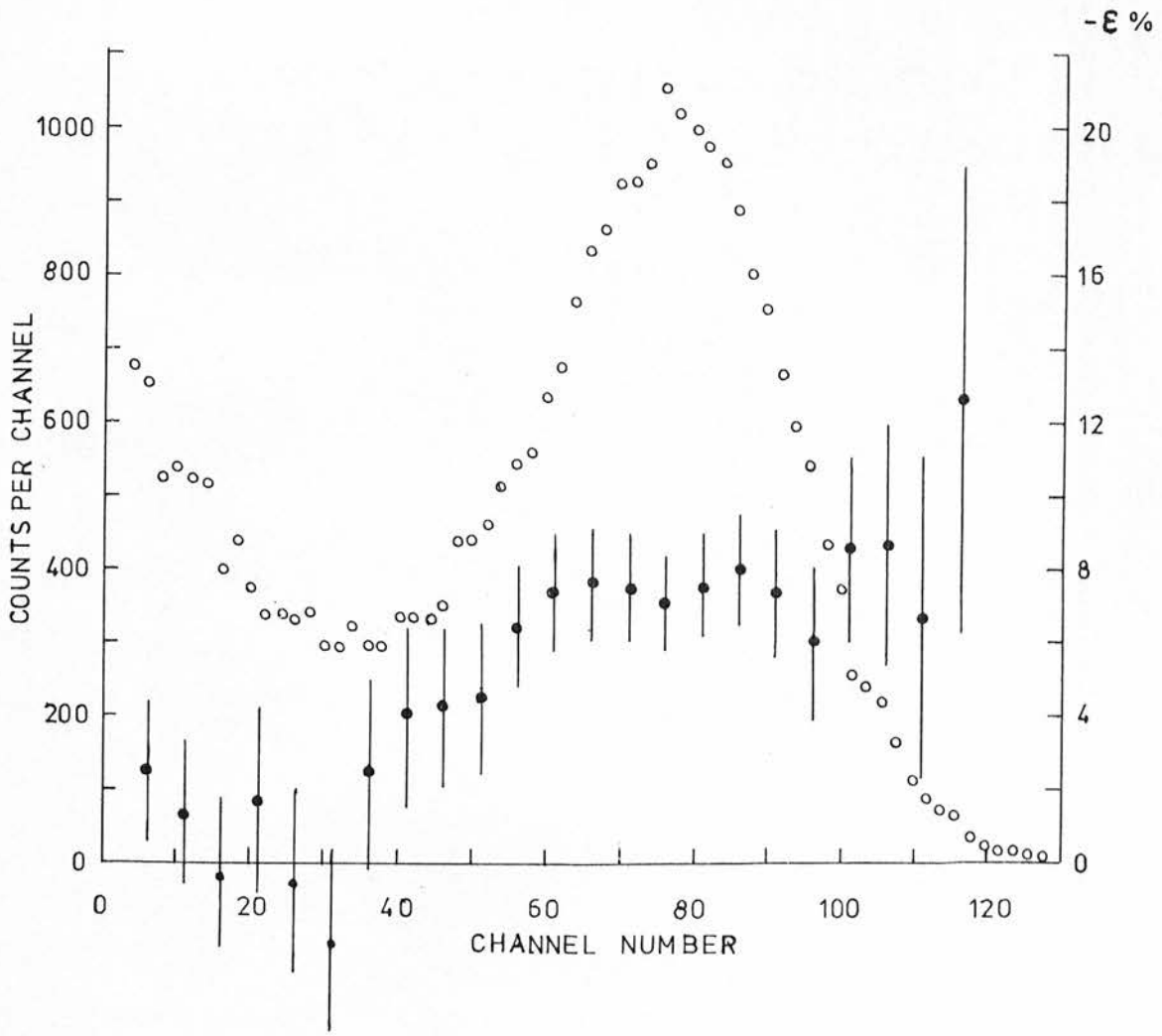
-ε %
1000
800
600
400
200
0
20
16
12
8
4
0
COUNTS PER CHANNEL
0
20
40
60
80
100
120
CHANNEL NUMBER

After coupling the polarimeter electronics through the interface unit, to the PDP-11/45 computer, special programs were written to operate the system and treat the resulting data.

The first program was written to allow the collection of data by the computer using a special code through the keyboard. Several facilities were added to this program. Thus through the keyboard one can select the following:

1. The running period required for the measurement with the cradle held at each one of the four cradle positions.
2. The sequence of the cradle positions (usually associated with the setting of switch SW2 of fig. 18 and described in section 3.6.1). This includes the number of cycles required at a particular run.
3. The run number for identifying particular data.
4. A six character label to identify the master file which contains the resulting data from a particular run.

After the end of a selected running cycle, two files will be produced and stored in the disk, one of these files will contain the individual sections joined together, each corresponding to a particular cradle position and identified by the run number and the cradle position. Thus any error in the data in any individual section, due to any sort of fault, can be deleted without affecting the other data. The deletion of any faulty data can be done by a special program available to the users of the PDP-11/45 computer.

The second file is the master file which was identified by a six character label. This file contains four sections joined together, each corresponding to the sum of the data resulting after several runs at a particular cradle position. Each section is identified by the cradle position and the last run number, i.e. the first section contains the sum of the data from several runs collected with the cradle held at position 1, the second, the third and the fourth sections contain the sum of data from several runs collected with the cradle held at positions 2,3 and 4, respectively. Any new data can be added to the master file if the same 6 identification characters are selected for every new run.

A third program has been written to deal with the individual sections in the first file. If these sections were joined together, using the available special code in the computer disk, the program calls for the appropriate keyword to obtain access to these sections, and then on the selection of any one of the 4 cradle positions, the program sums up the data corresponding to that position and stores them in a new section in a new file and identifies it by the selected cradle position. By selecting all the four cradle positions one by one, the resulting new file will be similar to the master file. This program can be used to sum the resulting data if for some reason the original master file contains unreliable data in any section.

For calculating the measured asymmetry a similar program to that used with the data produced by the P.H.A. has been used. An account has been taken of the difference in channel number between the P.H.A. (400 channel) and the computer (512 channel).

Running the polarimeter and treating the resulting data by the computer has saved a lot of time usually spent in feeding data tapes produced by the P.H.A. to the computer.

The analysis of the data will be discussed in the following chapter.

CHAPTER 5.

DATA ANALYSIS, RESULTS AND CONCLUSION.

CHAPTER 5.

DATA ANALYSIS, RESULTS AND CONCLUSION.

The results presented in this thesis come from a total of 33 individual runs. Each run corresponded to a particular deuteron energy. Some of these runs were repeated several times in order to achieve sufficient statistical accuracy especially with thin target measurements in the deuteron energy range up to 200 keV. The data for each run consists of 8 ^{4}He recoil spectra 4 real plus random spectra and 4 random spectra. In this chapter we will deal with the analysis of the data to yield neutron polarization.

In section 5.1, the methods used to calculate the average deuteron energy when using either thin or thick targets are described. In section 5.2, there is a description of how the uncorrected asymmetries and their statistical uncertainties were calculated. In section 5.3, we deal with the problem of the low energy tail observed in the helium recoil spectrum and the method used to correct the measured asymmetry for its effect on the data. In section 5.4, we deal with the analysing power calculation and the degree of agreement between the calculated helium analysing power from various phase shift data reported in the literature. In section 5.5, there is a description of how the mean analysing power is calculated and corrected for

the finite sizes of both the helium gas scintillator and the side detectors and is corrected for the variation in the D-D reaction cross section with the angle subtended by the gas scintillator at the target. The final results of neutron polarization and conclusion will be given in section 5.6. This includes comparison with published neutron polarization data and with the theoretical prediction of polarization by Boersma [27].

5.1 The Average Deuteron Energy Calculation.

In the present measurements both thin and thick Ti-D targets were used. The thin target stopping powers were taken from the compilations of Coon [75]. These compilations are based on extrapolations of theoretical predictions and experimental results. As these data were given in the energy range from 0.2 to 20 MeV, the stopping powers of the thin targets in the energy region below 200 keV were taken from the experimental results of Ormrod [76].

For targets mounted on the target holders which are inclined at 45° to the incident beam, the target thicknesses have to be increased by multiplying the given thicknesses by a factor of 1.4.

In the present measurements using thick Ti-D targets an expression was used to calculate the weighted average deuteron energy, at which the analysing power was evaluated, similar to

the expression used by Fick and Weiss [54]:

$$\bar{E}_d = \frac{\int_0^{E_d} \sigma_T(E_d) E_d dE_d}{\int_0^{E_d} \sigma_T(E_d) dE_d}$$

The total cross section $\sigma_T(E_d)$ of the $^2H(d,n)^3He$ reaction as a function of the deuteron energies were taken from the data compiled by Liskein and Paulsen [77].

The resulting average deuteron energies are in good agreement with published data to within the energy range of 3 to 8 keV.

The target thickness in mg/cm^2 and the calculated average deuteron energies are given in table 9.

5.2 Calculation of the Asymmetries and their Statistical Uncertainties.

The first stage in the analysis of polarization data is the calculation of the asymmetries. The asymmetries are obtained from the data contained in the helium recoil spectra.

For each incident deuteron energy the data consists of four numbers :

E_d keV	Target Thickness mg/cm^2	Target Thickness keV	$\bar{E}_d$ keV
350	3.04	Thick	240
300	3.04	Thick	210
250	3.04	Thick	180
200	3.04	Thick	150
150	3.04	Thick	115
350	0.32	150	275
300	0.32	150	225
250	0.20	110	195
200	0.11	40	180
150	0.08	30	135
125	0.11	40	105
100	0.08	30	85
100	0.11	40	80
75	0.11	40	55
50	0.11	30	35

Table 9. Target thickness and average deuteron energy.

R_{T1} = real plus random ^{4}He recoils, right side detector, first run.

R_{r1} = random ^{4}He recoils, right side detector, first run.

L_{T1} = real plus random ^{4}He recoils, left side detector, first run.

L_{r1} = random ^{4}He recoils, left side detector, first run.

For the second run the numbers R_{T2}, R_{r2}, L_{T2} and L_{r2} are obtained.

The real numbers of ^{4}He recoils are then :

$$I_{R1} = R_{T1} - R_{r1} \quad , \quad I_{L1} = L_{T1} - L_{r1}$$

$$I_{R2} = R_{T2} - R_{r2} \quad , \quad I_{L2} = L_{T2} - L_{r2}$$

The asymmetry can then be calculated by use of equation 1.3.6 :

$$\varepsilon = \frac{1 - A}{1 + A} \qquad \text{where}$$

$$A = \sqrt{\frac{I_{R1} \times I_{R2}}{I_{L1} \times I_{L2}}}$$

The propagation of the statistical counting error was accomplished by use of the relation :

$$(\Delta f)^2 = (\frac{\partial f}{\partial m_1})^2(\Delta m_1)^2 + (\frac{\partial f}{\partial m_2})^2(\Delta m_2)^2 + \ldots \quad (5.2.1)$$

where f is a function of m_1, m_2, ...

By applying this relation (5.2.1) to A, the uncertainty ΔA can be obtained :

$$\Delta A = \frac{A}{2}\left[\left(\frac{\Delta I_{R1}}{I_{R1}}\right)^2 + \left(\frac{\Delta I_{L1}}{I_{L1}}\right)^2 + \left(\frac{\Delta I_{R2}}{I_{R2}}\right)^2 + \left(\frac{\Delta I_{L2}}{I_{L2}}\right)^2\right]^{1/2} \quad (5.2.2)$$

Since R_{T1}, R_{r1}, etc. are numbers of ^{4}He recoils with normal counting statistics, then $\Delta R_{T1} = (R_{T1})^{1/2}$ and $\Delta R_{r1} = (R_{r1})^{1/2}$ etc. then $\Delta I_{R1} = (R_{T1} + R_{r1})^{1/2}$ (5.2.3) with similar expressions for ΔI_{R2}, ΔI_{L1} and ΔI_{L2}. Applying equation (5.2.1) to equation (1.3.6) and using the results of equations (5.2.2) and (5.2.3) the final expression is obtained :

$$\Delta\varepsilon = \frac{2\,\Delta A}{(1+A)^2}$$

$$= \frac{A}{(1+A)^2}\left[\frac{R_{T1}+R_{r1}}{(R_{T1}-R_{r1})^2} + \frac{L_{T1}+L_{r1}}{(L_{T1}-L_{r1})^2} + \frac{R_{T2}+R_{r2}}{(R_{T2}-R_{r2})^2} + \frac{L_{T2}+L_{r2}}{(L_{T2}-L_{r2})^2}\right]^{1/2} \quad (5.2.4)$$

The errors quoted for the asymmetries have been determined from expression (5.2.4).

5.3 The Tail and the Tail Correction.

The low energy tail observed in the helium recoil spectrum and its effect on the neutron polarization was discussed in references 66 and 78. The tail was attributed to neutrons scattered by the material surrounding the neutron detectors and the helium scintillator before being detected by the liquid scintillators. In the modified polarimeter the gas scintillator and the liquid scintillators were reorientated (as described in chapter 2) in order to reduce the amount of material in front of the incident neutron flux. The effect of this orientation has led to less unpolarized contribution to the valley and the peak

regions in the helium recoil spectra which slightly reduce the tail correction factor. Figure 34 shows two helium recoil spectra for neutrons emitted at 45° from D-D reaction with 200 keV deuterons. Spectrum (a) was obtained with the modified polarimeter and spectrum (b) with the original one.

For the treatment of the low energy tail, a Mont Carlo program was used in references 66 and 78, based on simulating a helium recoil spectrum which resulted when neutrons incident on the gas scintillator were scattered through different routes. The program was used to calculate the helium recoil spectrum resulting from scattering the incident neutrons in the following ways :

a. By the helium scintillator into the liquid scintillator.
b. By the helium scintillator then by the metal or the quartz window at the rear of the gas scintillator before being detected by the liquid scintillator.
c. By the metal or the quartz window then by the helium scintillator before being detected by the liquid scintillator.

These three spectra were added together. The resulting spectrum was similar to those obtained experimentally. One cannot rely completely on such a simulated spectrum when extrapolating the experimentally observed tail as several approximate assumptions were made in the calculation (e.g. the differential scattering cross section for the scattering of neutrons in the metal and quartz was assumed constant, the energy loss which takes place

Figure 34. The effect of the orientation of the gas scintillator and the neutron detectors on the helium recoil spectra. Both spectra obtained with neutrons from D-D reaction with 200 keV incident deuterons.
(a) Obtained with the modified polarimeter
(b) Obtained with the original polarimeter

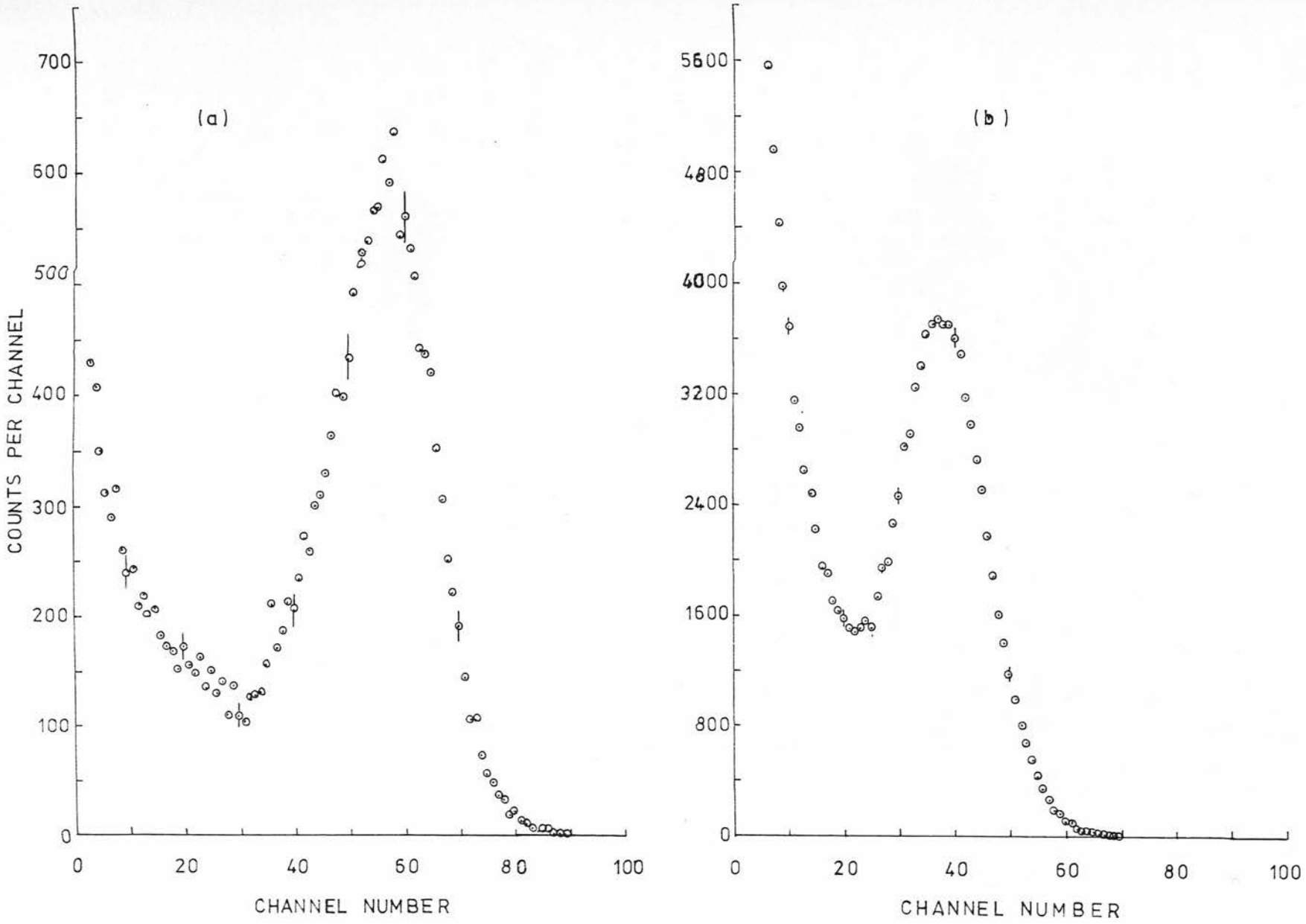
(a)
(b)
COUNTS PER CHANNEL
CHANNEL NUMBER
CHANNEL NUMBER
0
100
200
300
400
500
600
700
800
1600
2400
3200
4000
4800
5600
0
20
40
60
80
100

in the scatterer and the absorption of the neutron flux in the metal and quartz was ignored). Also contributions of other different routes of scattering (e.g. scattering from the cradle, scattering from the photomultiplier of the side detector and its brass container etc.) were ignored.

Thus a manual extrapolation to the tail in an observed spectrum has to be done by drawing a smooth curve through the tail continuing beneath the peak as can be seen from figure 35. The method of extrapolation was based on the results of asymmetry calculation made by integrating over an area of the recoil spectrum between points (A) and (B), (B) and (C) and (A) and (C). Points (A), (B) and (C) represents the midpoint of the low energy edge of the peak, the summit of the peak and the midpoint of the high energy edge of the peak, respectively. The results of these calculations showed that the second (area between (B) and (C)) and the third (area between (A) and (C)) calculated asymmetries agree well within the statistical accuracy while the first (area between (A) and (B)) calculated asymmetry showed a significant lower value, thus supporting the idea of fall off in the unpolarized contribution beneath the peak.

All the experimentally observed data was analysed by extrapolating the tails beneath their associated peaks in a similar way to that shown in figure 35 and such extrapolated tails were taken to be the unpolarized contribution to be corrected for.

Figure 35. The helium recoil spectrum for neutrons emitted at 45° from D-D reaction with 50 keV deuterons. The solid line showing the tail extrapolation.

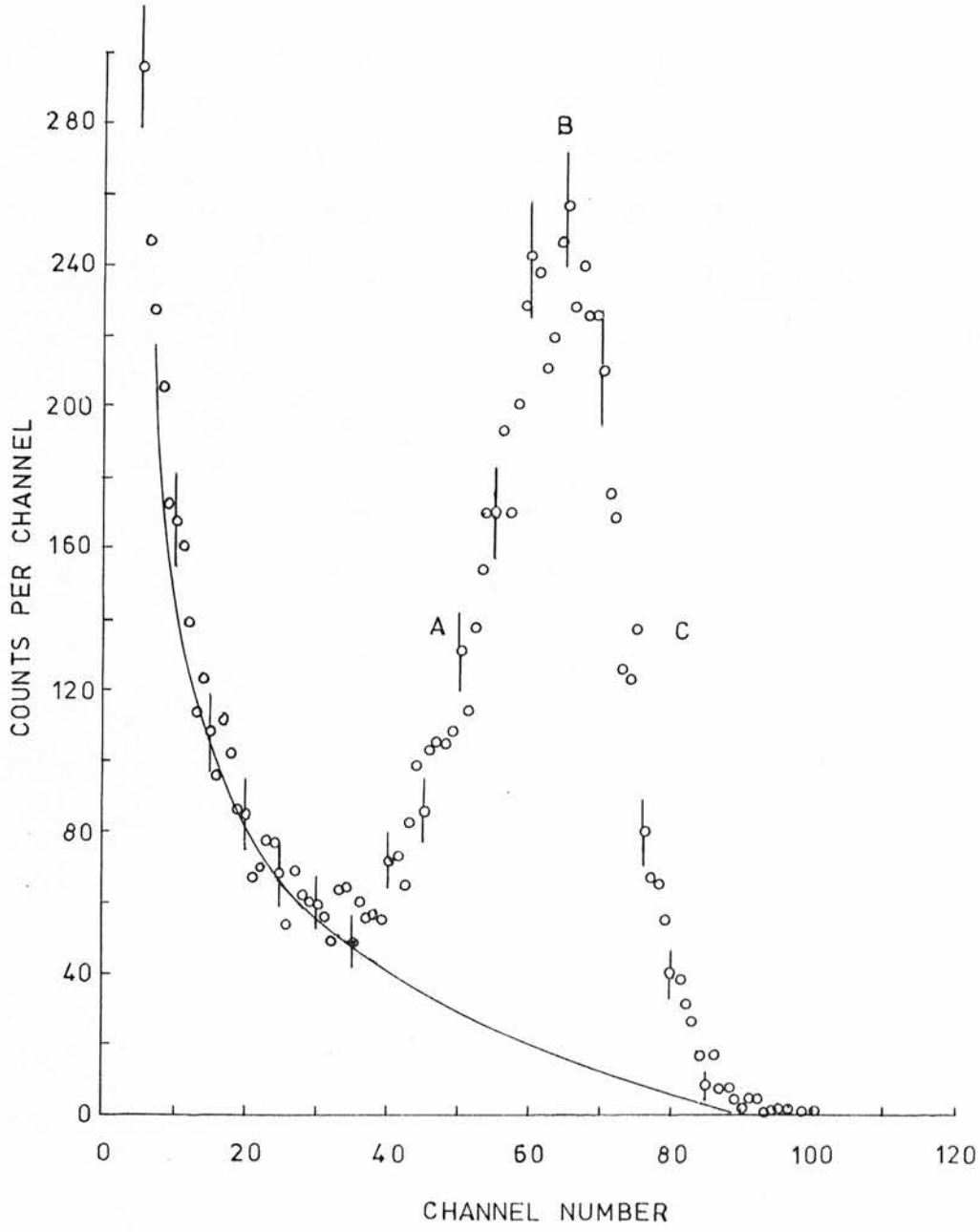
COUNTS PER CHANNEL
CHANNEL NUMBER
A
B
C
0
40
80
120
160
200
240
280
0
20
40
60
80
100
120

In order to reduce the unpolarized tail effect and in order not to lose much of the statistical accuracy, the asymmetry was calculated from an area of the spectrum between the midpoint of the lower energy edge of the peak and few channels after the midpoint of the high energy edge of the peak.

If T is the number of counts, between the selected limits, from the unpolarized tail in the recoil helium spectrum associated with the left and right neutron detectors together, and R is the total number of counts, between the same selected limits, in the helium recoil spectrum associated with left and right neutron detectors combined, then the factor $F = \frac{R}{R-T}$ is the unpolarized tail correction factor.

It was found that the measured asymmetries have to be multiplied by correction factors ranging from 1.07 to 1.18 where the lower corrections correspond to the better resolution spectra. These correction factors are listed with the measured asymmetries in tables 10 and 11.

In table 10 are given the resulting asymmetries as obtained by using thick Ti-D targets. In the first column are given the incident deuteron energies, followed by the mean deuteron energies as calculated using the method described in section 5.1, the measured asymmetries $\varepsilon(\%)$, the asymmetries detected in the vertical plane which is perpendicular to the reaction plane, the tail correction factor F, and the corrected asymmetries for the

E_d	$\bar{E}_d$	Measured ε	Vertical ε	F	Corrected ε	Average ε
keV	keV	(%)	(%)		(%)	(%)
350	240	-10.83 ± 0.70	-0.7 ± 1.2	1.16	-12.56 ± 0.80	
300	210	-09.86 ± 0.50	-0.2 ± 0.7	1.18	-11.63 ± 0.60	
300	210	-10.60 ± 0.60	-1.3 ± 2.9	1.12	-11.87 ± 0.70	
250	180	-09.20 ± 0.50	-0.2 ± 0.7	1.18	-10.86 ± 0.60	
200	150	-09.10 ± 0.43	-0.5 ± 0.8	1.16	-10.60 ± 0.50	
150	115	-09.06 ± 0.50		1.07	-09.69 ± 0.50	

Table 10. Resulting Asymmetries (Thick target)

E_d keV	$\bar{E}_d$ keV	Measured ε (%)	Vertical ε (%)	F	Corrected ε (%)	Average ε (%)
350	275	-11.16 ± 0.50	-0.4 ± 0.7	1.18	-13.17 ± 0.60	
300	225	-10.41 ± 0.38		1.18	-12.28 ± 0.45	
250	195	-11.03 ± 0.38		1.14	-12.57 ± 0.40	
200	180	-09.94 ± 1.76		1.13	-11.23 ± 1.99	-10.53 ± 0.50
		-09.14 ± 1.57	-1.0 ± 1.8	1.10	-10.10 ± 1.73	
		-08.14 ± 1.00	-0.2 ± 1.6	1.14	-09.30 ± 1.14	
		-09.98 ± 0.80	-1.5 ± 1.9	1.12	-11.18 ± 0.90	
		-09.60 ± 1.00	-1.3 ± 2.3	1.11	-10.66 ± 1.11	
150	135	-08.11 ± 1.33		1.11	-09.00 ± 1.48	-10.08 ± 0.40
		-09.30 ± 0.75		1.11	-10.32 ± 0.83	
		-08.30 ± 0.90		1.11	-09.21 ± 0.99	
		-10.60 ± 1.33		1.11	-11.80 ± 1.48	
		-09.01 ± 0.90		1.12	-10.09 ± 1.00	
		-09.16 ± 0.67		1.12	-10.23 ± 0.75	

Table 11. Resulting Asymmetries (Thin target)

E_d keV	$\bar{E}_d$ keV	Measured ε (%)	Vertical ε (%)	F	Corrected ε (%)	Average ε (%)
125	105	-06.50 ± 1.11		1.18	-07.70 ± 1.30	$-08.06 + 0.80$
		-07.00 ± 0.9		1.18	-08.30 ± 1.06	
100	85	-07.53 ± 1.00		1.14	-08.60 ± 1.14	
100	80	-07.33 ± 0.71		1.13	-08.30 ± 0.80	$-08.40 + 0.56$
		-07.54 ± 0.73		1.13	-08.50 ± 0.80	
75	55	-06.20 ± 1.34		1.16	-07.20 ± 1.55	$-07.35 + 0.70$
		-05.87 ± 1.47		1.17	-06.87 ± 1.72	
		-06.28 ± 1.07		1.17	-07.35 ± 1.25	
		-06.75 ± 1.24		1.16	-07.83 ± 1.44	
50	35	-04.77 ± 2.69		1.15	-05.48 ± 3.10	$-06.60 + 0.95$
		-06.33 ± 1.30		1.10	-06.96 ± 1.46	
		-05.17 ± 2.60		1.12	-05.79 ± 2.89	
		-06.09 ± 1.42		1.10	-06.70 ± 1.56	

Table 11. Resulting Asymmetries (Thin target) contd.

tail effect are given in the last column.

In table 11 are given the resulting asymmetries as obtained by using thin Ti-D targets. The results are given in the same arrangement as that of table 10. An extra column was added to contain the average asymmetries obtained by weighting the corrected asymmetries measured at a particular deuteron energy in several runs, often with a long time interval between them. The good agreement in these cases indicates the reproducability of the results and the freedom of the system from any spurious instrumental asymmetries.

5.4 The Analysing Power Calculation.

The analysing power of a scatterer of spin-zero nuclei can be calculated using the expression given by Baumgartner et al [79]. The expression is given in reference 7 as :

$$P = \frac{-2\ \mathrm{Im}(g^{*}h)}{|g|^{2} + |h|^{2}} \qquad (5.4.1)$$

where $g = (1/k)\ \sum_{l} P_l\ (\cos\theta)\ \left[(l+1)\sin\delta_l^{+}\ e^{i\delta_l^{+}} + l\sin\delta_l^{-}\ e^{i\delta_l^{-}}\right]$

$h = (1/k)\ \sum_{l} P_l'\ \sin(\delta_l^{+} - \delta_l^{-})\ e^{i(\delta_l^{+} + \delta_l^{-})}$

P_l and P_l' are the Legendre and associated polynomials

δ_l^{+} and δ_l^{-} are the phase shifts for $J = l + \frac{1}{2}$ and $J = l - \frac{1}{2}$ respectively.

In the case of n - ^{4}He scattering experiments the phase shifts were derived from the measured total cross section,

differential cross section and polarization. Several phase shifts were derived from the available data, by various authors, and published in the literature. In order to examine the degree of agreement between these various phase shifts a brief review of the existing data is given in that which follows.

Initially the phase shifts were obtained from P - ^{4}He scattering data as experimental P - ^{4}He information was more abundant and reliable. Dodder and Gammel (DG) [29] deduced nucleon - ^{4}He phase shifts from fitting P - ^{4}He cross section data at 5.81 and 9.48 MeV. These phase shifts were then supported by n - ^{4}He cross section measurement carried out by Seagrave [17] up to 14 MeV incident neutron energy. Later P - ^{4}He cross section and polarization for energies >10 MeV were analysed in terms of phase shifts by Gammel and Thaler [80]. These phase shifts, however, disagree with the neutron data above 15 MeV and disagree with the phase shifts obtained from the experimental data in the energy range below 4 MeV. After this unreliable situation Hoop and Barschall [12] determined n - ^{4}He phase shifts in the energy range from 6 to 30 MeV. Their data is a continuation of those of Austin and Barschall [20] who contributed a set of n - ^{4}He phase shifts which cover the energy range up to 8 MeV. These phase shifts agree with those of Dodder and Gammel [29] which were published by Seagrave [17] in the energy range below 10 MeV.

More n - ^{4}He phase shifts were derived by Sawers et al [81] at 1.01 and 2.44 MeV, Morgan et al [82] in the energy range between 0.2 and 7 MeV, and by Satchler et al [40] who applied an optical model fit to the data of Morgan et al [82] and predicted phase shifts for neutron - ^{4}He up to 18 MeV energy. Arndt and Roper [84] published their set which was obtained from fitting the existing experimental data. Their data cover the energy range up to 20 MeV. Stammbach and Walter [85] deduced phase shifts from the available n - ^{4}He and P - ^{4}He data up to 20 MeV. Their description of both nucleon - ^{4}He systems is the more complete in the mentioned energy range.

In order to examine the degree of agreement between the most commonly used phase shifts, the angular distribution of the analysing power of helium in the Lab. system is plotted in figure 36 and figure 37. The analysing power was computed using the expression 5.4.1 applying various phase shifts. Figure 36 shows the analysing power of helium for a neutron energy of 3 MeV as computed using the phase shifts of Hoop et al [12], Morgan et al [82], Satchler et al [40] and Stammbach et al [85]. Figure 37 shows the analysing power of helium for neutron energy of 6 MeV as computed using the phase shifts taken from the same authors.

As can be seen from the two figures the agreement between the curves is much better at the backward scattering maximum than at the forward scattering minimum. For 3 MeV neutrons the

Figure 36. Angular dependence of the analysing power of ^{4}He in the Lab. system for 3 MeV neutrons as calculated using four different sets of phase shifts.

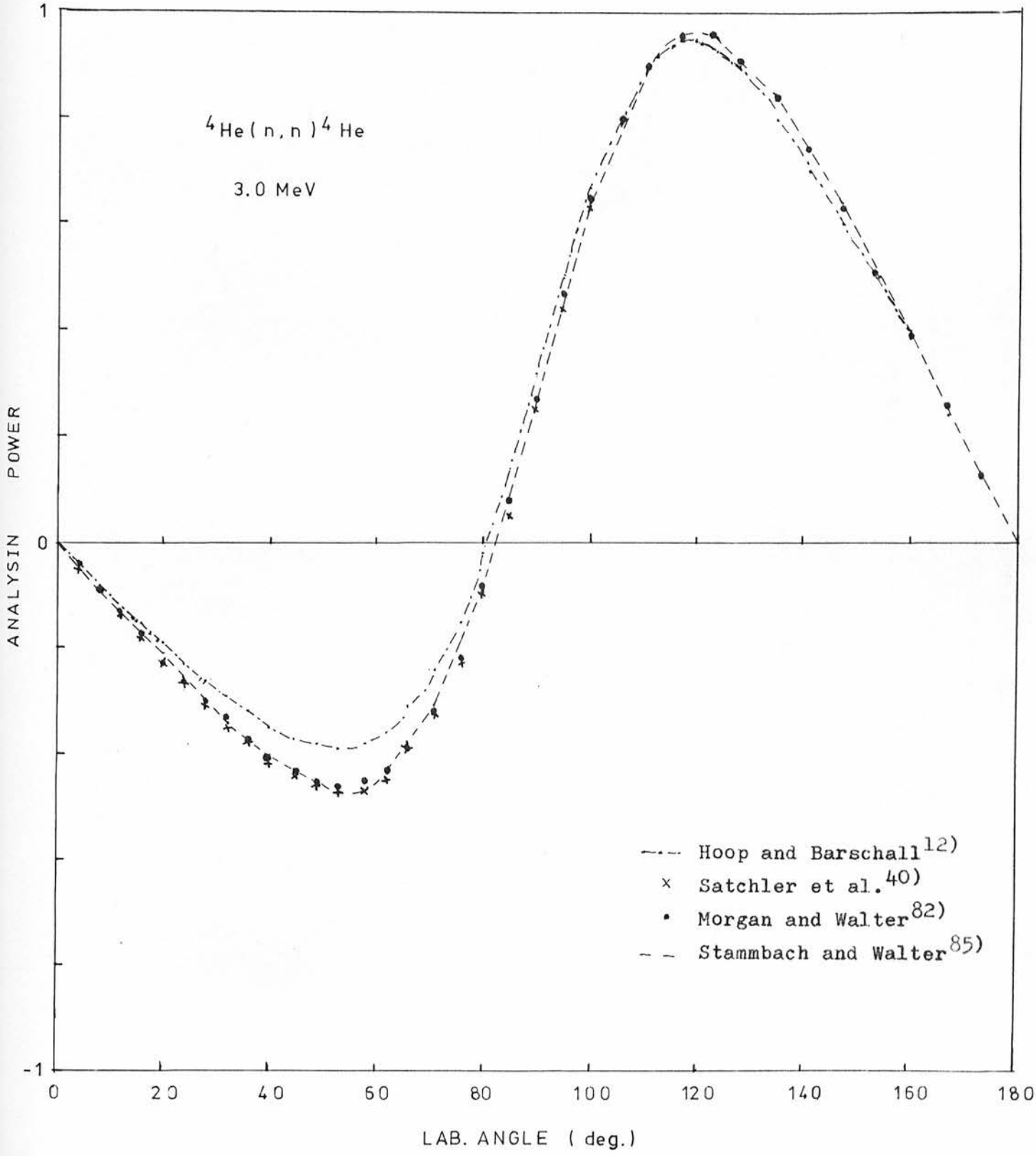
^{4}He(n, n)^4 He
3.0 MeV
ANALYSIN POWER
1
0
-1
0
20
40
60
80
100
120
140
160
180
LAB. ANGLE (deg.)
Hoop and Barschall[12)]
Satchler et al.[40)]
Morgan and Walter[82)]
Stammbach and Walter[85)]

Figure 37. Angular dependence of the analysing power of ^{4}He in the Lab. system for 6 MeV neutrons as calculated using four different sets of phase shifts.

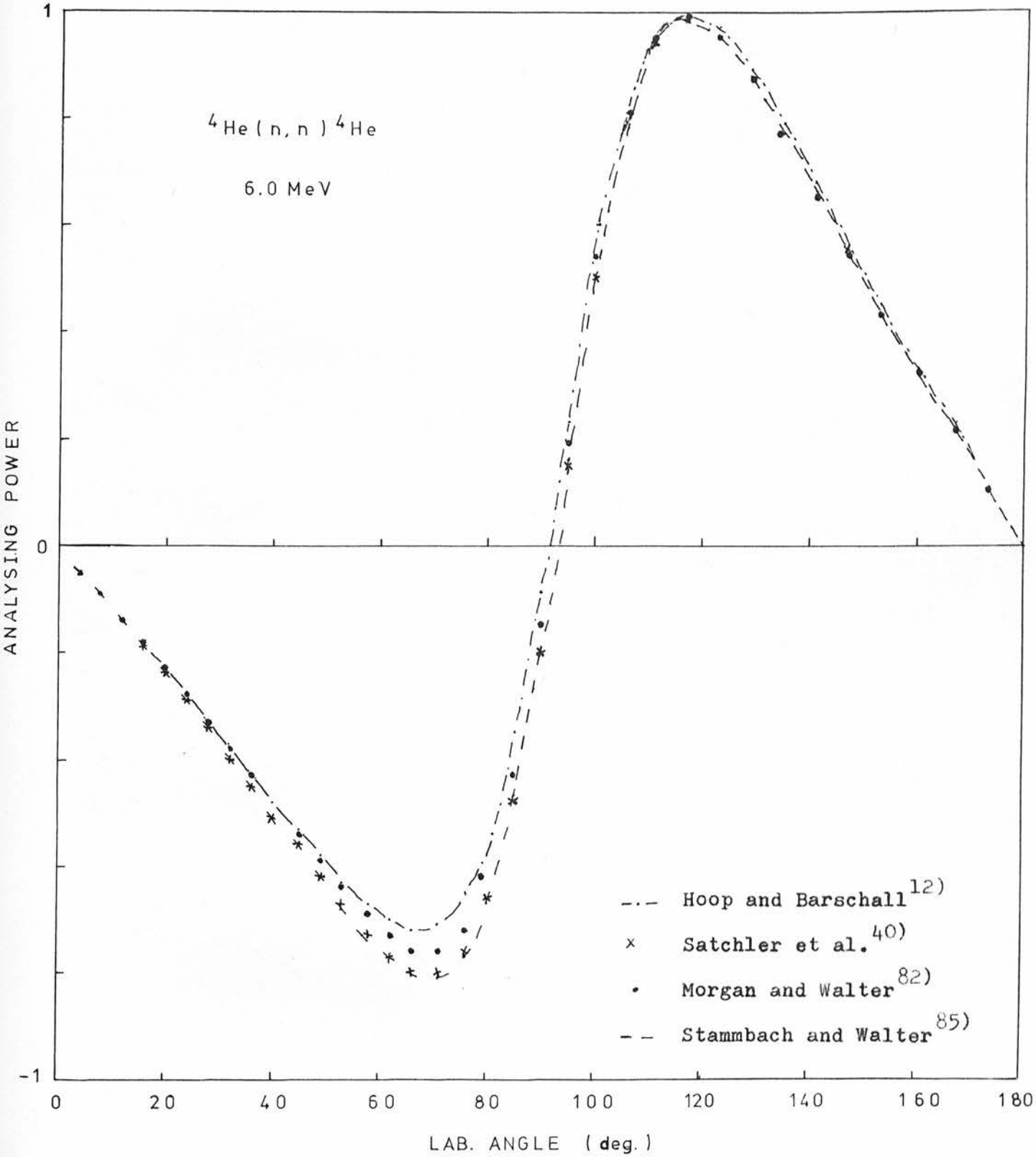
$^4He(n,n)^4He$
6.0 MeV
ANALYSING POWER
1
0
-1
0
20
40
60
80
100
120
140
160
180
LAB. ANGLE (deg.)
Hoop and Barschall[12)]
Satchler et al.[40)]
Morgan and Walter[82)]
Stammbach and Walter[85)]

analysing power differs by nearly 20% at the forward minimum and about 3% difference exists at the backward maximum.

The analysing power of helium reported in this thesis was computed using the phase shifts of Hoop and Barschall [12]. The selection of these phase shifts is based on the agreement of the experimental results of the neutron double scattering on ^{4}He experiment of Tornow [86] and the neutron polarization experiment of Sikkema and Steendam [55], with the predicted phase shifts of Hoop and Barschall [12]. Also the results of neutron polarization measurement using small angle scattering experiment of Lugo [64] agree very well with the present results using the phase shifts of Hoop and Barschall [12].

The latest set of phase shifts which was reported by Stammbach and Walter [85] yield values of the analysing power of helium which differ by less than 0.02 from those calculated using the Hoop and Barschall [12] phase shifts. It is estimated that these differences decrease the present values of polarization by about 0.002 which is within the statistical accuracy involved.

5.5 The Mean Analysing Power Calculation.

The measured asymmetry, according to formula 1.2.9 of section 1.2, can be used to calculate the neutron polarization P_n if the analysing power of the scatterer is known. As expression 5.4.1 can be used to calculate the analysing power of the scatterer,

(in the present case helium), two factors have to be taken into account. First is the scattering angles involved due to the finite dimentions of both the helium gas scintillator and the side detectors. Second is the variation in cross section for the D-D reaction over the solid angle subtended by the gas scintillator at the target. The analysing power calculated with account of these two factors is called the mean analysing power $< P >$ and will be discussed in this section.

When a uniform monoenergetic neutron flux N, impinges upon the gas scintillator, the number of neutrons per second detected by a small volume element dv' of the right liquid scintillator after having been scattered by a small volume element dv of the helium gas scintillator can be given according to formula 1.2.7 of section 1.2 as:

$$\frac{Ns_R n\sigma(\theta)\left[1 + PP_n\cos\phi\right]dvdv'}{r^2} \qquad (5.5.1)$$

where s_R is the probability of a scattered neutron being detected, n is the number of helium nuclei per unit volume and r is the distance between dv and dv'. In the present experimental arrangement the target is located at a definite distance k from the helium scintillator and the neutron flux N has to be considered in such a case. The reaction angle θ, for a neutron emitted from the target and scattered at a point (a,b,c) from the origin of coordinates (x,y,z) which is located at the centre of the helium scintillator will be given as:

$$\theta = \langle\theta\rangle - \frac{b}{c + k} \qquad (5.5.2)$$

where $\langle\theta\rangle$ is the mean reaction angle. As the fractional variation of D-D reaction cross section may be considered as a constant, say α, for small deviation from $\langle\theta\rangle$, the neutron flux N at a point (a,b,c) within the gas scintillator will be given by [66]:

$$N = \frac{N'}{a^2 + b^2 + c^2}\left(1 - \frac{b}{c + k}\right) \qquad (5.5.3)$$

and since $k \gg |a|$, $|b|$ and $|c|$ the expression can be approximated to:

$$N = N''(1 + \gamma b) \qquad (5.5.4)$$

where γ is the fractional variation of the D-D reaction differential cross section per unit length traversed in the Y direction in the helium gas scintillator. γ depends on the deuteron energy and the polarimeter geometry and it is evaluated at the centre of the gas scintillator.

The result of combining expressions 5.5.1 and 5.5.4 will be:

$$\frac{N''s_R n\sigma(\theta)(1 + \gamma b)(1 + PP_n\cos\phi)dvdv'}{r^2} \qquad (5.5.5)$$

Thus the total number of neutrons detected per second by the 'Right' liquid scintillator after scattering by the helium gas scintillator is:

$$I_R = N''s_R n \int \frac{\sigma(\theta)(1 + \gamma b)(1 + PP_n\cos\phi)}{r^2}\, dvdv' \qquad (5.5.6)$$

and the total number for the 'Left' liquid scintillator which is symmetrical to the 'Right' one will be:

$$I_L = N''s_L n \int \frac{\sigma(\theta)(1 - \gamma b)(1 - PP_n \cos\phi)}{r^2} \, dvdv' \qquad (5.5.7)$$

Expression 1.3.6 of section 1.3 is used to calculate the asymmetry where the detection efficiencies cancel entirely. by using expressions 5.5.6 and 5.5.7 expression 1.3.6 will be:

$$\varepsilon = P_n \left[\frac{\int \frac{\sigma(\theta) P \cos\phi}{r^2} dvdv' + \frac{\gamma}{P_n} \int \frac{b\sigma(\theta)}{r^2} dvdv'}{\int \frac{\sigma(\theta)}{r^2} dvdv' + \gamma P_n \int \frac{b\sigma(\theta) P \cos\phi}{r^2} dvdv'} \right]$$

$$= P_n \left[\frac{J_1 + \frac{\gamma}{P_n} J_1'}{J_2 + \gamma P_n J_2'} \right] = P_n \langle P \rangle \qquad (5.5.8)$$

where J_1, J_1', J_2 and J_2' are double volume integrals calculated throughout the volumes of both the helium scintillator and side detectors.

The expression for the mean analysing power $\langle P \rangle$ includes both corrections for finite geometry as well as the variation of the $^2H(d,n)^3He$ cross section with angle and can be approximated [66] as:

$$\varepsilon = P_n \frac{J_1}{J_2} + \gamma \frac{J_1'}{J_2}$$

$$= P_n \langle P_1 \rangle + m \qquad (5.5.9)$$

where m is the false asymmetry due to the variation of the reaction angle and $< P_1 >$ is the analysing power corrected only for the finite geometry.

In order to evaluate the mean analysing power of helium a Mont Carlo program, used before by Davie [66] and Maayouf [78] based on expression 5.5.8 and 5.5.9 was employed. This program is modified to the requirement of the geometry of the new polarimeter. The volumes of the helium gas scintillator and the liquid scintillator were sampled in a random way. The 'rectangular' random number distribution used in this process being generated by a power residue method [83]. The program has to be supplied with n - ^{4}He phase shifts, the fractional variation of the D-D reaction cross section and an estimation of neutron polarization P_n.

The fractional variation of the D-D reaction cross section was evaluated using the cross section data compiled by Liskien and Paulsen [77] for each deuteron energy at the employed reaction angle of 45°. As the angle subtended by the helium gas scintillator at the target was about 3.5°, the value of γ was very small.

The n - ^{4}He phase shifts, supplied to the computer code, were obtained by interpolation, for each neutron energy, from the data of Hoop and Barschall.[12]

The measured asymmetries were used as estimations of P_n and this resulted in values of $< P >$ with enough accuracy. By

supplying the code with the calculated P_n using this $< P >$ value, as a more accurate estimation of P_n, the resulting value of $< P >$ did not differ significantly from the previous one.

The results of the calculation, using the program, gave values of $< P_1 >$, $< P >$ and m where m was always less than the statistical accuracy associated with the results for all the present measurements.

5.6 Results and Conclusion.

The asymmetry in the scattering of the neutrons in the plane normal to the reaction plane was measured several times at different deuteron energies and the resulting asymmetries have been given in tables 1o and 11. These results show that there are no appreciable asymmetries in the system.

Contribution to the measured polarization from multiple scattering in the helium gas scintillator and scattering in the target assembly etc. has been proved [66] to be insignificant.

Thus the neutron polarization has been evaluated from the corrected asymmetries given in tables 10 and 11 and the mean analysing power of helium calculated as described in section 5.5.

The results of the present measurements for both thin and thick targets are given in table 12. For each incident deuteron

E_d	$\bar{E}_d$	E_n	$\langle P_{He} \rangle$	P_n (%)	Target
keV	keV	MeV			
350	240	2.94	0.856	-14.7 ± 0.9	Thick
300	210	2.91	0.853	-13.6 ± 0.7	Thick
300	210	2.91	0.869	-13.7 ± 0.8	Thick
250	180	2.87	0.864	-12.6 ± 0.7	Thick
200	150	2.82	0.859	-12.3 ± 0.6	Thick
150	115	2.77	0.842	-11.5 ± 0.6	Thick
350	275	2.99	0.878	-15.0 ± 0.7	Thin
300	225	2.93	0.854	-14.4 ± 0.5	Thin
250	195	2.89	0.852	-14.7 ± 0.5	Thin
200	180	2.87	0.851	-12.4 ± 0.6	Thin
150	135	2.80	0.847	-11.9 ± 0.5	Thin
125	105	2.75	0.843	-09.6 ± 0.9	Thin
100	85	2.72	0.840	-10.2 ± 1.4	Thin
100	80	2.71	0.839	-10.0 ± 0.7	Thin
75	55	2.66	0.835	-08.8 ± 0.8	Thin
50	35	2.62	0.830	-08.0 ± 1.1	Thin

Table 12. The resulting $^2H(d,n)^3He$ polarization at a reaction angle of 45^o Lab.

energy, the following quantities are given: $\bar{E}_d$ is the average deuteron energy, E_n the neutron energy at an emission angle of 45° Lab., $< P_{He} >$ the mean analysing power of the ^4He and P_n the neutron polarization (%) at 45° Lab.

A comparison of the results of the present measurements with the values obtained so far by other authors for a reaction angle of $45^\circ \pm 5^\circ$ Lab. and average deuteron energies below 400 keV is shown in figure 38. Both thin and thick target results are represented in this figure.

The present results show no sign of a peak in the polarization values near 100 keV deuteron energy. As most of the published results with a resonance-like behaviour were observed with carbon used as an analyser (the results of Hansgen et al.[22], Rogers and Bond [21], Kane [18] and Prade and Csikai [36]) and because of the rapid increase of the analysing power of carbon in this energy range and their effect on the polarization values, those results are excluded from the discussion. Also the results of Thomas and Hofmann [33] are excluded because of the width of the peak in their polarization values is less than the energy spread of the deuterons reacting in the target. The results of Pasma [14] are also excluded because of the criticism by Boersma et al [15] that this data should be corrected for instrumental asymmetries and background effect. The Pasma [14] data was also excluded from the review of Walter [35] for the same reasons.

Figure 38. Comparison of the neutron polarization values as determined in the present work with other published values.

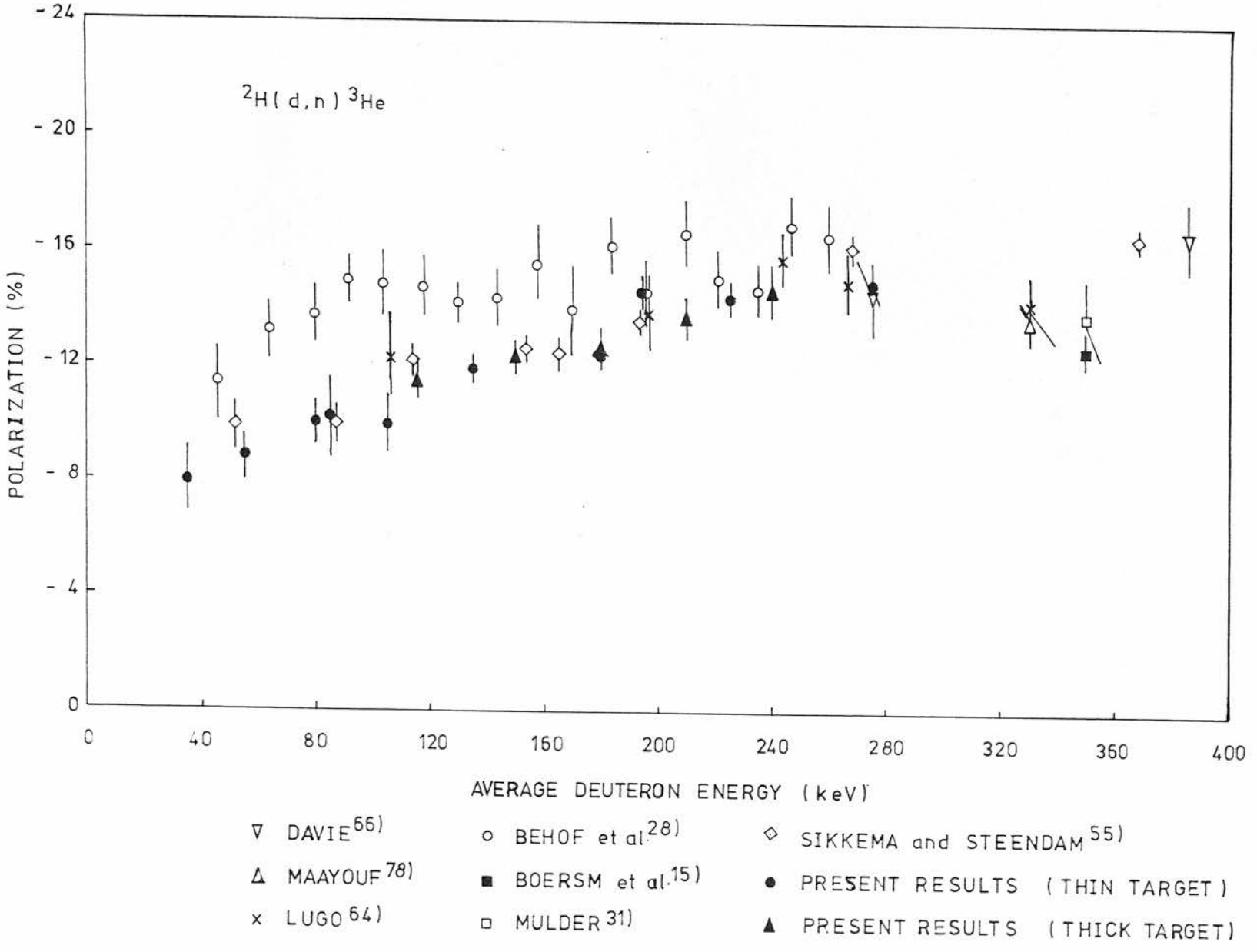
$^{2}H(d,n)^{3}He$
POLARIZATION (%)
0
- 4
- 8
- 12
- 16
- 20
- 24
0
40
80
120
160
200
240
280
320
360
400
AVERAGE DEUTERON ENERGY (keV)
▽ DAVIE 66)
△ MAAYOUF 78)
× LUGO 64)
○ BEHOF et al. 28)
■ BOERSM et al. 15)
□ MULDER 31)
◇ SIKKEMA and STEENDAM 55)
● PRESENT RESULTS (THIN TARGET)
▲ PRESENT RESULTS (THICK TARGET)

As can be seen from figure 38 the present results differ from those of Behof et al [28]. Behof et al [28] have measured the neutron polarization with a polarimeter similar to the present modified one. But they used the difference in the time of flight of the neutrons and γ-rays between the gas scintillator and the side neutron detectors to reject γ-rays. This method might result not only in a rejection of γ-rays but also in a substantial reduction in the tail remote from the peak [66]. Thus if the recoil spectra have been recorded, then the tail resulting from the fast timing to reject γ-rays might lead to a false extrapolation and a consequent introduction of error. This might explain the high values of polarization obtained by Behof et al [28] which are higher than all of the published results in this energy region.

The present results came in very good agreement with the recent results of Sikkema and Steendam [55]. They have used a new type of helium recoil polarimeter based on a helium-filled multiwire proportional chamber. Their method of measurement has been briefly described in section 1.4 of chapter 1.

The present results came also in very good agreement with the very recent results of Lugo [64] who used a small angle scattering experiment to obtain the polarization values. His polarimeter consists of two neutron detectors to measure the asymmetry in the scattering of neutrons from lead. Pulse shape discrimination technique, similar to the one used in the present experiment, was used to reject γ-rays. In the small angle

experiment the polarization can be calculated from measured cross sections without the need for any phase shift analysis [7]. The results of Lugo [64] were measured using a thin Ti-D target and neutrons emitted at a Laboratory angle of 45^{o} in the deuteron energy range from 100 to 330 keV.

The results of the present experiment, together with the results of Sikkema and Steendam [55] and Lugo [64], indicate that the polarization is monotonically increaisng with energy in the region below 400 keV average deuteron energy.

In order to compare the present results with the theoretical prediction of polarization by Boersma [27] those expressions given by him and discussed in chapter 1 will be used in this section.

The neutron polarization P_n is related to the anisotropy coefficient A_2/A_o by expression 1.5.8 and both P_n and A_2/A_o depend on the deuteron energy E_d according to expressions 1.5.9 and 1.5.3 respectively.

The experimental values of A_2/A_o in the low energy limit as published by several authors and as calculated from the anisotropy coefficient A using expression 1.5.2 as given by Boersma [28] have been plotted in figure 6 in chapter 1. These experimental results were fitted with two curves calculated from expression 1.5.3. One of these curves was obtained by Boersma [28] by selecting the constant values α and β in expression 1.5.3 to fit the experimental

data of Theus et al [46] and Eliot et al [51]. The other curve was obtained from Fick and Weiss [54] who found different values for α and β in order to fit those values along with more recent values of A_2/A_o.

From the present results it was found that both the neutron polarization values and the anisotropy coefficient values can be well represented by expressions 1.5.9 and 1.5.3 respectively with $\alpha = 3.8$ and $\beta = 5$.

With these values A_2/A_o was calculated as a fuction of E_d with expression 1.5.3 and plotted (solid curve) with the experimental values in figure 39. A_2/A_o as calculated using the values α and β given by Fick and Weiss [54] with their maximal errors are also plotted (dashed curves) in the same figure. As can be seen from the figure the values A_2/A_o as calculated using the obtained α and β are lying within those of Fick and Weiss [54] and in good agreement with most of the experimental values even at higher energies.

The obtained values of α and β are used to calculate the neutron polarization as a function of deuteron energy with expression 1.5.9.

A value of $c = -0.160$ was obtained by letting the polarization value at 135 keV coincide with the calculated one. Using this value of c, P_n was calculated and the resulting values are plotted in

Figure 39. The A_2/A_o values for the $^2H(d,n)^3He$ reaction as a function of the average deuteron energy. The dashed curves represent the maximum and minimum values of A_2/A_o obtained from expression 1.5.3 with the values of $\alpha = 3.2 \pm 0.3$ $\beta = 4.9 \pm 0.2$ as given by Fick and Weiss [54]. The solid curve represents the A_2/A_o values obtained from expression 1.5.3 with $\alpha = 3.8$ and $\beta = 5$.

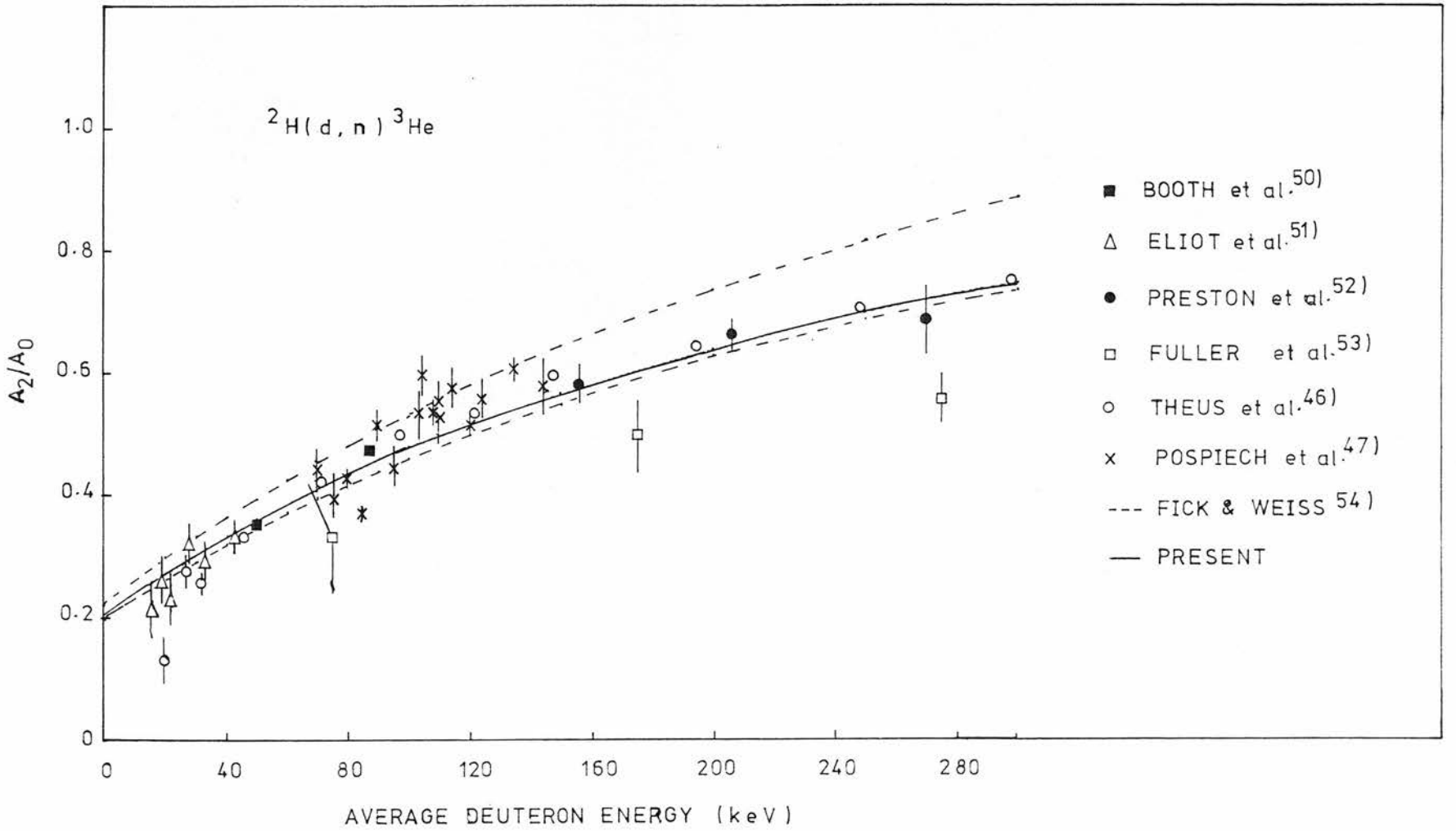
$^2H(d,n)^3He$
A_2/A_0
1.0
0.8
0.6
0.4
0.2
0
0
40
80
120
160
200
240
280
AVERAGE DEUTERON ENERGY (keV)
BOOTH et al.[50]
ELIOT et al.[51]
PRESTON et al.[52]
FULLER et al.[53]
THEUS et al.[46]
POSPIECH et al.[47]
--- FICK & WEISS [54]
— PRESENT

Figure 40. Comparison of the neutron polarization values as determined in the present work with those determined from the theoretical expression 1.5.9 with the values α, β and c obtained in the current section.

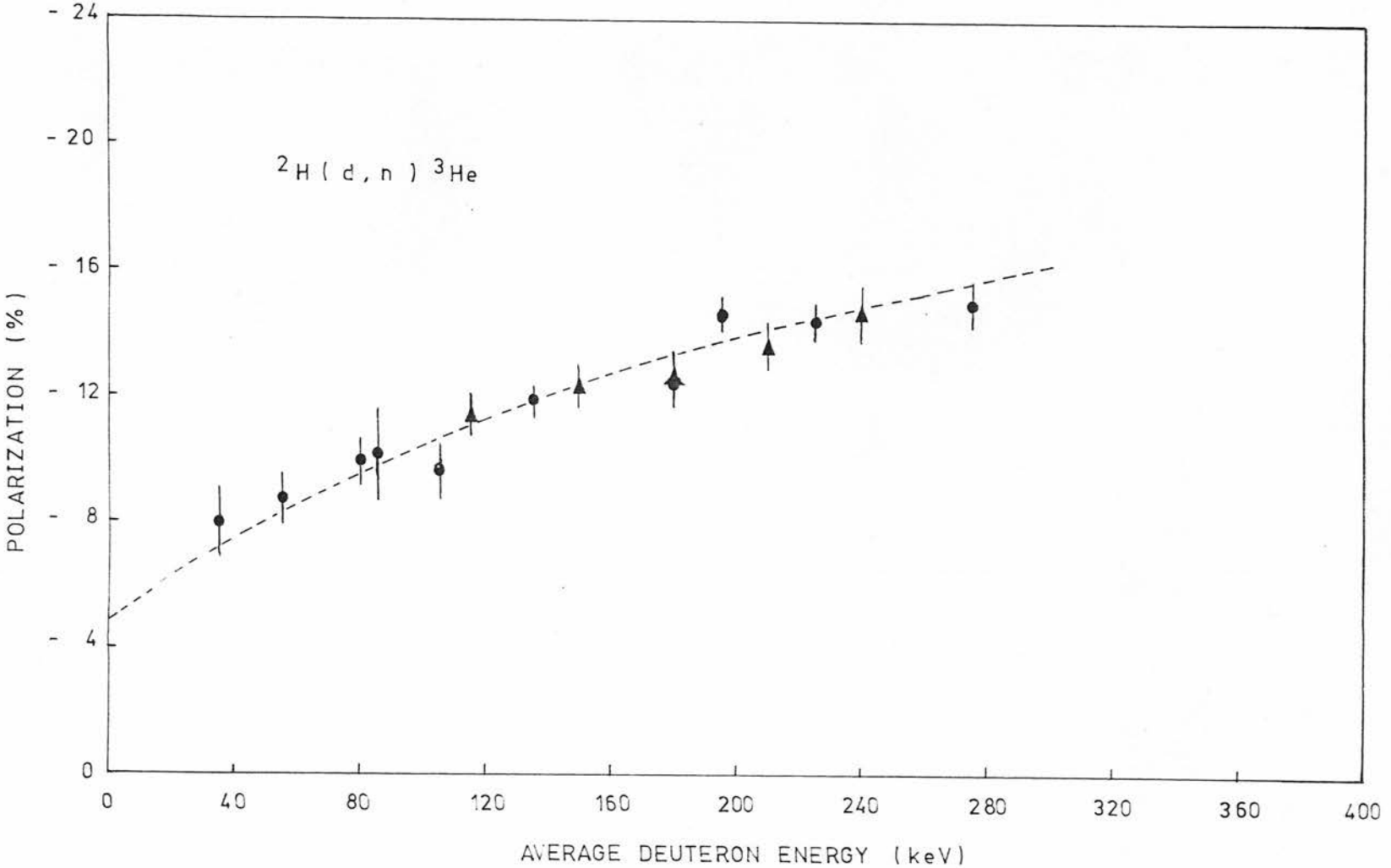

▲ PRESENT RESULTS (THICK TARGET)

● PRESENT RESULTS (THIN TARGET)

DASHED CURVE THEORETICAL EXP. (1.5.9)

figure 40 together with the present experimental results. As can be seen from the figure, the calculated P_n values came in good agreement with most of the present results even for energies higher than 200 kev, where expression 1.5.9 loses validity.

It is concluded that the $^2H(d,n)^3He$ reaction provides a source of polarized neutrons with a polarization varying in magnitude from 0.08 to 0.16 in the energy range from 35 to 400 keV average deuteron energy at a reaction angle of 45^o.

The excellent agreement of the present results with the experimental results of Sikkema and Steendam [55] and Lugo [64] and the theoretical prediction of polarization by Boersma [27] could provide the users of $^2H(d,n)^3He$ reaction with sufficient information in this energy range and angle in order to study the scattering of polarized neutrons from this reaction by different materials.

The demonstrated applicability of the present ^4He scattering polarimeter should encourage studies of neutron polarization from various reactions.

REFERENCES.

REFERENCES.

1. E.J.Konopinski and E.Teller, Phys.Rev. 73, 822 (1948)
2. L.Wolfenstein, Phys.Rev. 75, 342 (1949)
3. J.Schwinger, Phys.Rev. 69, 681 (1946)
4. P.Huber and E.Baumgartner, Helv.Phys.Acta 26, 420 (1953)
5. R.Ricamo, Helv.Phys.Acta 26, 423 (1953)
6. R.Ricamo, Nuovo Cimento 10, 1607 (1953)
7. W.Haeberli, Fast Neutron Physics, edited by J.B.Marion and J.L.Fowler (Interscience Publishers, New York 1960), Part II, Chapter V.G.
8. R.B.Galloway, Nucl.Inst.&Meth. 92, 537 (1971); Errata 95, 393 (1971)
9. F.O.Purser, J.R.Sawers, Jr., and R.L.Walter, Phys.Rev. 140, B870 (1965)
10. R.B.Galloway, A.S.Hall, R.M.A.Maayouf and D.G.Vass, Nucl.Phys. A242, 122 (1975)
11. F.M.Beiduk, J.R.Prutt and E.J.Konopinski, Phys.Rev. 77, 622 (1950)
12. B.Hoop and H.H.Barschall, Nucl.Phys. 83, 65 (1966)
13. J.E.Wills, J.K.Blair, H.O.Cohn and H.B.Willard, Phys.Rev. 109, 891 (1958)
14. P.J.Pasma, Nucl.Phys. 6, 141 (1958)
15. H.J.Boersma, C.C.Jonker, J.G.Nijenhuis and P.J.Van Hall Nucl.Phys. 46, 660 (1963)
16. R.Van Wageningen, Intern Rapport Natuurkundig Laboratorium IR 15 (Groningen 1954)

17. J.D.Seagrave, Phys.Rev. 92, 1222 (1953)

18. P.P.Kane, Nucl.Phys. 10, 429 (1959)

19. R.W.Meier, P.Scherrer and G.Trumpy, Helv.Phys.Acta 27, 577 (1954)

20. S.M.Austin, H.H.Barschall and R.E.Shamu, Phys.Rev. 126, 1532 (1962)

21. J.T.Rogers and C.D.Bond, Nucl.Phys. 53, 297 (1964)

22. H.Hansgen, H.Pose, G.Schirmer and D.Seeliger, Nucl.Phys. 73, 417 (1965)

23. P.Szydlik and C.Werntz, Phys.Rev. 138, B866 (1965)

24. J.Cerny, C.Detraz and R.Phel, Phys.Rev.Lett. 15, 300 (1965)

25. J.J.Schmidt, Neutron cross sections for fast reactor materials (Karlsruhe, 1968).

26. F.Ajzenberg-Selove, Nucl.Phys. A152, 1 (1970)

27. H.J.Boersma, Nucl.Phys. A135, 609 (1969)

28. A.F.Behof, T.H.May and W.I.McGarry, Nucl.Phys. A108, 250 (1968)

29. D.C.Dodder and J.L.Gammel, Phys.Rev. 88, 520 (1952)

30. G.P.Lietz, S.F.Trevino, A.F.Behof and S.E.Darden, Nucl.Phys. 67, 193 (1965)

31. J.P.F.Mulder Phys.Lett. 23, 589 (1966)

32. W.G.Stoppenhagen and R.W.Finlay, Bull.Am.Phys. A108, 250 (1968)

33. K.Thomas and A.Hofmann Z.Phys. 217, 128 (1968)

34. D.Fick and H.W.Franz Phys.Lett. 27B, 541 (1968)

35. R.L.Walter, Polarization Phenomena in Nuclear Reactions (Ed. H.H.Barschall and W.Haeberli, Univ. Wisconsin Press, Madison 1970) P. 317

36. H.Prade and J.Csikai, Nucl.Phys. A123, 365 (1969)

37. H.Davie and R.B.Galloway, Nucl.Inst.&Meth. 108, 581 (1973)

38. R.M.A.Maayouf and R.B.Galloway, Nucl.Inst.&Meth. 118, 343 (1974)

39. R.B.Galloway and R.M.A.Maayouf, Nucl.Phys. A212, 182 (1973)

40. G.R.Satchler, L.W.Owen, A.J.Elwyn, G.L.Morgan and R.L.Walter, Nucl.Phys. A112, 1 (1968)

41. H.Davie and R.B.Galloway, Nucl.Inst&Meth. 92, 547 (1971)

42. J.V.Lepore, Phys.Rev. 79, 137 (1950)

43. M.Fierz, Helv.Phys.Acta 25, 629 (1952)

44. H.W.Franz and D.Fick, Nucl.Phys. A122, 591 (1968)

45. N.Ying, B.B.Cox, B.K.Barnes and A.W.Barrows, Jr., Nucl.Phys. A206, 481 (1973)

46. R.B.Theus, W.I.McGarry and L.A.Beach, Nucl.Phys. 80, 273 (1966)

47. G.Pospiech, H.Genz, E.H.Marlinghaus, A.Richter and G.Schrieder, Nucl.Phys. A239, 125 (1975)

48. H.Hansgen and M.Nitzsche, Nucl.Phys. A165, 401 (1971)

49. H.D.Knox, J.M.Cox, R.W.Finlay and R.O.Lane, Nucl.Phys. A217, 611 (1973)

50. D.L.Booth, G.Preston and P.F.D.Shaw, Proc.Phys.Soci. A69, 265 (1956)

51. E.A.Eliot, D.Roaf and P.F.D.Shaw, Proc.Roy.Soci. A216, 57 (1953)

52. G.Preston, P.F.D.Shaw and S.A.Young, Proc.Roy.Soci. A226, 206 (1954)

53. J.C.Fuller, W.E.Dance and D.C.Ralph, Phys.Rev. 108, 91 (1957)

54. D.Fick and U.Weiss, Z.Phys. 265, 87 (1973)

55. C.P.Sikkema and S.P.Steendam, Nucl.Phys. A245, 1 (1975)

56. F.A.Guckel and D.Fick, Z.Phys. 271, 39 (1974)

57. B.P.Ad'Yasevich, V.G.Antonenko and D.E.Fomenko, Sov.J.Nucl.Phys. 11, 411 (1970)

58. R.J.Blin-Stoyle, Proc.Phys.Soc. A64, 700 (1951)

R.J.Blin-Stoyle, Proc.Phys.Soc. A65, 949 (1952)

59. M.Cini, Nuovo Cimiento 8, 1007 (1951)

60. R.J.Rook and L.J.B.Goldfarb, Nucl.Phys. 27, 79 (1961)

61. H.Davie and R.B.Galloway, Nucl.Inst.&Meth. 92, 547 (1971)

62. Texas Instruments Ltd., 74 Series TTL, 1972 Edition (Quarandon Electronics, Derby, 1972).

63. P.Hillman, G.H.Stafford and Whitehead, Nuovo Cimiento 4, 67 (1956)

64. R.Lugo, Ph.D. Thesis, Edinburgh University, 1976

65. J.G.Jenkin and R.E.Shamu, Nucl.Inst.&Meth. 34, 116 (1965)

66. H.Davie, Ph.D. Thesis, Edinburgh University, 1972

67. M.L.Rouch, M.A.Wilson and W.F.Hornyak, Nucl.Inst.&Meth. 31, 112 (1964)

68. J.D.Seagrave, Los Alamos report LAMS - 2162, 1958

69. J.A.D'cunha, 'Electronics' circuit designer casebook (McGraw-Hill Publication, New York, 1971) P.4

70. R.B.Galloway and A.Waheed, Nucl.Inst.&Meth. 128, 505 (1975)
Nucl.Inst&.Meth. 128, 515 (1975)

71. S.E.Hunt and W.M.Jones, Phys.Rev. 89, 1283 (1953)

72. F.Ajzenberg-Selove and T.Lauritsen, Nucl.Phys. 11, 1 (1959)

73. J.B.Marion, Rev.Mod.Phys. 33, 139 (1961)

74. F.M.Watson, private communication

75. J.H.Coon, Fast Neutron Physics, Interscience, New York, 1960 Chapter IV.D.

76. J.H.Ormrod, Nucl.Inst.&Meth. 95, 49 (1971)

77. H.Liskein and A.Paulsen, Nucl.Data Tables 11, 587 (1973)

78. R.M.A.Maayouf, Ph.D. Thesis, Edinburgh University, 1973

79. E.Baumgartner and P.Huber, Helv.Phys.Acta 26, 545 (1953)

80. J.L.Gammel and R.M.Thaler, Phys.Rev. 109, 2041 (1958)

81. J.R.Sawers, G.L.Morgan, L.A.Schaller and R.L.Walter, Phys.Rev. 168, 1102 (1968)

82. G.L.Morgan and R.L.Walter, Phys.Rev. 168, 1114 (1968)

83. I.B.M. Manual C20 - 8011, Random Number Generation and Testing.

84. R.A.Arndt and L.D.Roper, Phys.Rev. C1, 903 (1970)

85. Th.Stammbach and R.L.Walter, Nucl.Phys. A180, 225 (1972)

86. W.Tornow, Z.Phys. 266, 357 (1974)

ACKNOWLEDGEMENTS.

I thank Professor N. Feather, F.R.S., for the facilities provided for this research. The advice, encouragement and guidance of Dr. R.B. Galloway, my supervisor, is gratefully acknowledged.

I thank Dr. G. Bradford and Mr. L. Kennedy for their advice and help in matters connected with the automatic control system.

I thank my colleagues, A.S. Hall and F.M. Watson for their willing assistance, also R. Maayouf, A. Waheed and R. Lugo for interesting and useful discussion.

I am grateful to Mr. H.J. Napier for maintaining and operating the accelerator, often at inconvenient hours, and to Mr. G. Turnbull for his willing assistance.

I thank the University of Riyadh, Saudi Arabia, for their financial support during the course of this research.